

Nucleon Electro-Magnetic Form Factors

- Introduction
- Formalism
- Instrumentation
- Review of data
- Theory
- Summary

Kees de Jager
Jefferson Lab
SUSSP 58
August 23 - 27, 2004



Thomas Jefferson National Accelerator Facility

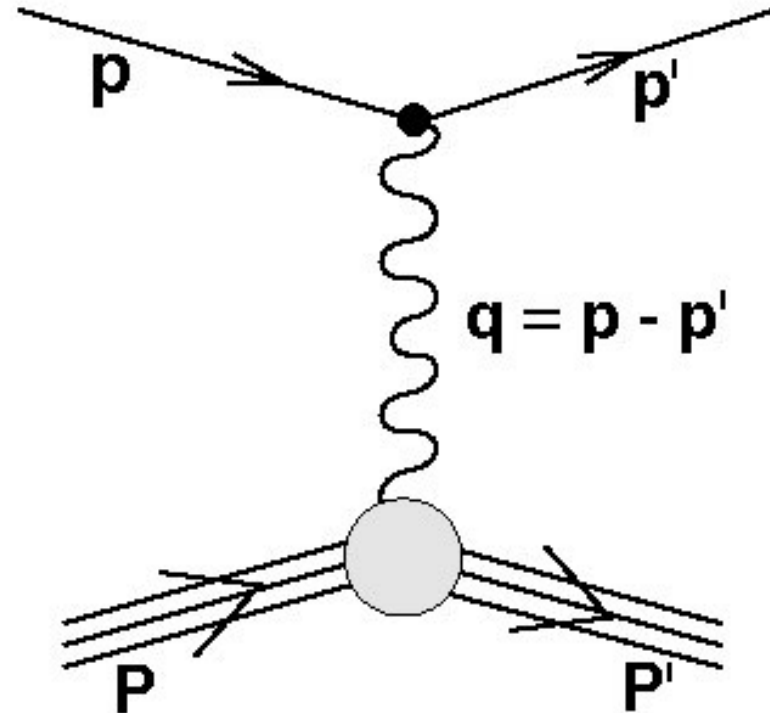
Introduction

- **Form Factor**

response of system to probe with wavelength λ
(or momentum transfer Q), often normalized
to that of point-like system

Examples:

- ← scattering of photons by bound atoms
- ← nuclear beta decay
- ← X-ray scattering from crystal
- ← electron scattering off nucleon

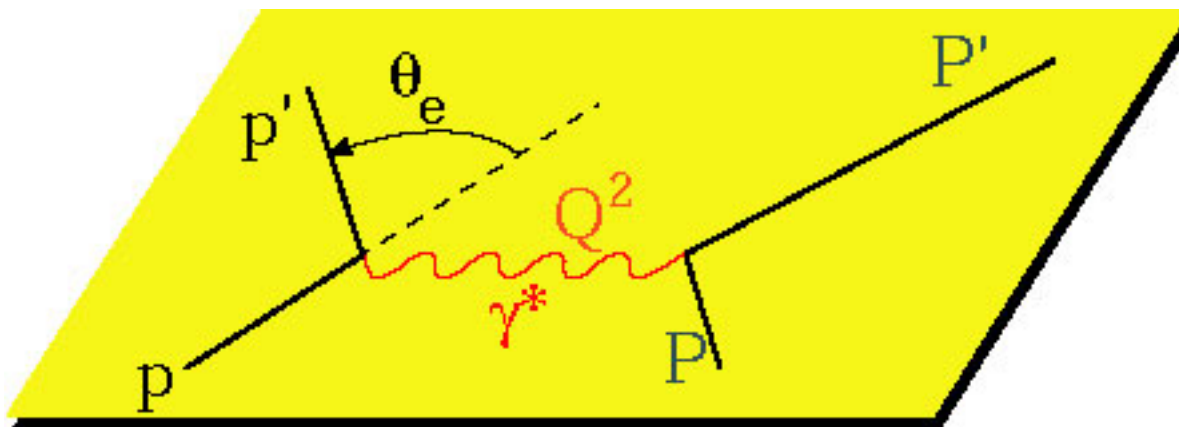


Nucleon Electro-Magnetic Form Factors

- ▲ Fundamental ingredients in "Classical" nuclear theory
- A testing ground for theories constructing nucleons from quarks and gluons
 - probes spatial distribution of charge and magnetization of the nucleon
 - wavelength of probe can be tuned by selecting momentum transfer Q :
 - < 0.1 GeV^2 integral quantities (charge radius,...)
 - $0.1\text{-}10 \text{ GeV}^2$ internal structure of nucleon
 - > 20 GeV^2 pQCD scaling

Caveat: If Q is several times the nucleon mass (\sim Compton wavelength), dynamical effects due to relativistic boosts are introduced, making physical interpretation more difficult

Kinematics



$$\vec{q} = \vec{p} - \vec{p}'$$

$$\omega = E_e - E_e'$$

$$-Q^2 \equiv t \equiv q^2 = \omega^2 - \vec{q}^2$$

$$Q^2 \approx 4EE' \sin^2 \theta_e / 2$$

$$J_\mu = \bar{U}(P') \left\{ \gamma_\mu F_1(Q^2) + \frac{i\sigma^{\mu\nu} q_\nu}{2M_p} \kappa F_2(Q^2) \right\} U(P)$$

$Q^2 > 0$ space-like region, studied through elastic electron scattering

$Q^2 < 0$ time-like region, studied through creation or annihilation

$e^+ + e^- \rightarrow N + N$ or $N + N \rightarrow e^+ + e^-$

In the isovector channel ($T = 1$) two pions can contribute, so $Q^2 < -4m_\pi^2$

In the isoscalar channel ($T = 0$) only an odd number of pions can couple, so $Q^2 < -9m_\pi^2$

Formalism

Cross section or spin-dependent properties provide information on **nucleon vertex**

In eN scattering, **lepton vertex** known from QED

$$i\mathcal{M} = \frac{-i}{q^2} \left[ie\bar{v}(P')\Gamma^\mu(P',P)v(P) \right] \left[ie\bar{u}(p')\gamma_\mu u(p) \right] \quad |\mathcal{M}|^2 = \left(\frac{e^2}{q^2} \right)^2 W^{\mu\nu} L_{\mu\nu}$$

Breit frame

$$W^{00} = 4M^2 G_E^2$$

$$W^{11} = Q^2 G_M^2$$

$$W^{22} = Q^2 G_M^2$$

$$L_{\mu\nu} = 2p_\mu p'_\nu + 2p_\nu p'_\mu - 2g_{\mu\nu} p p'$$

$$L_{00} = 4E^2 - Q^2 = Q^2 \cot^2 \theta_e / 2$$

$$L_{11} = 4p_1^2 + Q^2 = Q^2 (1 + \cot \theta_e / 2)$$

$$L_{22} = Q^2$$

Lab frame

$$|\mathcal{M}|^2 = \left(\frac{e^2}{q^2} \right)^2 4M^2 Q^2 \left[2\tau G_M^2 + \frac{\cot^2 \theta_e / 2}{1 + \tau} (G_E^2 + G_M^2) \right]$$

Formalism

Dirac (non-spin-flip) F_1 and Pauli (spin-flip) F_2 Form Factors

$$\frac{d\sigma}{d\Omega}(E, \theta) = \frac{\alpha^2 E' \cos^2\left(\frac{\theta}{2}\right)}{4E^3 \sin^4\left(\frac{\theta}{2}\right)} [(F_1^2 + \kappa^2 \tau F_2^2) + 2\tau(F_1 + \kappa F_2)^2 \tan^2\left(\frac{\theta}{2}\right)]$$

with E (E') incoming (outgoing) energy, θ scattering angle, κ anomalous magnetic moment and $\tau = Q^2/4M^2$
 Alternatively, Sachs Form Factors G_E and G_M

$$F_1 = G_E + \tau G_M \quad F_2 = \frac{G_M - G_E}{\kappa(1 + \tau)} \quad \tau = \frac{Q^2}{4M^2}$$

$$\frac{d\sigma}{d\Omega}(E, \theta) = \sigma_M \left[\frac{G_E^2 + \tau G_M^2}{1 + \tau} + 2\tau G_M^2 \tan^2\left(\frac{\theta}{2}\right) \right]$$

$$\sigma_M = \frac{\alpha^2 E' \cos^2\left(\frac{\theta}{2}\right)}{4E^3 \sin^4\left(\frac{\theta}{2}\right)}$$

In the Breit (centre-of mass) frame the Sachs FF can be written as the Fourier transforms of the charge and magnetization radial density distributions

Early Measurements of G_E^p

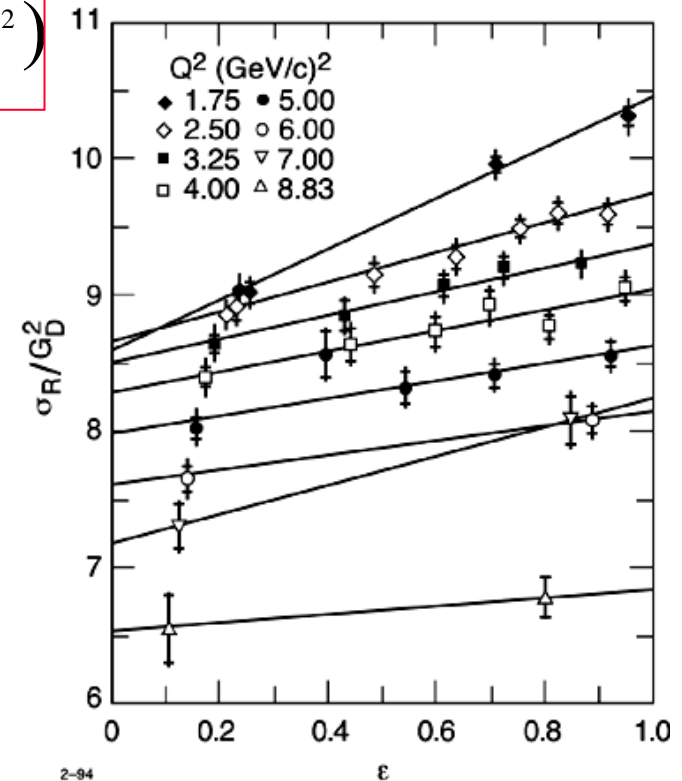
- relied on Rosenbluth separation
 - measure $d\sigma/d\Omega$ at constant Q^2
 - G_E^p inversely weighted with Q^2 , increasing the systematic error above $Q^2 \sim 1 \text{ GeV}^2$

$$\sigma_R(Q^2, \varepsilon) = \varepsilon \left(1 + \frac{1}{\tau}\right) \frac{E}{E'} \frac{\sigma(E, \theta)}{\sigma_{Mott}} = (G_M^p)^2(Q^2) + \frac{\varepsilon}{\tau} (G_E^p)^2(Q^2)$$

$$Q^2 = 4EE' \sin^2\left(\frac{\theta}{2}\right)$$

$$\varepsilon = \frac{1}{1 + 2(1 + \tau) \tan^2(\theta/2)}$$

- At $Q^2=6 \text{ GeV}^2$ σ_R changes by only 8% from $\varepsilon=0$ ($\theta=180^\circ$) to $\varepsilon=1$ ($\theta=0^\circ$) if $G_E^p = G_M^p / \mu_p$
- Hence, measurement of G_E^p with 10% accuracy requires 1.6% cross-section measurement



G_E^n without Polarization

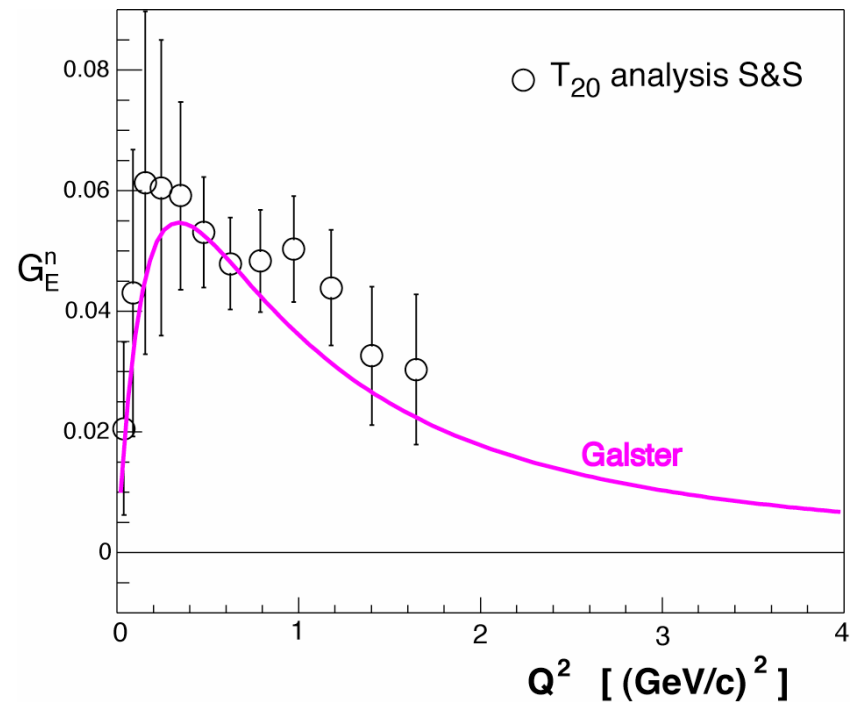
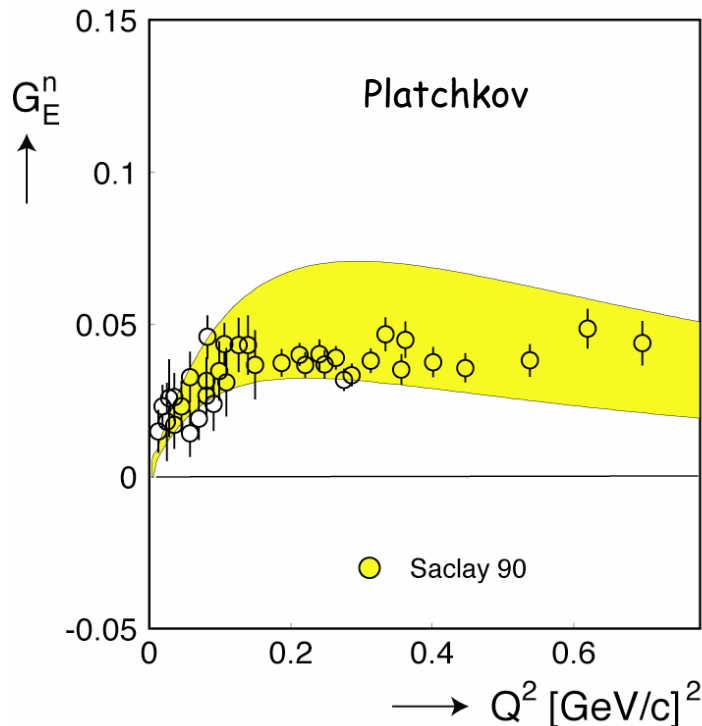
No free neutron target available, early experiments used deuteron
 Large systematic errors caused by subtraction of proton contribution

Elastic e-d scattering

$$\frac{d\sigma}{d\Omega} \propto \{A + B \tan^2(\theta_e / 2)\} \propto (G_E^p + G_E^n)^2 \int [u^2(r) + w^2(r)] j_0\left(\frac{Qr}{2}\right) dr + \dots$$

Quadrupole Form Factor

$$T_{20}(Q^2) \propto G_Q(Q^2) = (G_E^p + G_E^n) \int w(r) \{u(r) - w(r) / \sqrt{8}\} j_2\left(\frac{Qr}{2}\right) dr$$



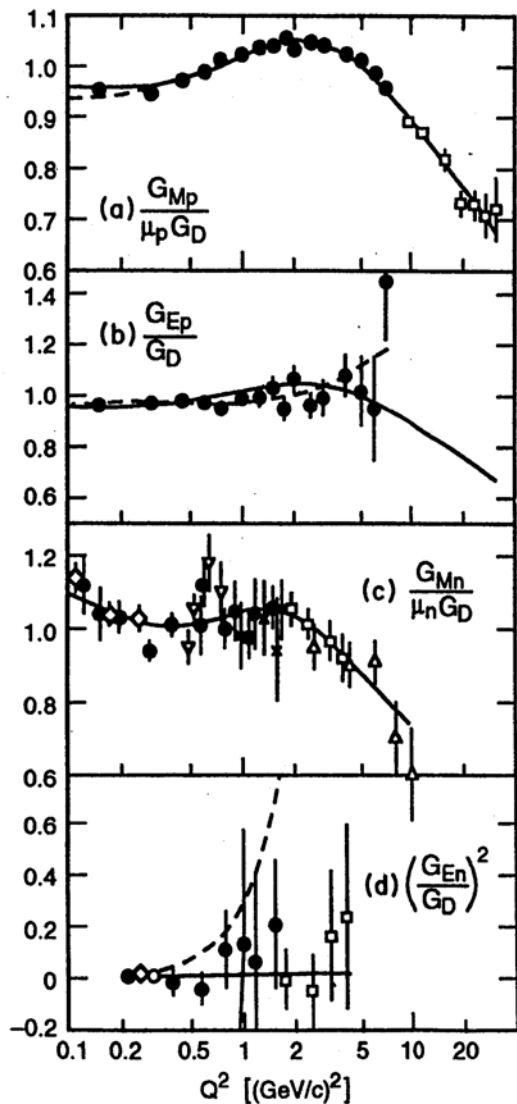
The Pre-JLab Era

- Stern (1932) measured the proton magnetic moment $\mu_p \sim 2.5 \mu_{\text{Dirac}}$ indicating that the proton was not a point-like particle
- Hofstadter (1950's) provided the first measurement of the proton's radius through elastic electron scattering
- Subsequent data (≤ 1993) were based on:
Rosenbluth separation for proton,
severely limiting the accuracy for G_E^p at $Q^2 > 1 \text{ GeV}^2$
- Early interpretation based on Vector-Meson Dominance
- Good description with phenomenological dipole form factor:

$$G_D = \left\{ \frac{\Lambda^2}{\Lambda^2 + Q^2} \right\}^2 \quad \text{with } \Lambda = 0.84 \text{ GeV}$$

corresponding to ρ (770 MeV) and ω (782 MeV) meson resonances in timelike region and to exponential distribution in coordinate space

Global Analysis



P. Bosted *et al.*
PRC 51, 409 (1995)

$$G_E^p = G_M^p = \left(1 + \sum_{i=1}^5 a_i Q^i\right);$$

$$G_M^n = \left(1 + \sum_{i=1}^4 b_i Q^i\right); G_E^n = 0$$

Three form factors very similar

G_E^n zero within errors \rightarrow accurate data on G_E^n early goal of JLab

First JLab G_E^p proposal rated B+!

Modern Era

Akhiezer et al., Sov. Phys. JETP 6 (1958) 588 and
Arnold, Carlson and Gross, PR C 23 (1981) 363
showed that:

accuracy of form-factor measurements can be significantly improved by
measuring an interference term $G_E G_M$ through the beam helicity
asymmetry with a polarized target or with recoil polarimetry

$$\frac{G_E^{n,p}}{G_M^{n,p}} = -\frac{P_t}{P_l} \frac{E_e + E_{e'}}{2M} \tan\left(\frac{\theta_e}{2}\right)$$

Had to wait over 30 years for development of

- Polarized beam with
high intensity ($\sim 100 \mu A$) and high polarization ($> 70\%$)
(strained GaAs, high-power diode/Ti-Sapphire lasers)
- Beam polarimeters with 1-3 % absolute accuracy
- Polarized targets with a high polarization or
- Ejectile polarimeters with large analyzing powers

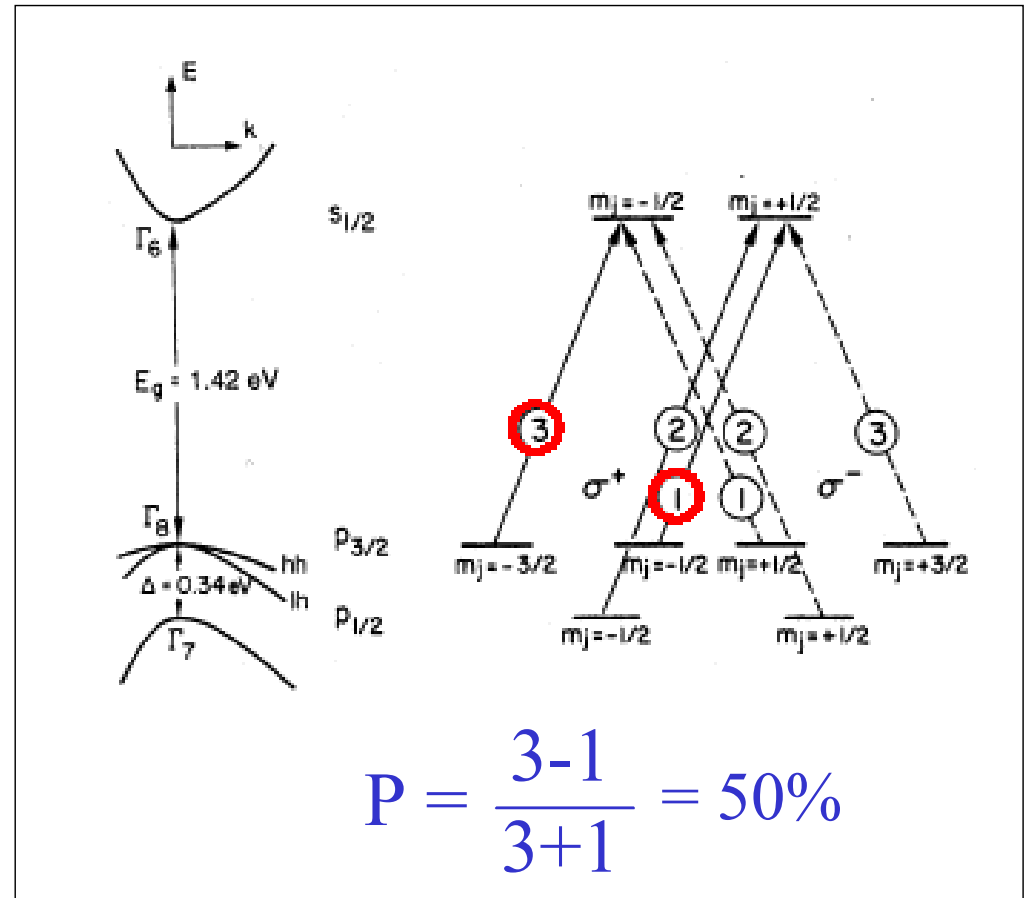
Instrumentation

- Polarized beam
- Beam polarimeters
 - Møller polarimeter
 - Compton polarimeter
- Polarized targets
 - Polarized hydrogen/deuterium target
 - Atomic beam source
 - Polarized helium-3 target
- Particle detection
- Recoil polarimeter



How to produce polarized electrons?

- Use thin layer of semiconductor (GaAs)
- Illuminate with high-intensity circularly polarized laser light
- Preferentially excite electrons of one helicity state to conduction band through optical pumping
- Extract electrons with ~100 kV potential
- Transport and bunch electrons to accelerator, while orienting the polarization vector

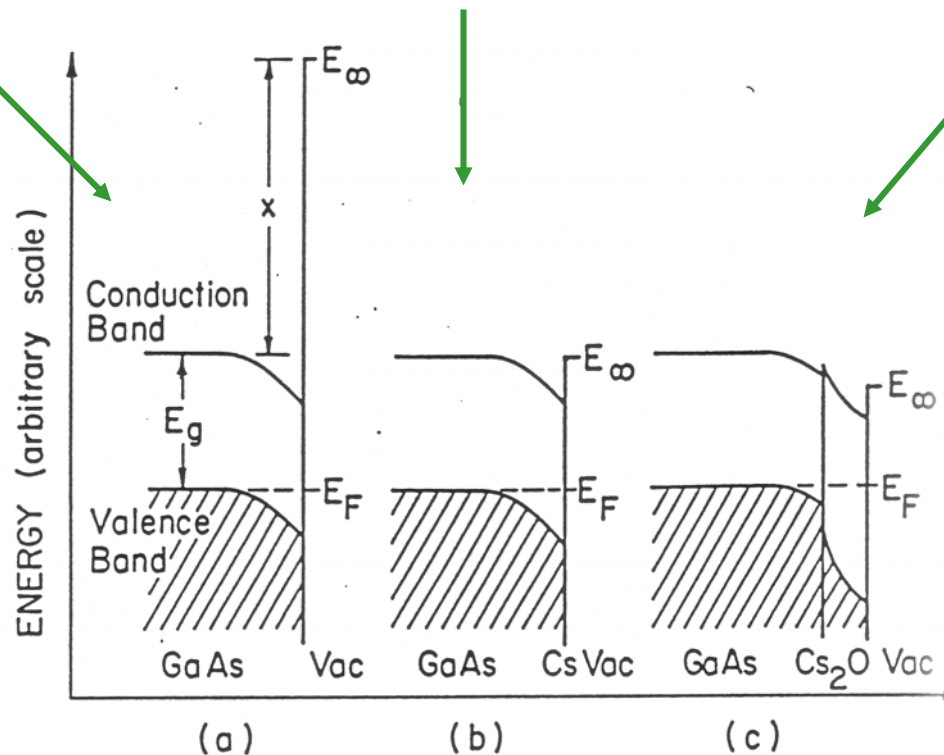


Photoemission from GaAs

Bare GaAs surface;
Big work function.
No electrons

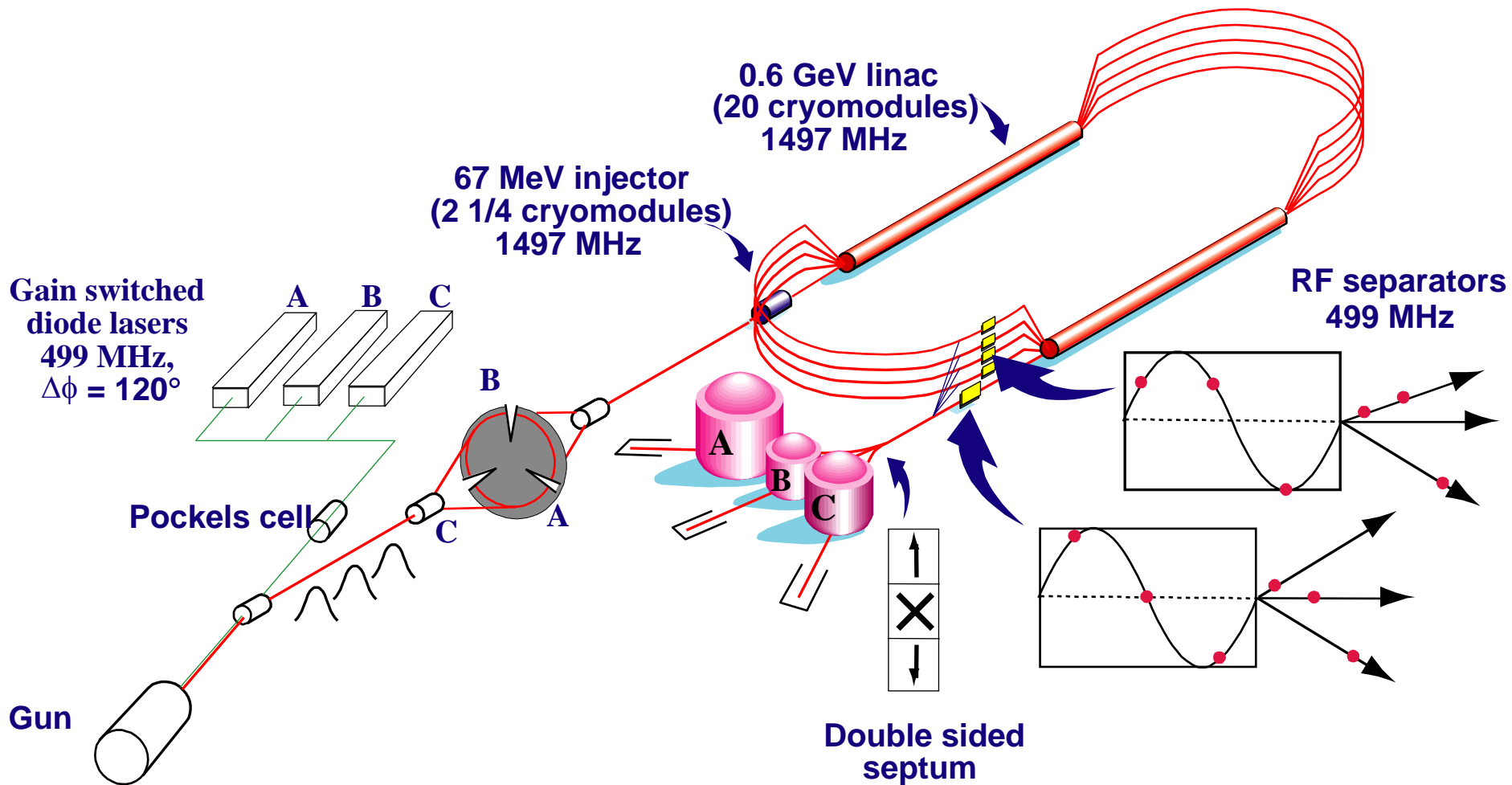
Cesium reduces
work function.
Some electrons

Cesium + Oxygen
"Negative Electron Affinity".
Many electrons

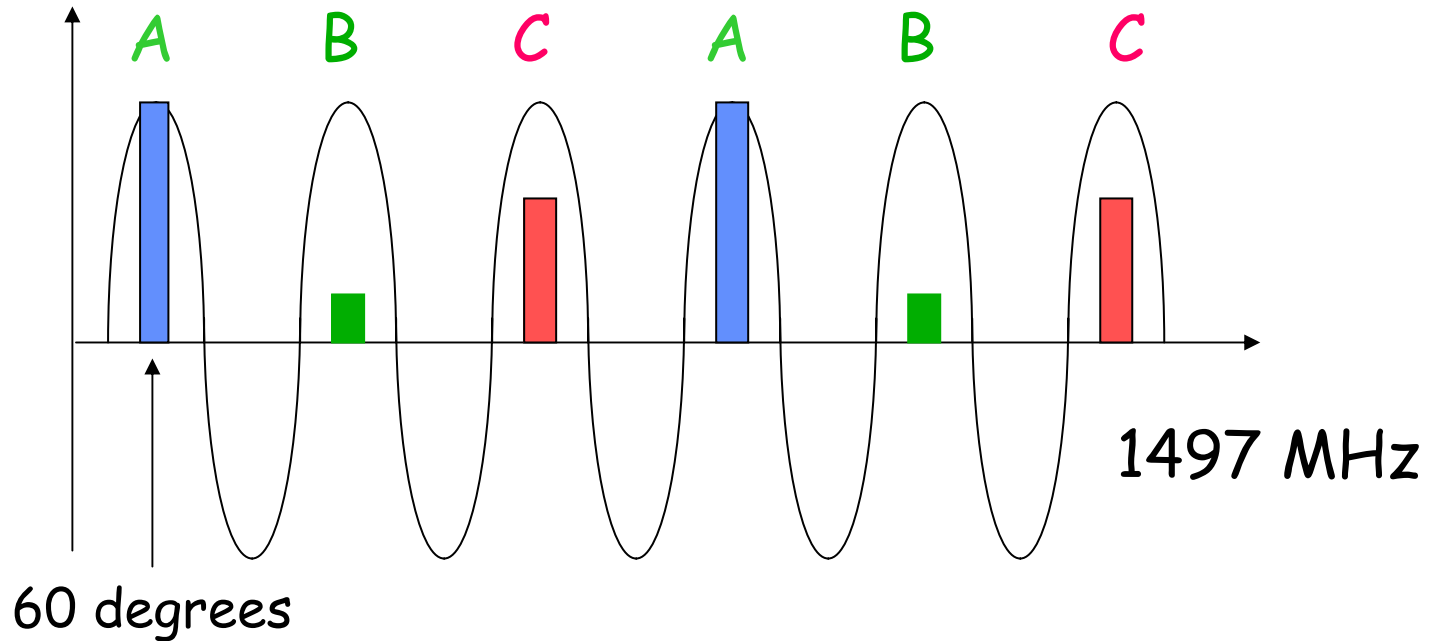


Quantum efficiency: Number of electrons extracted per laser photon

Continuous Electron Beam Accelerator Facility

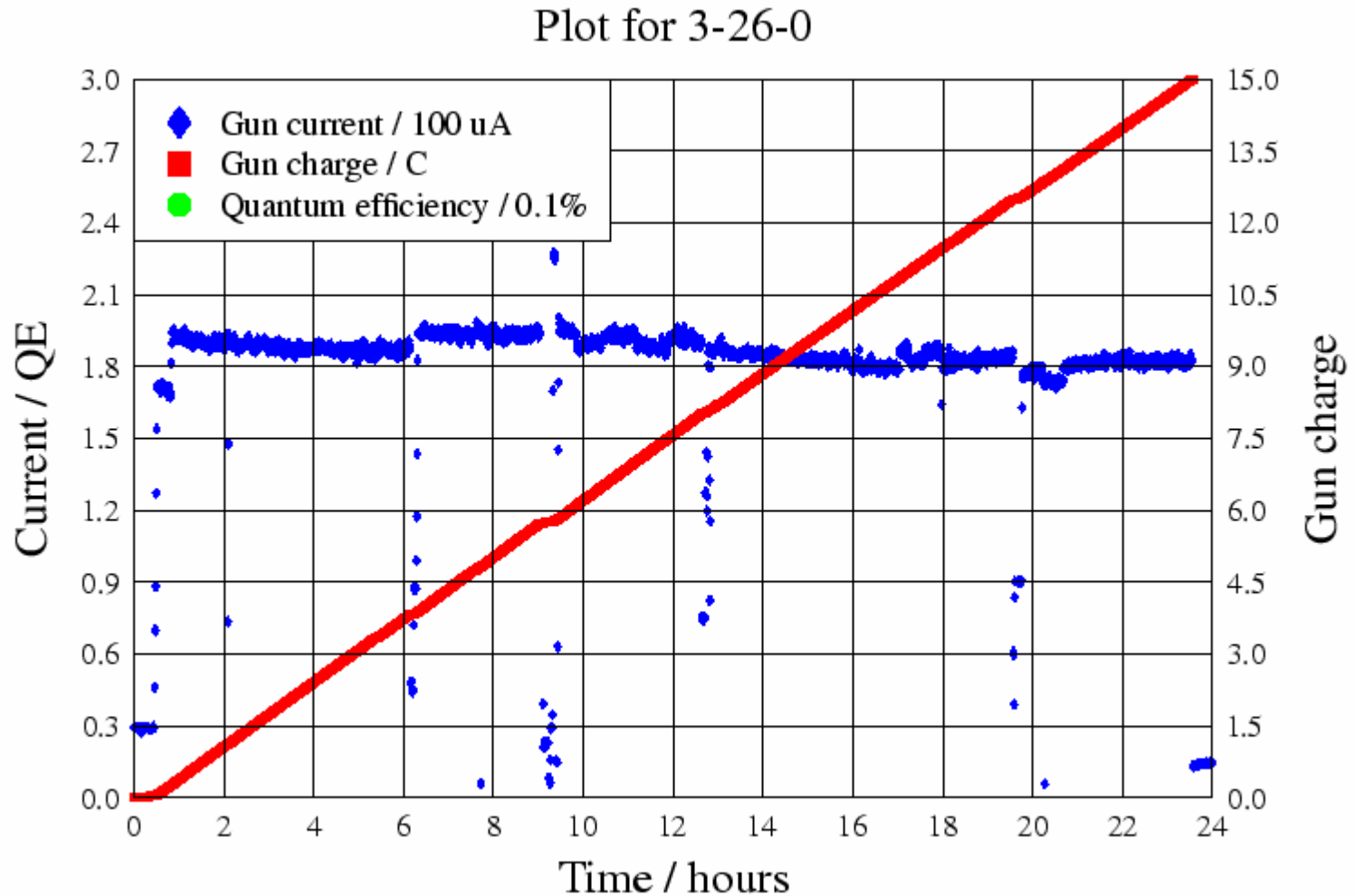


Synchronous Photoinjection



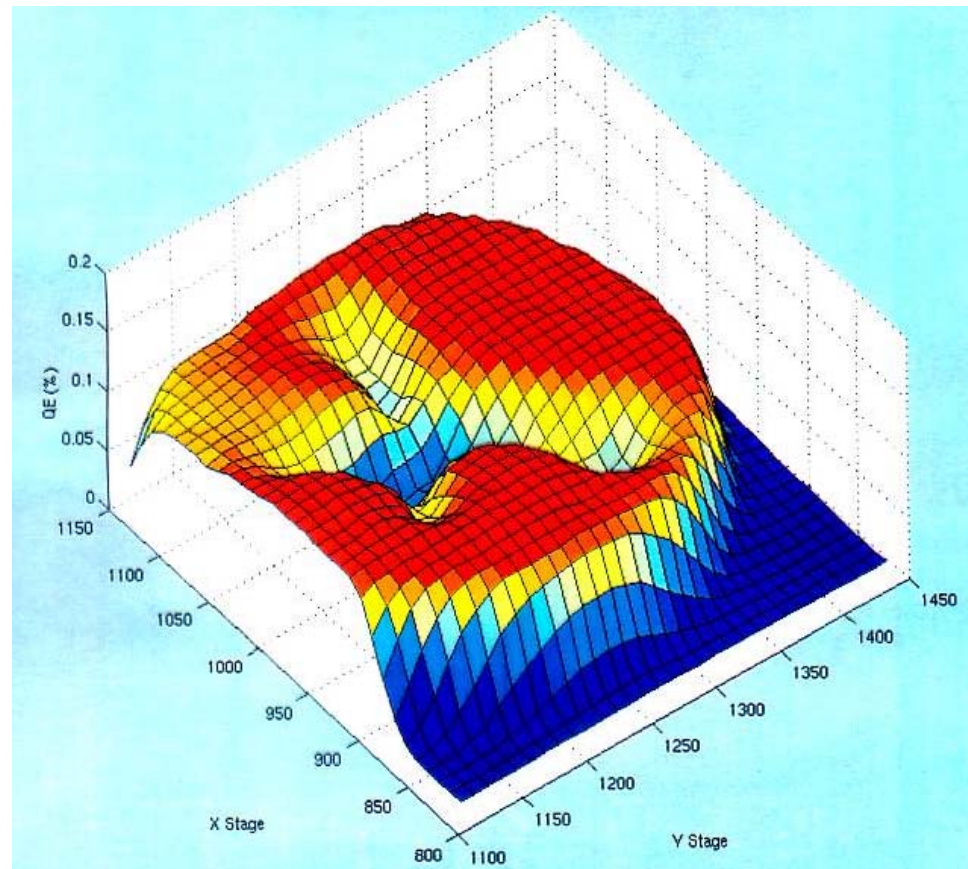
- Use pulsed light to extract electrons only when we need them.
- This prolongs operating lifetime of the gun.

A good day when...



Photocathode Lifetime

Vacuum not perfect. QE degrades via ion backbombardment



Gun Issues Today and Tomorrow

- Lifetime at High Current (vacuum issues)
- Adequate photocathode QE and polarization
- Adequate Laser Power with RF pulse structure
- Control of Helicity Correlated Systematics
- Beam handling (space charge induced emittance growth)



Møller Polarimeter

Basic principle (absolute accuracy 1-3 %)

- Scatter the polarized electron beam off polarized atomic electrons in a magnetized iron foil

Advantages:

- High analyzing power and small systematics at $\theta_{CM} = 90^\circ$
- Large cross section
- Two particles ion final states with appr. equal energy
 - Coincidence between incoming and scattered electron eliminates background

Disadvantages

- Invasive measurement
- Relatively low polarization $\sim 8\%$
- Beam current limited ($\sim 1 \mu A$) because of target heating
- Systematic errors on target polarization
- Kinematic distortion from scattering off K,L shell electrons (Levchuk effect)



Møller Polarimeter (cont.)

$\bar{e}^- + e^- \rightarrow e^- + e^-$ QED (Møller, 1932)

$$\frac{d\sigma}{d\Omega_{CM}} = \frac{d\sigma_0}{d\Omega_{CM}} \left(1 + \sum_{i=X,Y,Z} (A_{ii} P_{i \text{ arg } beam}^i) \right)$$

$$\frac{d\sigma_0}{d\Omega_{CM}} \approx \frac{r_e^2}{4\gamma^2} \frac{(4 - \sin^2 \theta_{CM})^2}{\sin^4 \theta_{CM}}$$

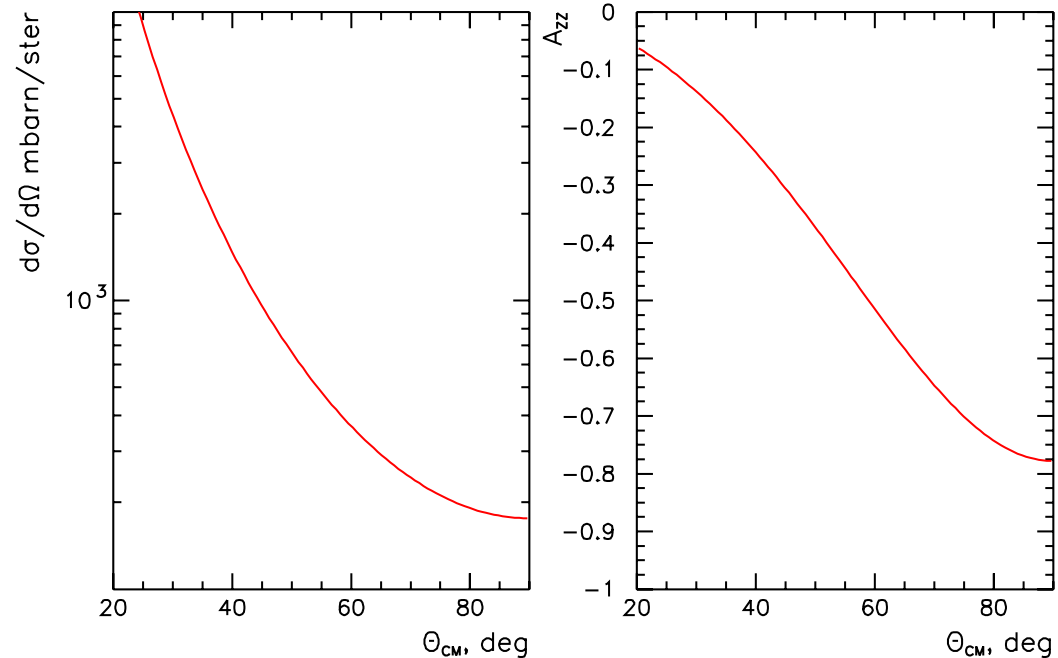
$$\left. \frac{d\sigma_0}{d\Omega_{CM}} \right|_{\theta_{CM} = 90^\circ} \approx 176 \text{ mb/sr in LAB}$$

Asymmetry:

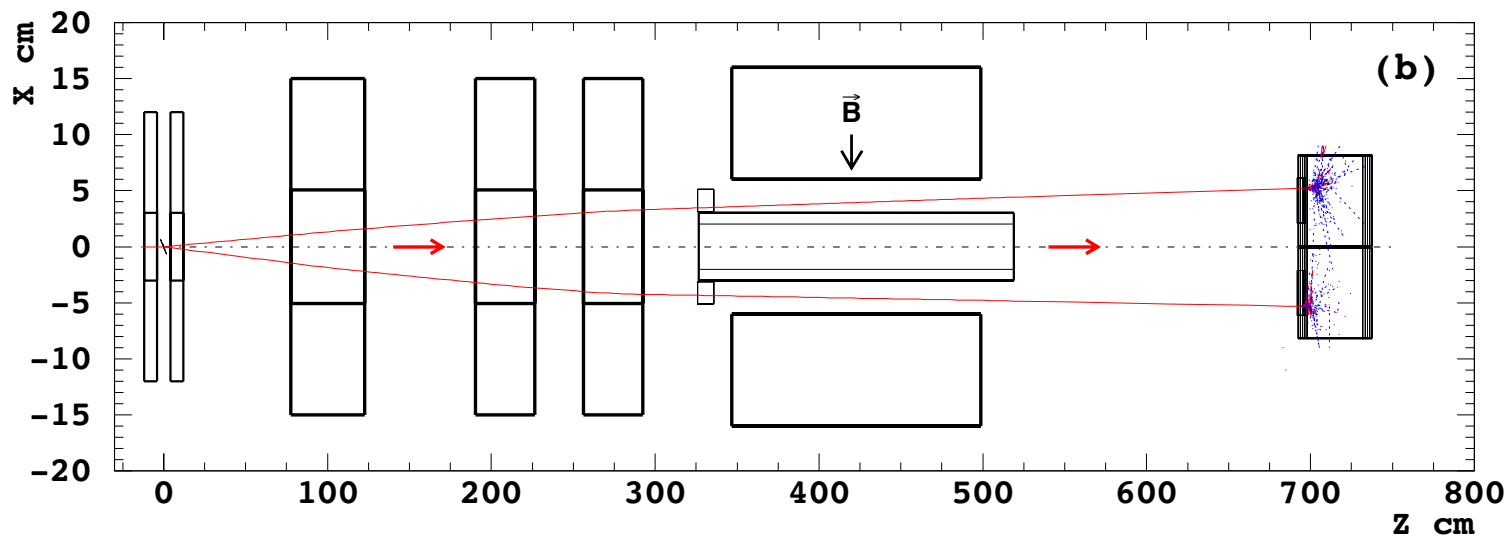
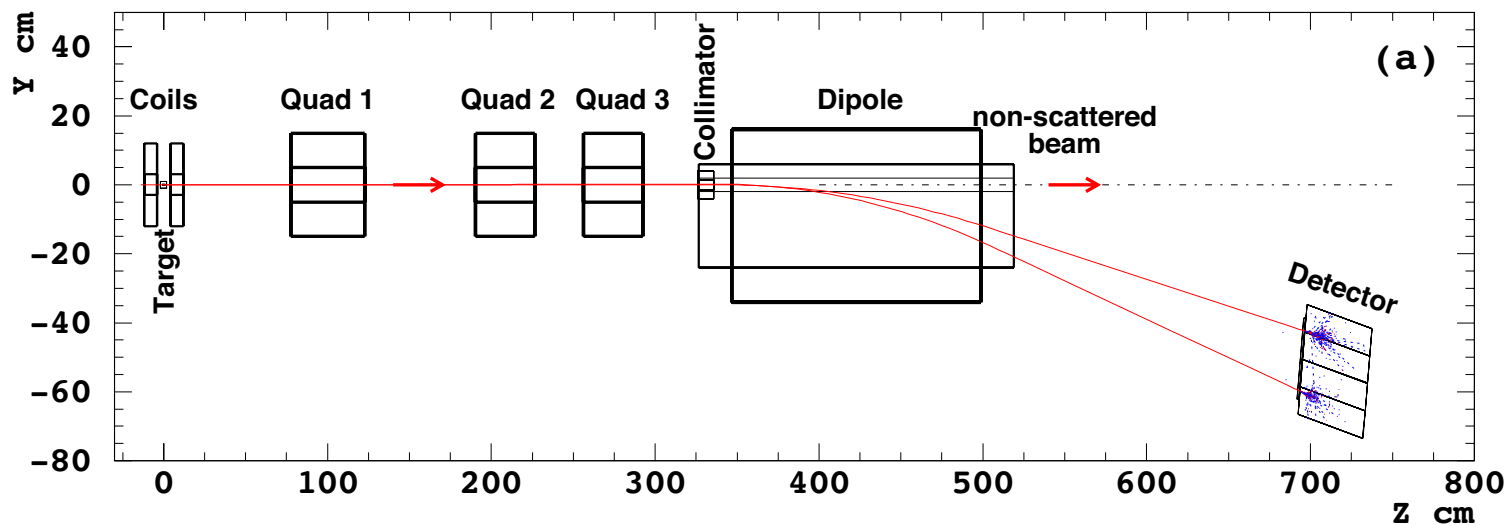
$$A_{ZZ} = -\frac{\sin^2 \theta_{CM} (7 + \cos^2 \theta_{CM})}{(3 + \cos^2 \theta_{CM})^2}$$

$$A_{XX} = -\frac{\sin^4 \theta_{CM}}{(3 + \cos^2 \theta_{CM})^2} \quad A_{YY} = -A_{XX}$$

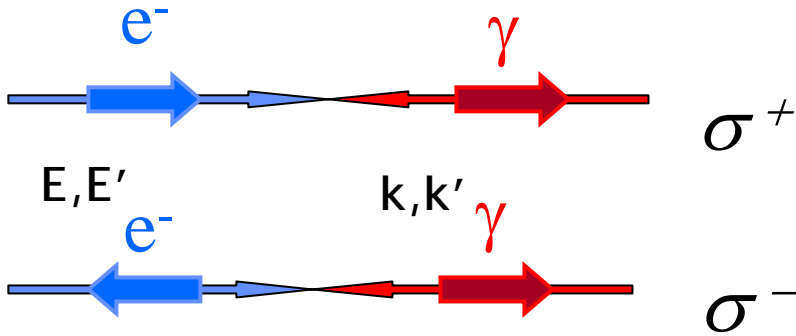
$$\text{At } \theta_{CM} = 90^\circ \quad A_{ZZ} = 7/9 \quad A_{YY} = -A_{XX} = 1/9$$



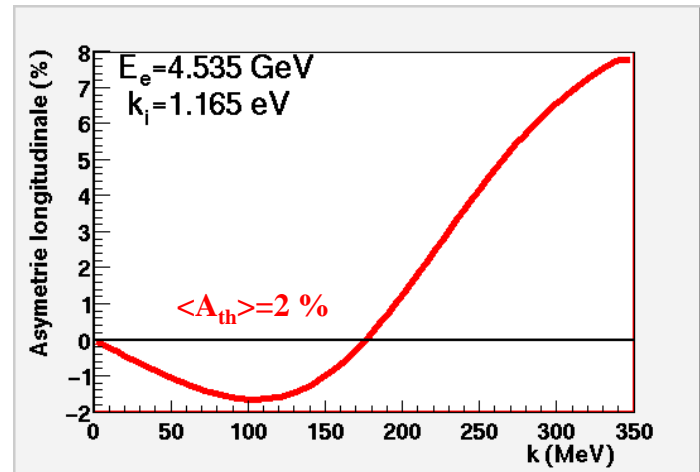
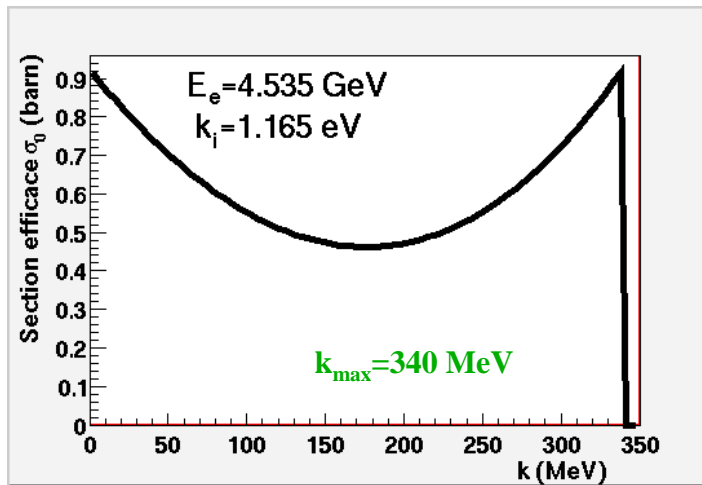
Møller Polarimeter (cont.)



Compton Polarimetry



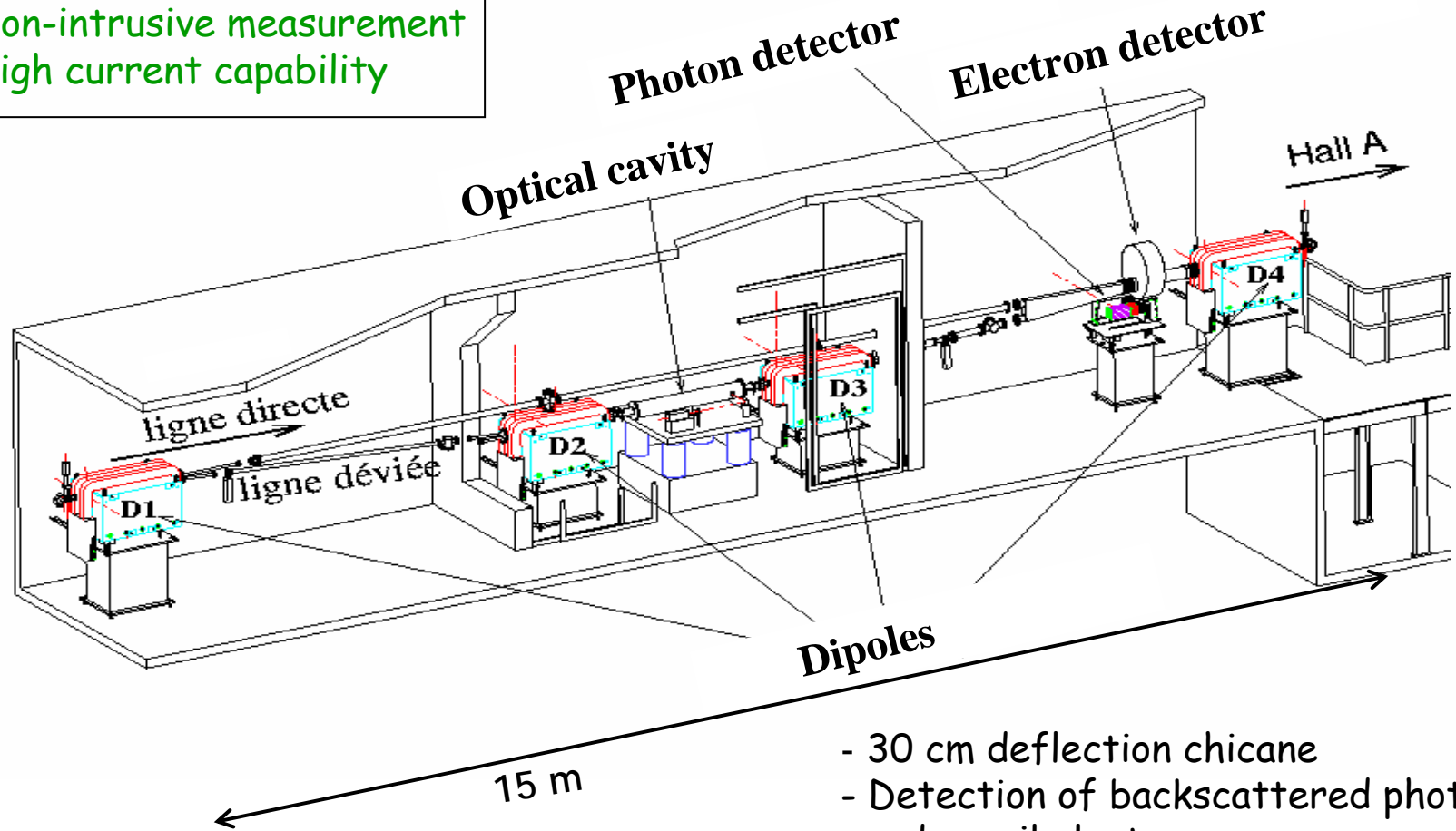
$$A_{\text{exp}} = \frac{n^+ - n^-}{n^+ + n^-} = P_\gamma \times P_e \times \langle A_{\text{th}} \rangle$$



- Figure-of-Merit $\sim \sigma \times A^2 \sim k^2 \times E^2$
- Differential Measurements yield higher $\langle A \rangle$
- Absolute accuracy 0.5 - 1.5%

Hall A Compton Polarimeter

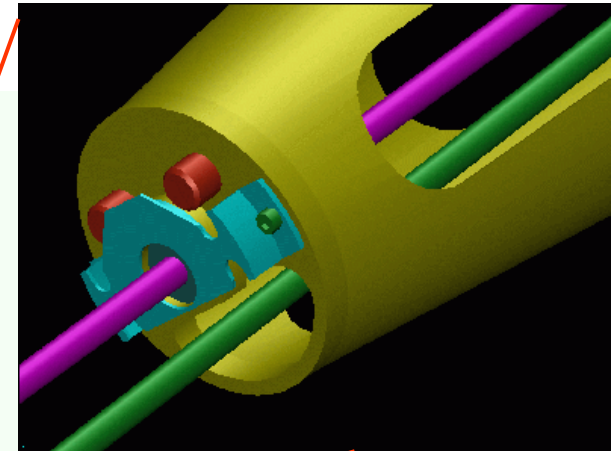
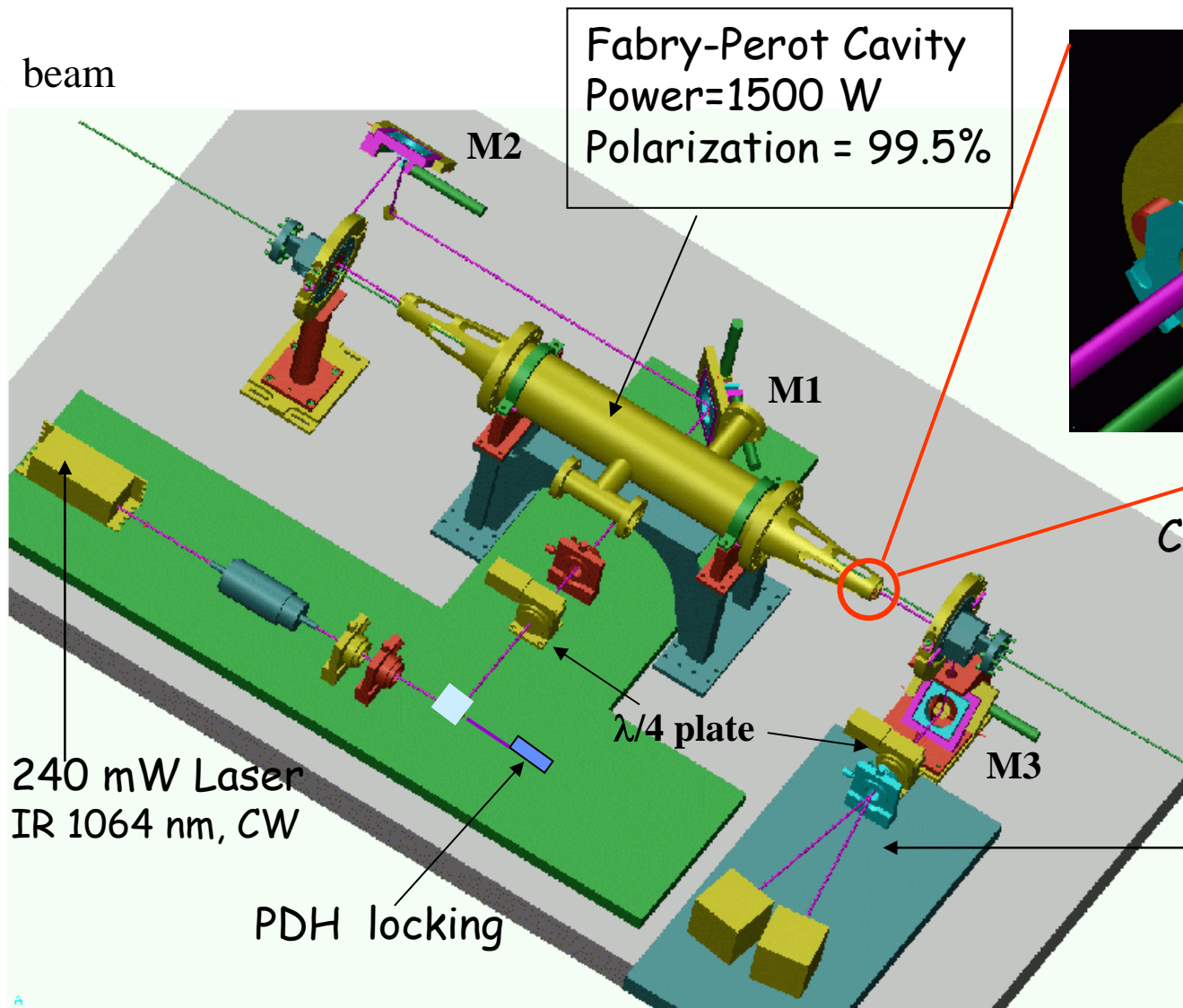
Non-intrusive measurement
High current capability



- 30 cm deflection chicane
- Detection of backscattered photons and recoil electrons

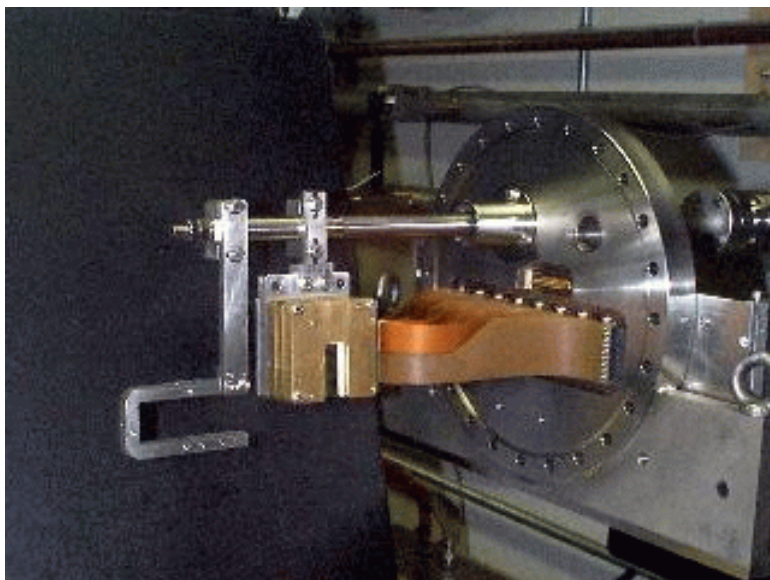
Optical setup

e beam



Crossing angle: 23 mrad

Electron detector



4 planes of 48 silicon strips

- Width : 650 mm
- Energy range for 1 strip:
~ 0.13% of E_{beam}

e- detector

4th dipole

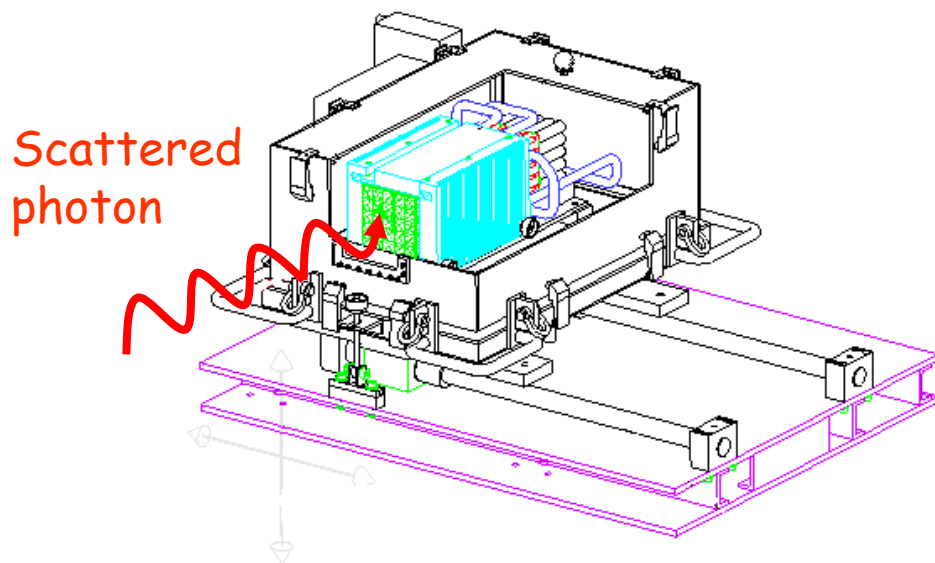
3-7 mm gap

3rd dipole

PbWO4

γ detector

Photon calorimeter



5x5 PbWO_4 scintillators ($2 \times 2 \times 23 \text{ cm}^3$)

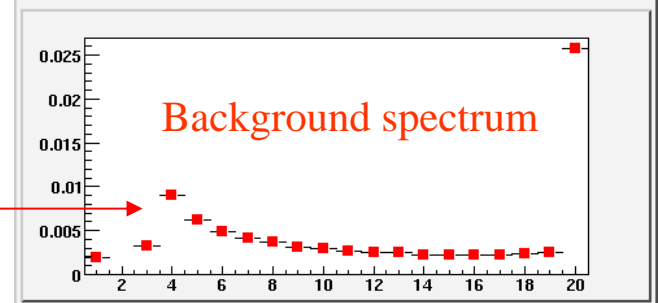
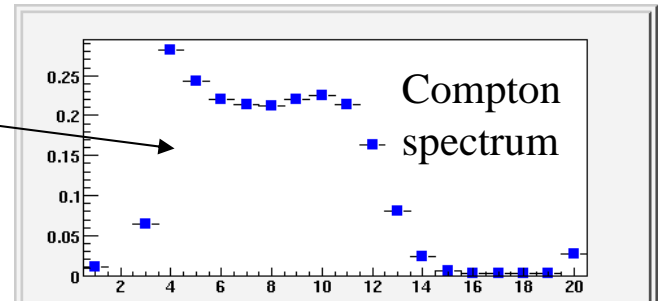
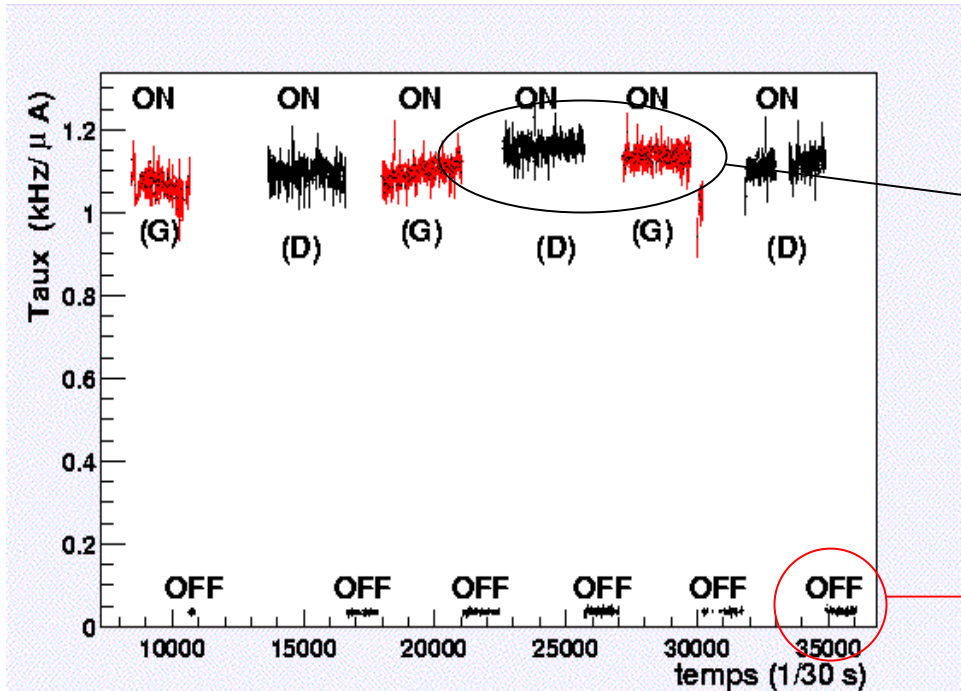
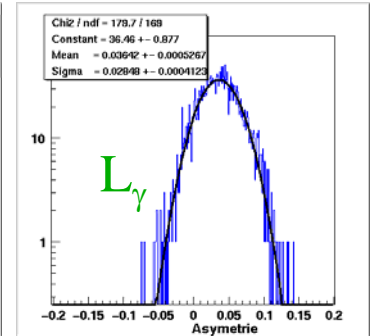
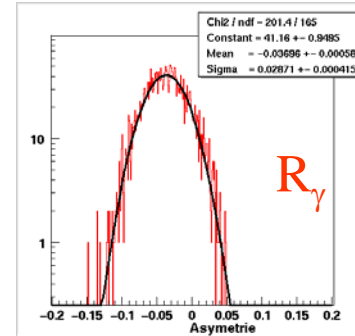
- *Fast response*
- *Compact ($\chi_0 = 0.85 \text{ cm}$, $R_M = 2.2 \text{ cm}$)*
- *Radiation hard*



Typically, only the central crystal of the 5 x 5 matrix is used

Data taking

- 30 Hz Electron helicity flip
- 3 min Laser polarization cycle
Right-off-Left-off
- Signal-to-background > 10 (typ.)



Summary and Future Plans

- Compton polarimetry provides non-intrusive high accuracy beam polarization measurements
- High Gain Fabry-Perot cavity offers superior signal-to-background ratio and better control over systematic errors
- Present 1064 nm IR laser is adequate down to 3 GeV

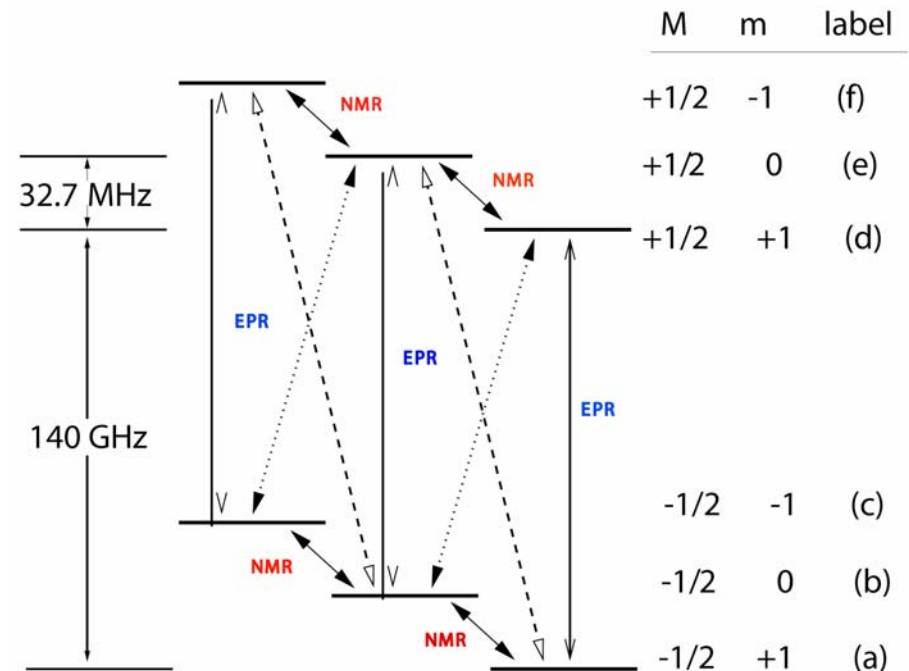
Future plans to improve accuracy down to 1 GeV:

- ▲ 532 nm green laser
- ▲ 200 μm pitch electron detector
- ▲ High light-yield calorimeter

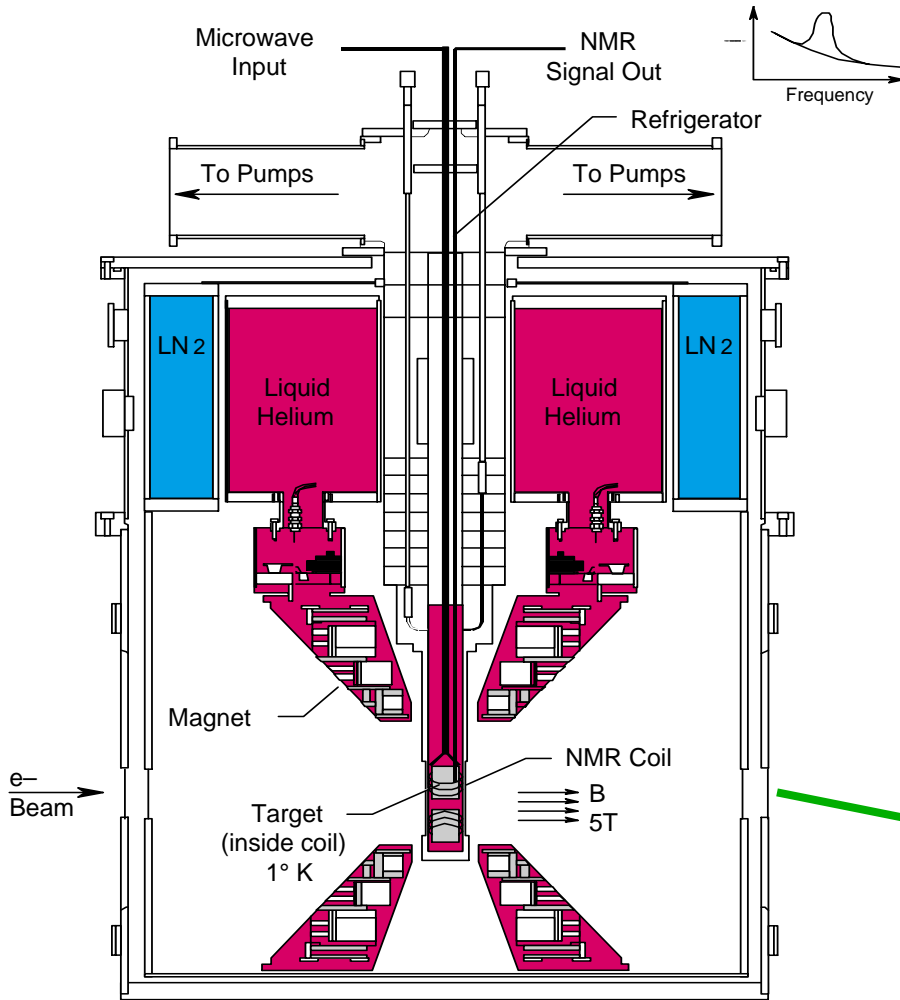


Dynamically Nuclear Polarized ND₃ Target

- ▲ Frozen (doped) ¹⁵ND₃
- ▲ ⁴He evaporation refrigerator
- ▲ 5 T polarizing field
- ▲ Remotely movable insert
- ▲ Dynamic nuclear polarization:
 - Doping with free radicals by radiation damage
 - In ~5 T field at ~1 K free electrons in radicals are polarized to ~99%
 - Induce transitions to preferred nuclear spin orientation by RF field
 - Electrons relax much quicker than nuclei, resulting in ~80% polarization for deuterons and ~30% for protons

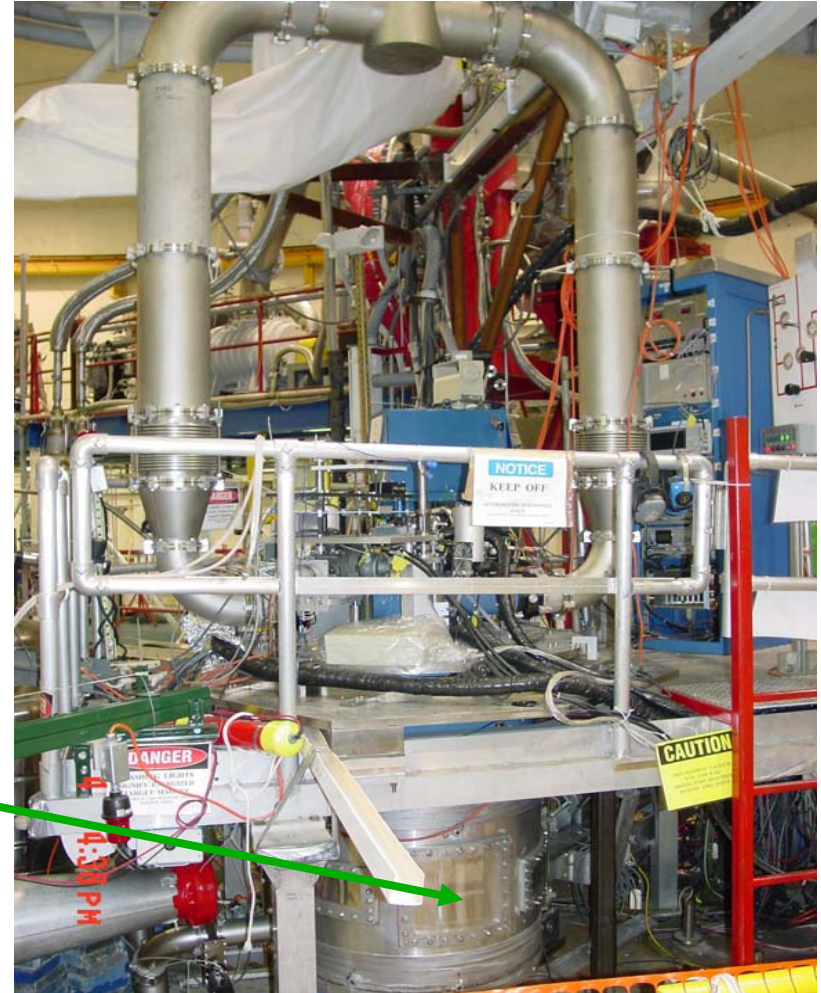


Dynamically Nuclear Polarized ND_3 Target



4-94

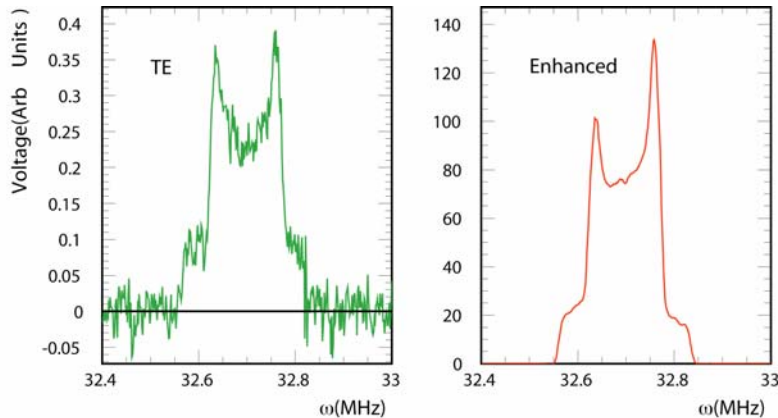
7656A1



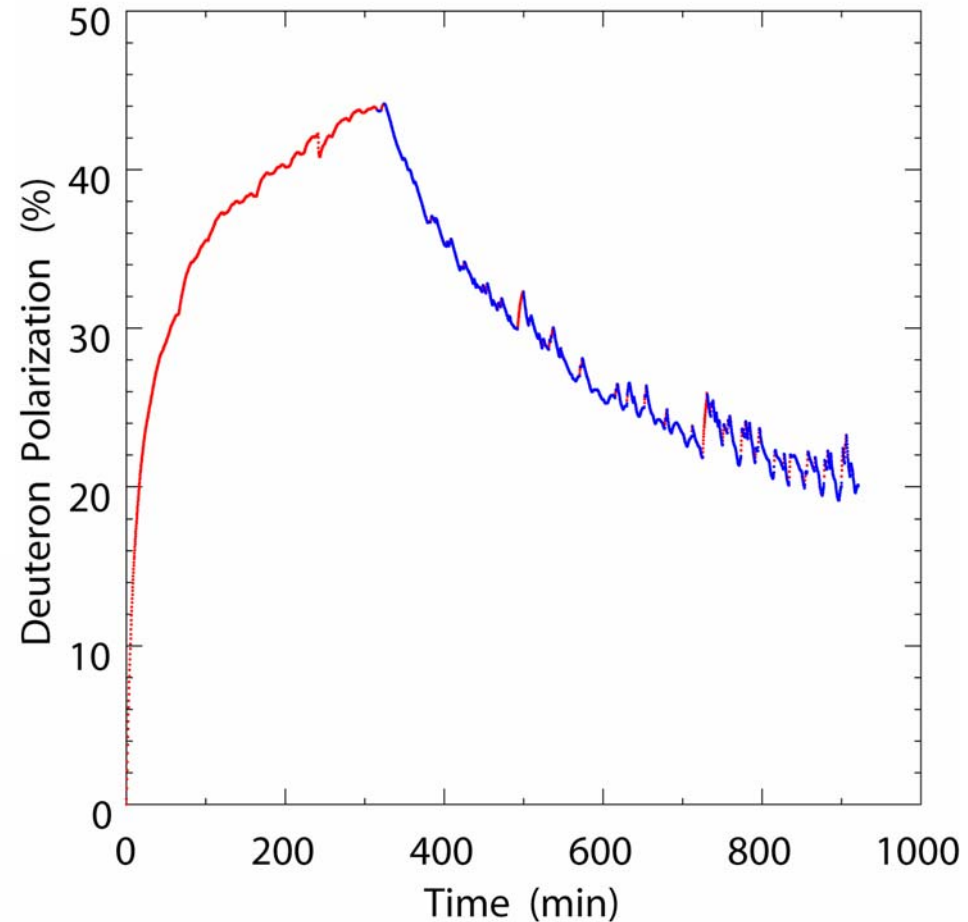
NMR polarimetry

- Sweep RF frequency
- Measure absorptive part of response
- Polarization proportional to signal

$$P_{TE} = \frac{4 \tanh(\mu B / 2kT)}{3 + \tanh^2(\mu B / 2kT)} \approx 0.07\%$$



GEn Target Performance 10 Sep 01



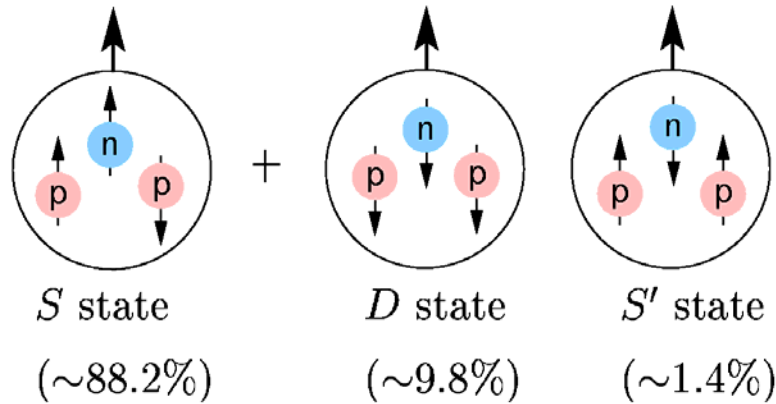
Average Polarization 25%

Polarized ^3He Target

- Polarized ^3He is best approximation of polarized neutron $P_n=87\%$ and $P_p=2.7\%$
- Requires corrections for nuclear medium, investigated by many theorists
- Basic principle:
 - Optical pumping of Rb, followed by polarization transfer to ^3He through spin-exchange collisions
- Target polarization measured by EPR/NMR
- ▲ New technologies and their probable impact
 - Hybrid alkali spin-exchange optical pumping
 - Progress with laser technology
 - Sol-gel coatings and cell production



Polarized ^3He as an effective polarized neutron



Effective nucleon polarizations:

$$P_n = 86\%, P_p = -2.8\%$$

$$\boxed{^3\vec{\text{He}} \approx \vec{n}}$$

Effective
Neutron
Target

Polarized ^3He as an effective polarized neutron

CONVOLUTION APPROACH

C. degli Atti et.al., *Phys.Rev.* **C48**, 968(1993); *Phys. Lett.* **B404**, 223(1997)

- ^3He consists S, S', D
- Three body calculation using Fadeev wavefunction

$$\tilde{g}_1^n = \frac{1}{\rho_n} (g_1^{^3\text{He}} - 2\rho_p g_1^p)$$
$$\tilde{A}_1^n = \frac{W_1^{^3\text{He}}}{W_1^n} \frac{1}{\rho_n} (A_1^{^3\text{He}} - 2 \frac{W_1^p}{W_1^{^3\text{He}}} \rho_p A_1^p)$$

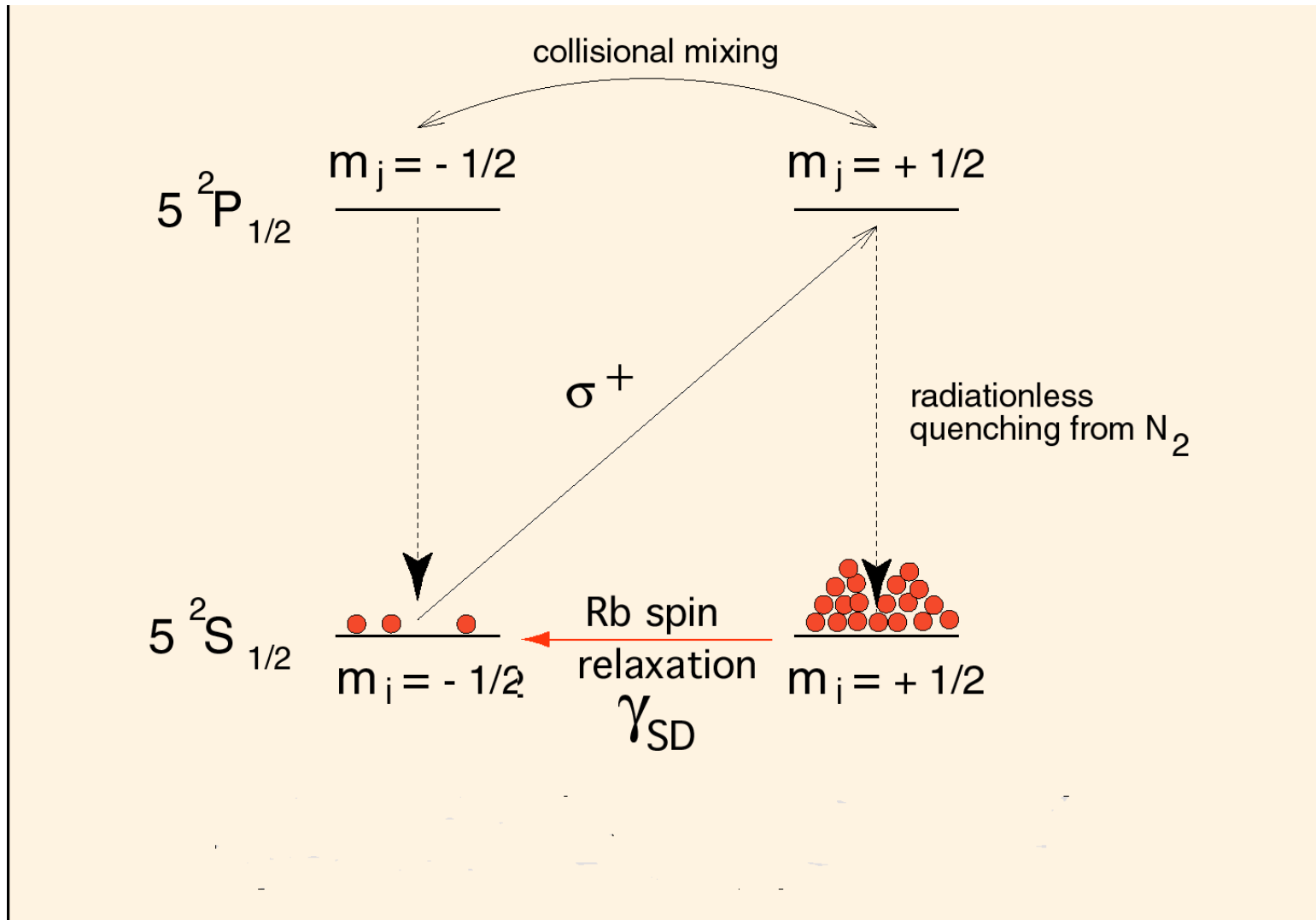
COMPLETE ANALYSIS

F. Bissey et. al., [hep-ph/0109069](https://arxiv.org/abs/hep-ph/0109069)

- S, S', D, Δ isobar in ^3He wavefunction

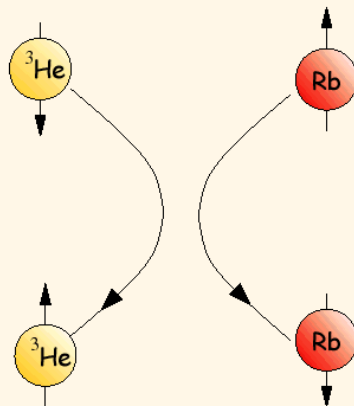
$$A_1^n = \frac{F_2^{^3\text{He}}}{P_n F_2^n (1 + \frac{0.056}{P_n})} [A_1^{^3\text{He}} - 2 \frac{F_2^p}{F_2^{^3\text{He}}} P_p A_1^p (1 - \frac{0.014}{2P_p})]$$

Optical pumping in Rb

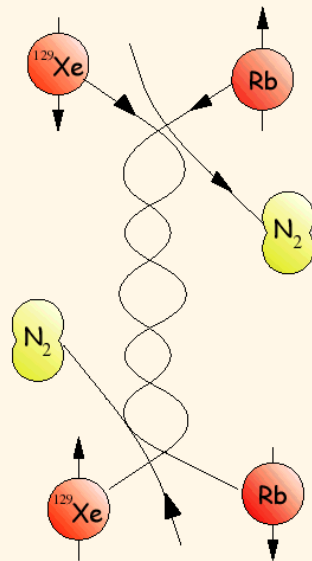


Alkali-metal/noble gas spin exchange

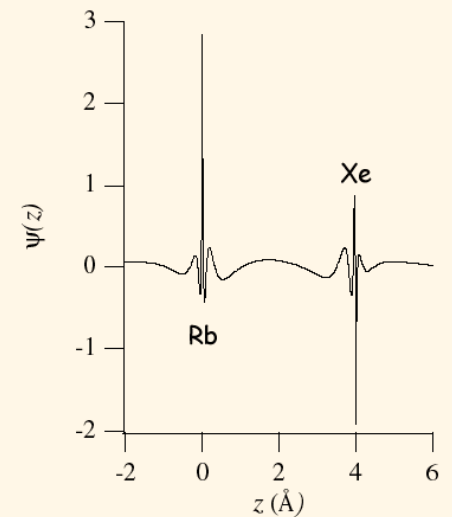
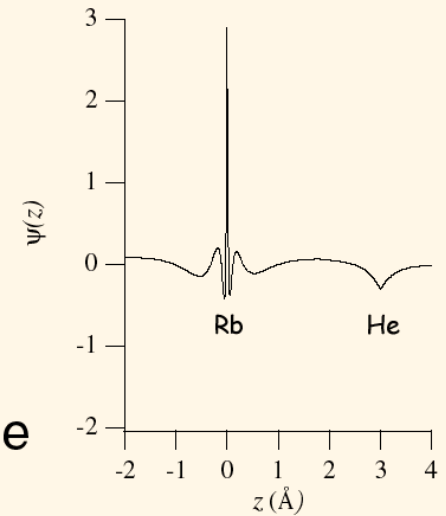
Binary collisions



van der Waals molecules



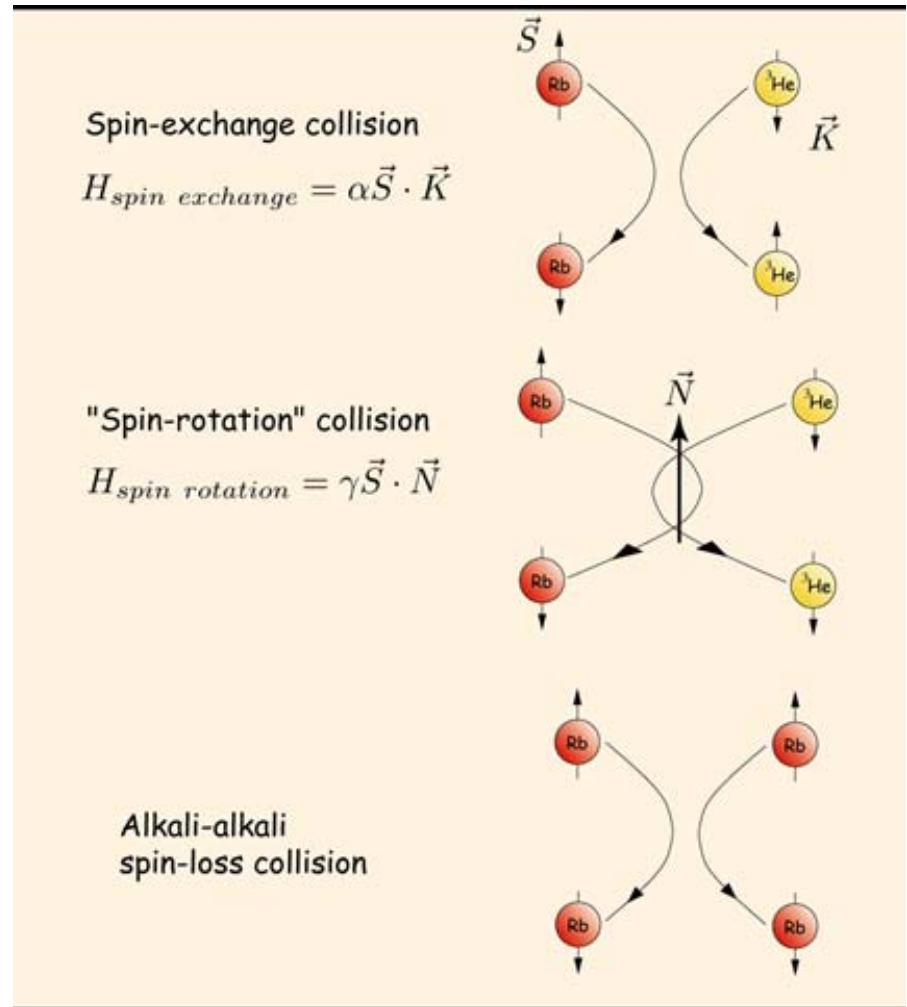
Spin-exchange occurs due to hyperfine interactions.



Spin-exchange efficiency

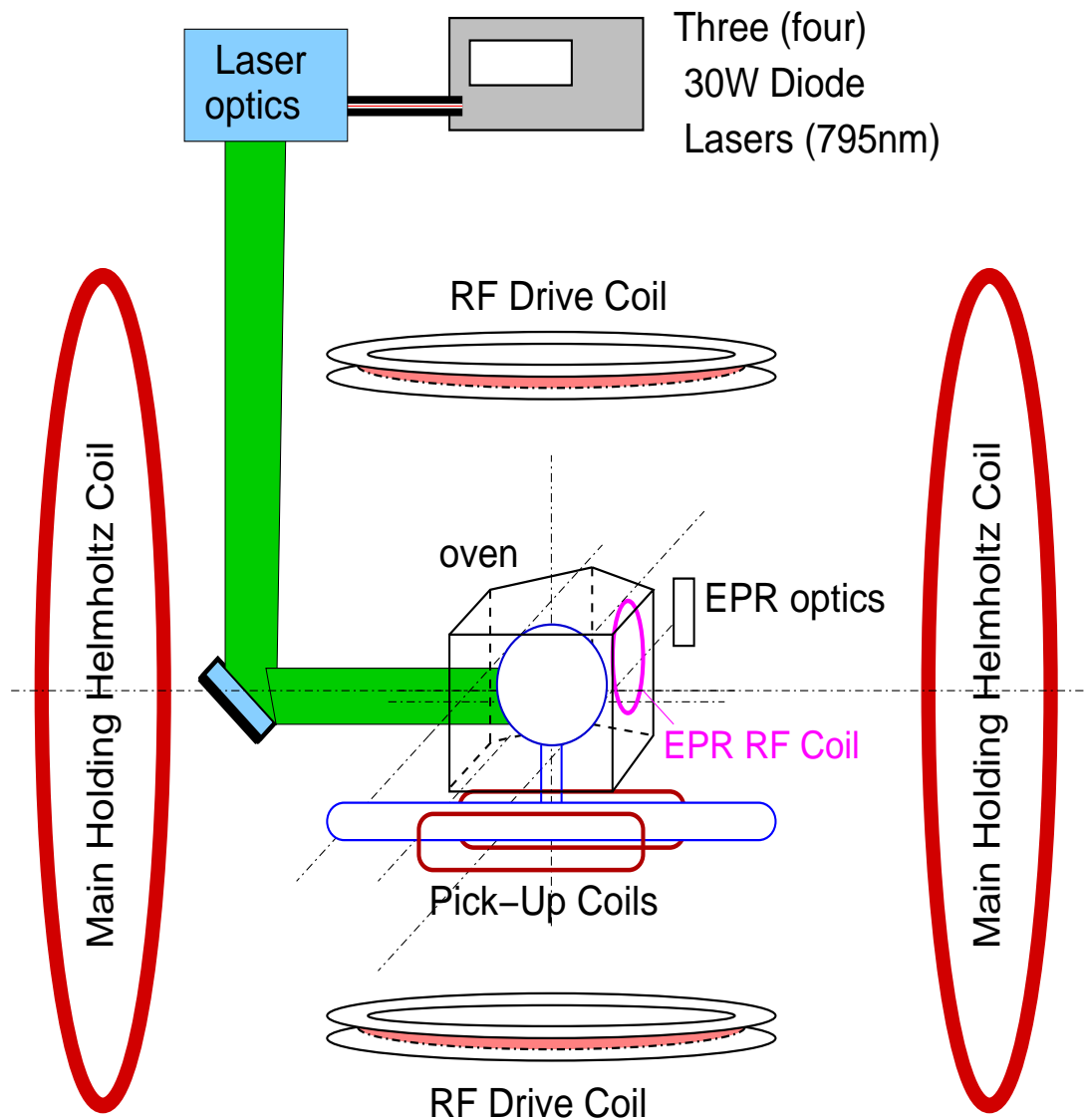
How many polarized alkali-metal atoms does it take to polarize a ^3He nucleus?

It depends on how much angular momentum goes into spin exchange and how much is lost into other processes.

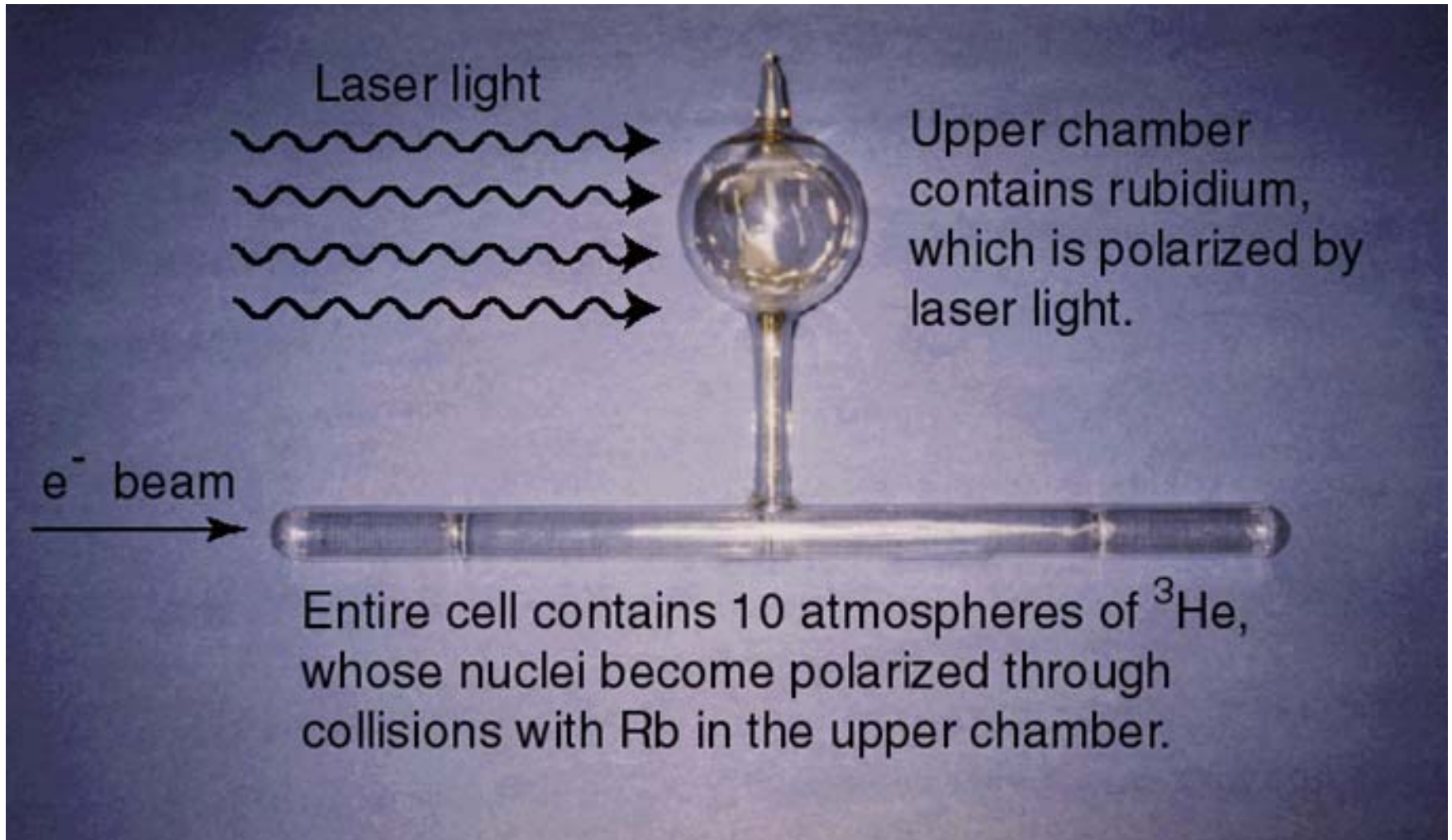


$$\eta_{SE} = \frac{\text{angular momentum lost by spin exchange}}{\text{angular momentum lost by all processes}}$$

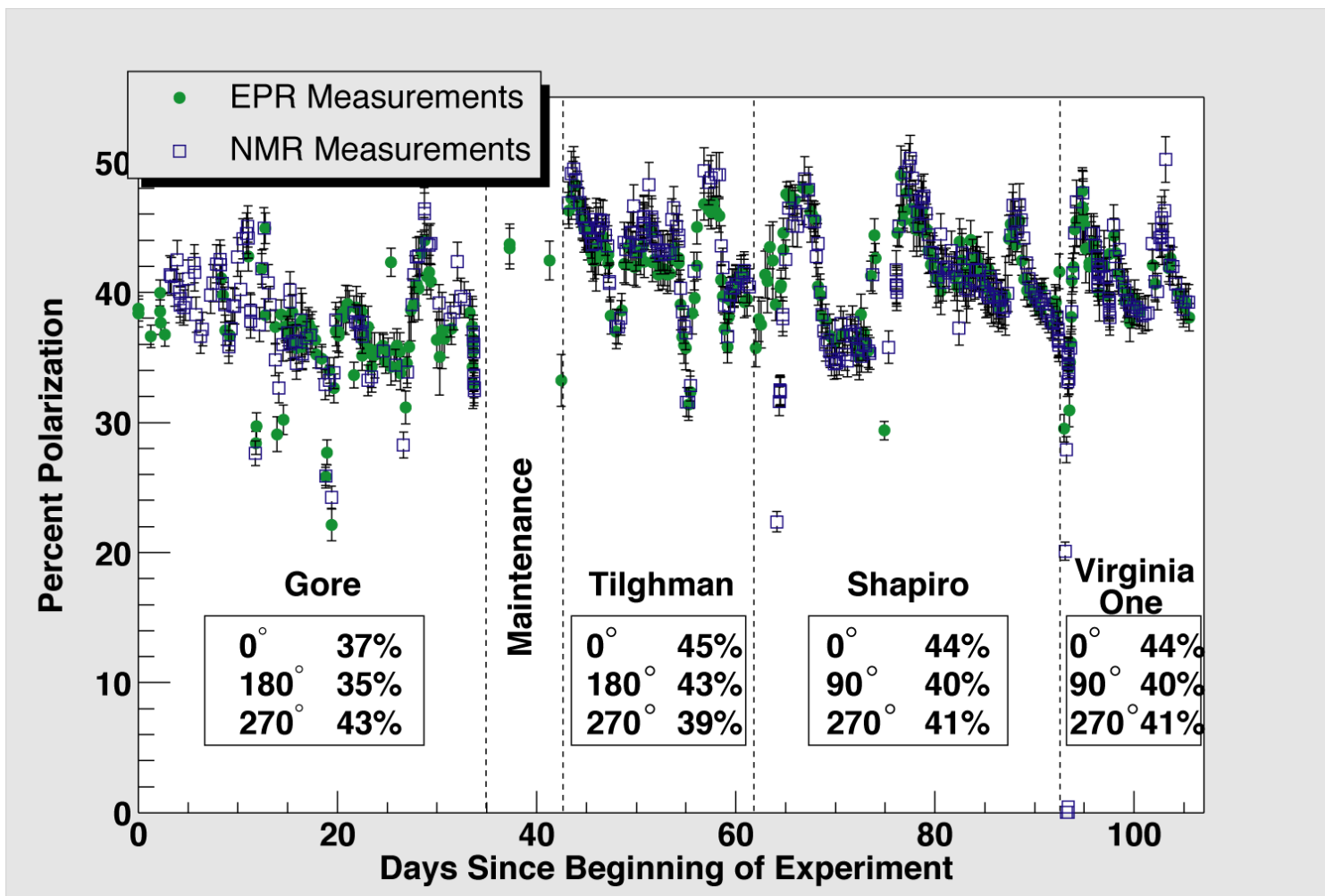
Schematic of JLab polarized ^3He target



JLab target cell

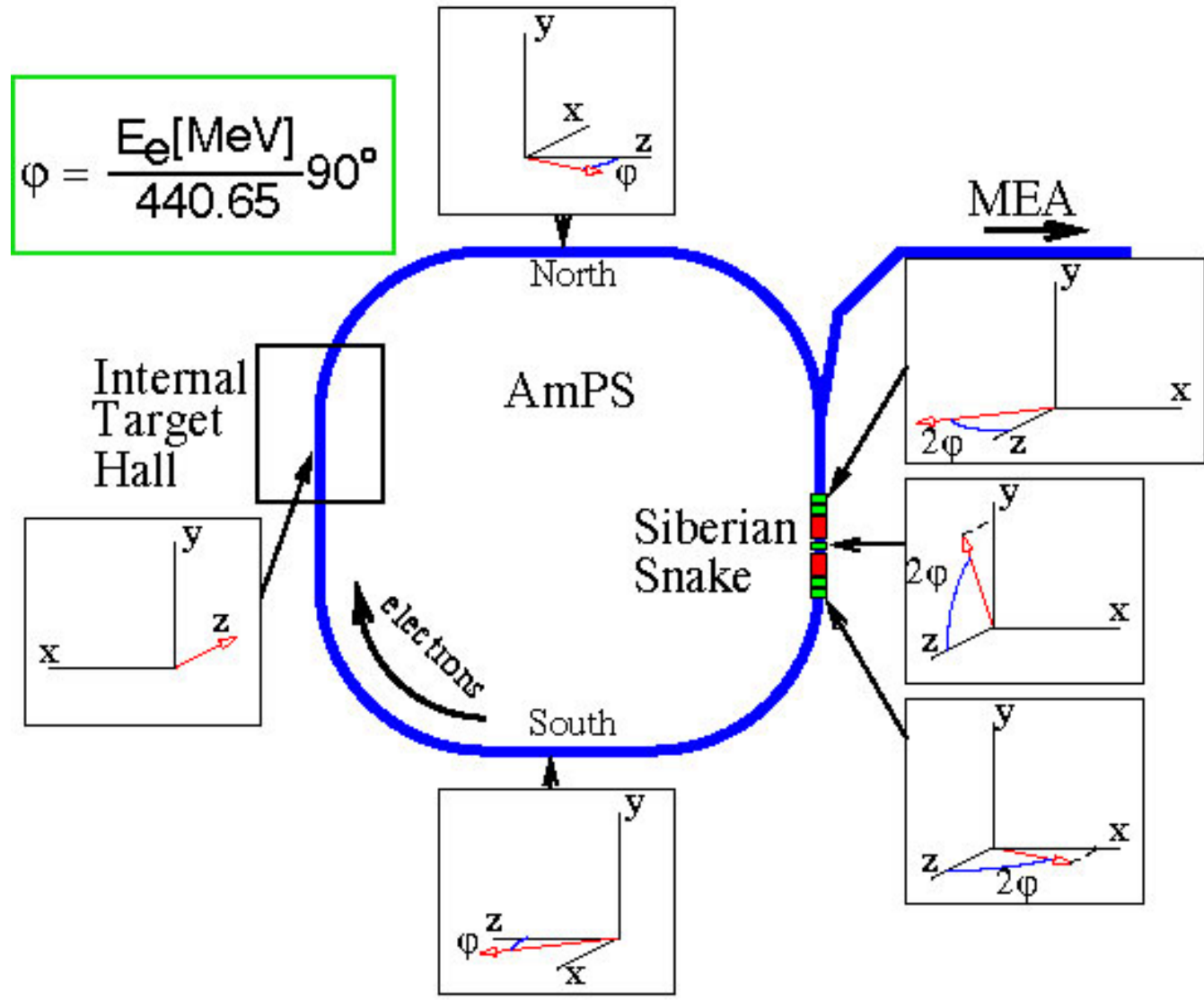


^3He target polarization during E99-117 and E97-103



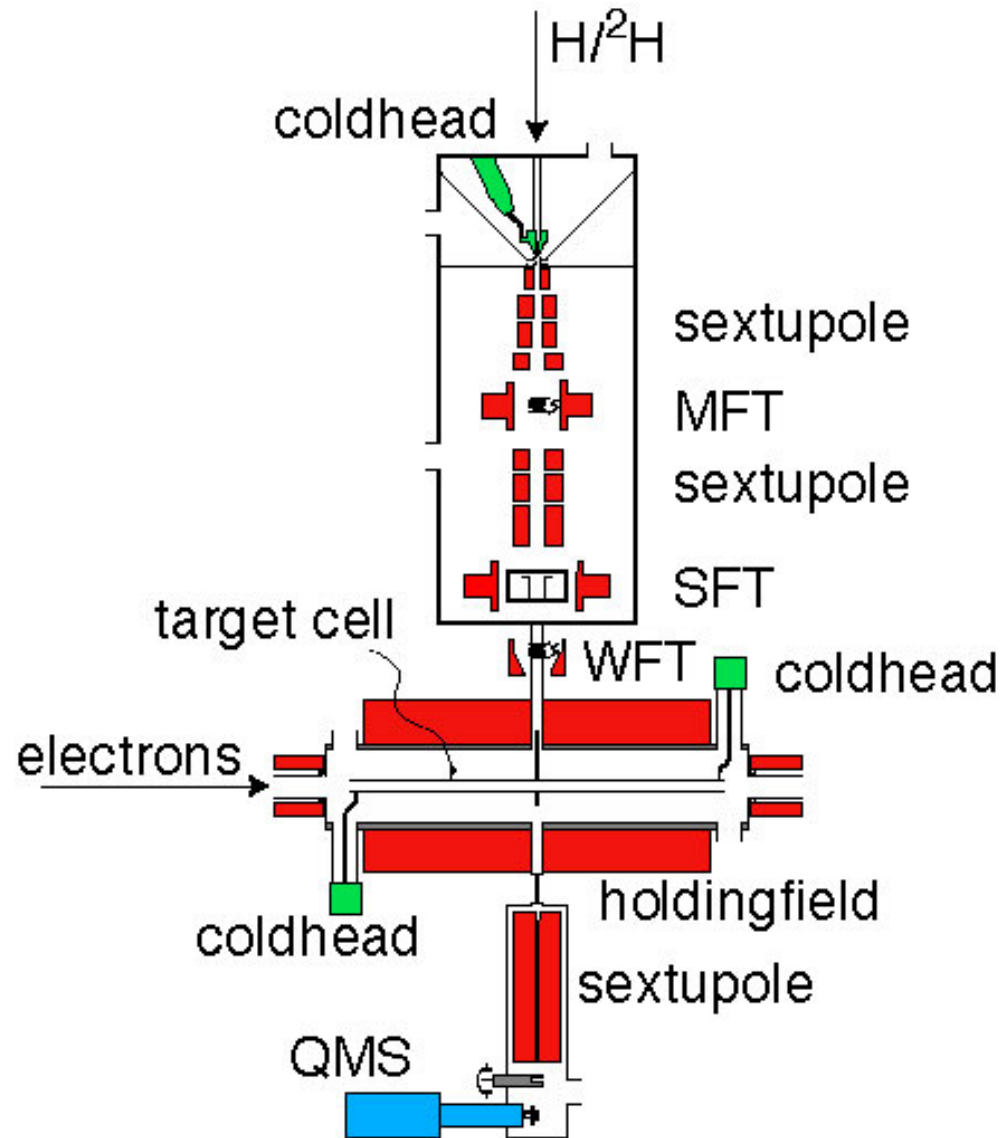
Storage Ring

- Couple storage ring to accelerator
- Inject polarized beam with such a polarization direction that it will be **longitudinal** at the internal target location
- Use **Siberian Snake** 180° from target to flip beam polarization
- Stored currents can be in excess of **100 mA**



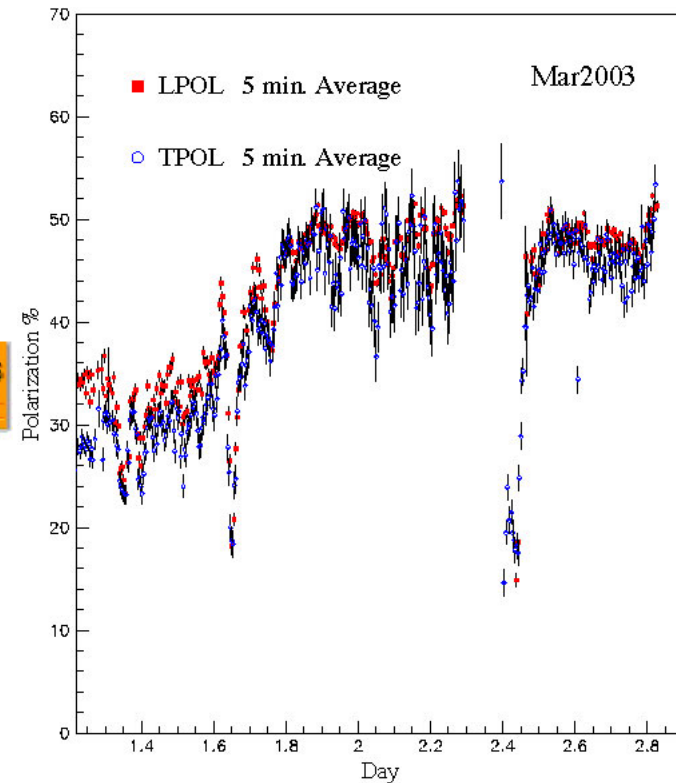
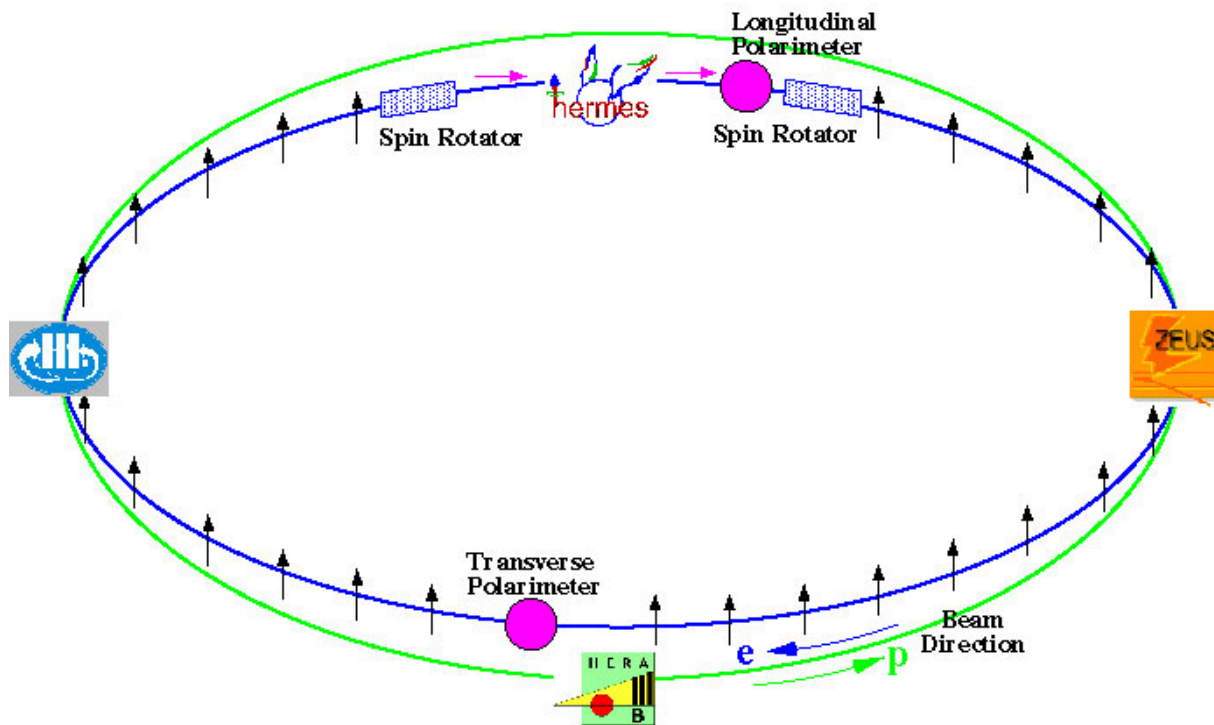
Polarized Internal Targets

- Produce atomic beam of hydrogen or deuterium with **dissociator** and cooled nozzle
- Separate atoms with different electron spin direction through **Stern-Gerlach** technique
- Induce transitions between different hyperfine states with RF units to obtain **nuclear polarization**
- Feed polarized atomic beam into **open-ended storage cell**, coated to minimize recombination
- Need **magnetic field** to orient polarization vector
- Result is target thickness of $2 \cdot 10^{14}$ nuclei/cm² at ~80% polarization

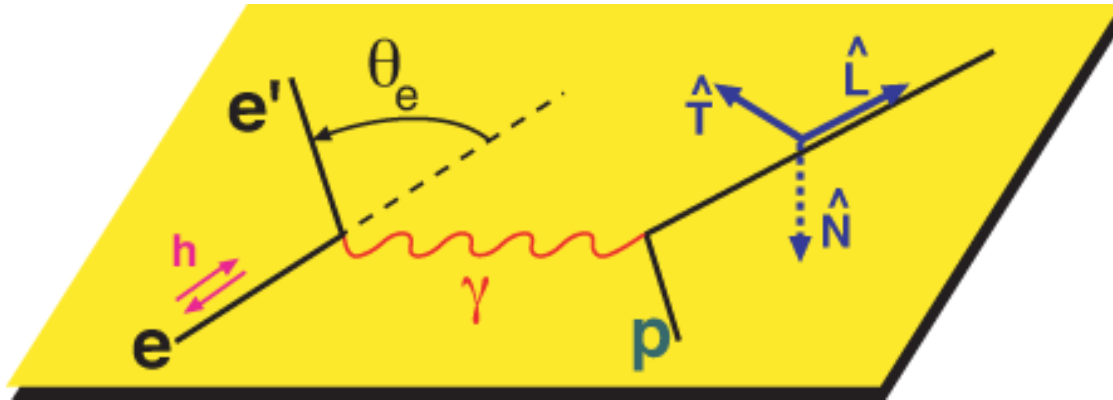


High-Energy Storage Ring

- At high energy an unpolarized stored beam becomes **transversely** polarized due to the difference in synchrotron radiation production for different beam helicities
- Need **spin rotator** to rotate polarization to longitudinal before interaction point and back to transverse after.



Spin Transfer Reaction ${}^1\text{H}(\vec{e}, e'\vec{p})$



$$P_n = 0$$

$$\pm hP_t = \mp h 2\sqrt{\tau(1+\tau)} G_E^p G_M^p \tan\left(\frac{\theta_e}{2}\right) / I_0$$

$$\pm hP_l = \pm h(E_e + E_{e'}) (G_M^p)^2 \sqrt{\tau(1+\tau)} \tan^2\left(\frac{\theta_e}{2}\right) / M / I_0$$

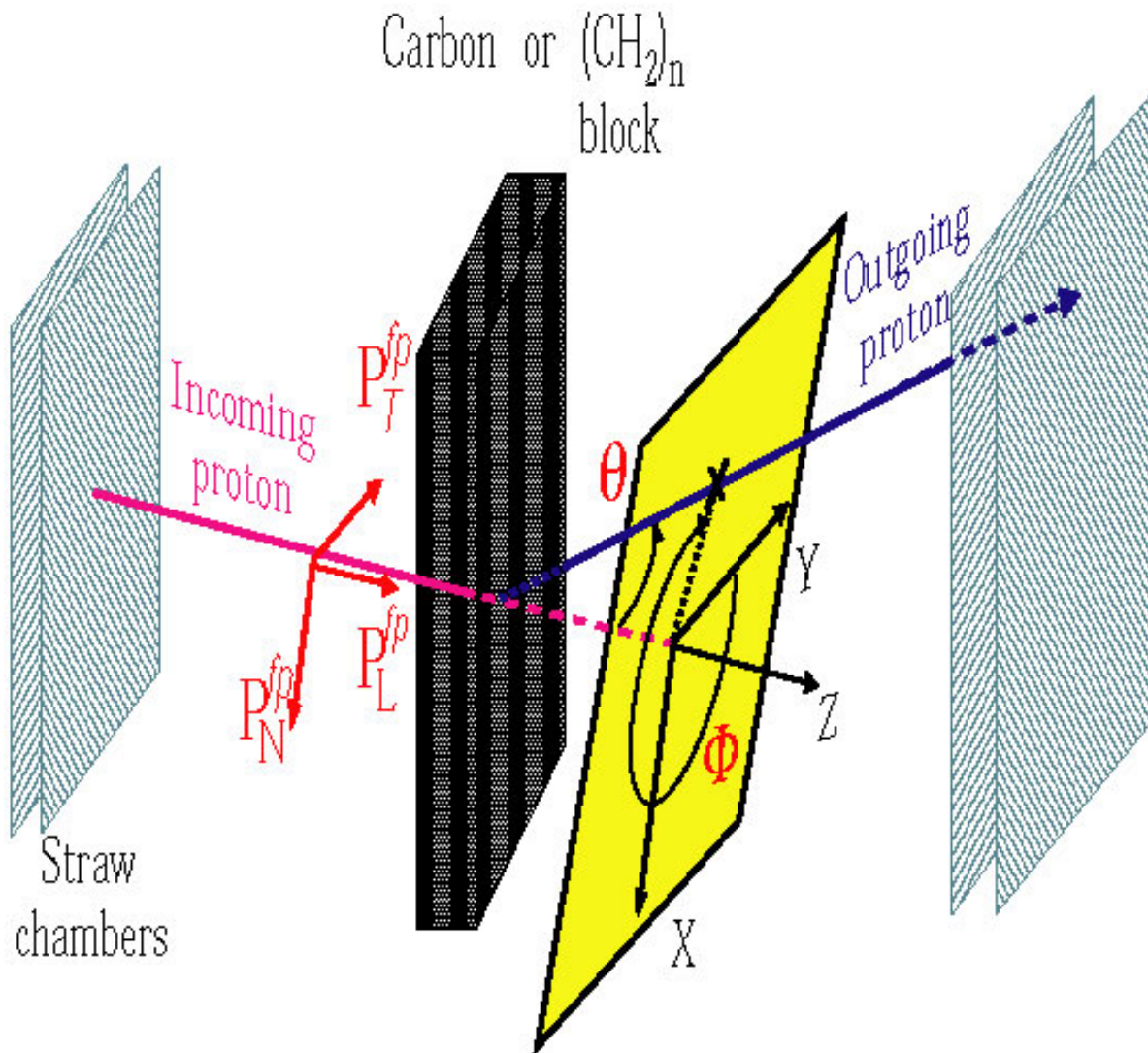
$$I_0 = \{G_E^p(Q^2)\}^2 + \tau \{G_M^p(Q^2)\}^2 \left[1 + 2(1+\tau) \tan^2\left(\frac{\theta_e}{2}\right) \right]$$

$$\frac{G_E^p}{G_M^p} = -\frac{P_t}{P_l} \frac{E_e + E_{e'}}{2M} \tan\left(\frac{\theta_e}{2}\right)$$

No error contributions from

- analyzing power
- beam polarimetry

Focal Plane Polarimeter

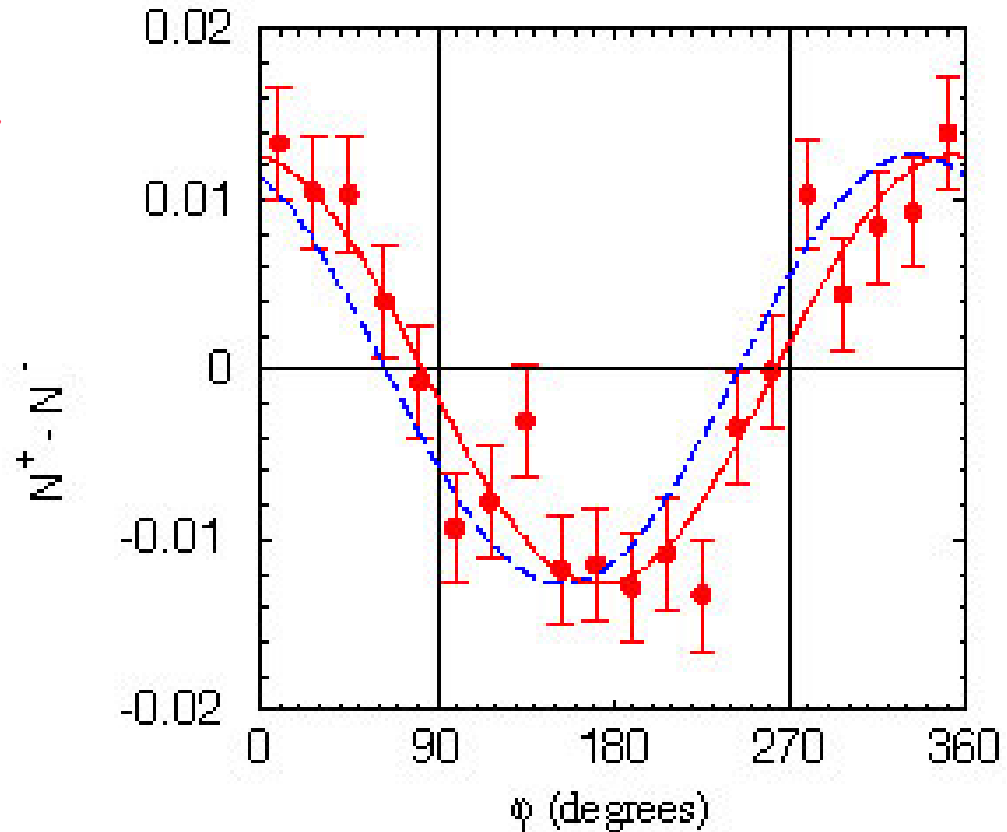


Rutgers, W&M, Georgia, NSU

Azimuthal Distributions

$$N^{\pm}(\theta, \varphi) = N_0^{\pm}(\theta) \left[1 + \{ \mp h A_C(\theta) P'_n + b_i \} \cos \varphi + \{ \pm h A_C(\theta) P'_t + a_i \} \sin \varphi \right]$$

- Polarimeter only sensitive to polarization components **transverse** to proton momentum
- Take helicity (h) difference of azimuthal distributions
- $A_C(\theta)$ is the $^{12}\text{C}/\text{CH}_2$ analyzing power
- a_i, b_i are the instrumental asymmetries, determined from the helicity sum



blue $G_E/G_M = 1$
red final fit



Spin Precession in Spectrometer-A (Mainz)

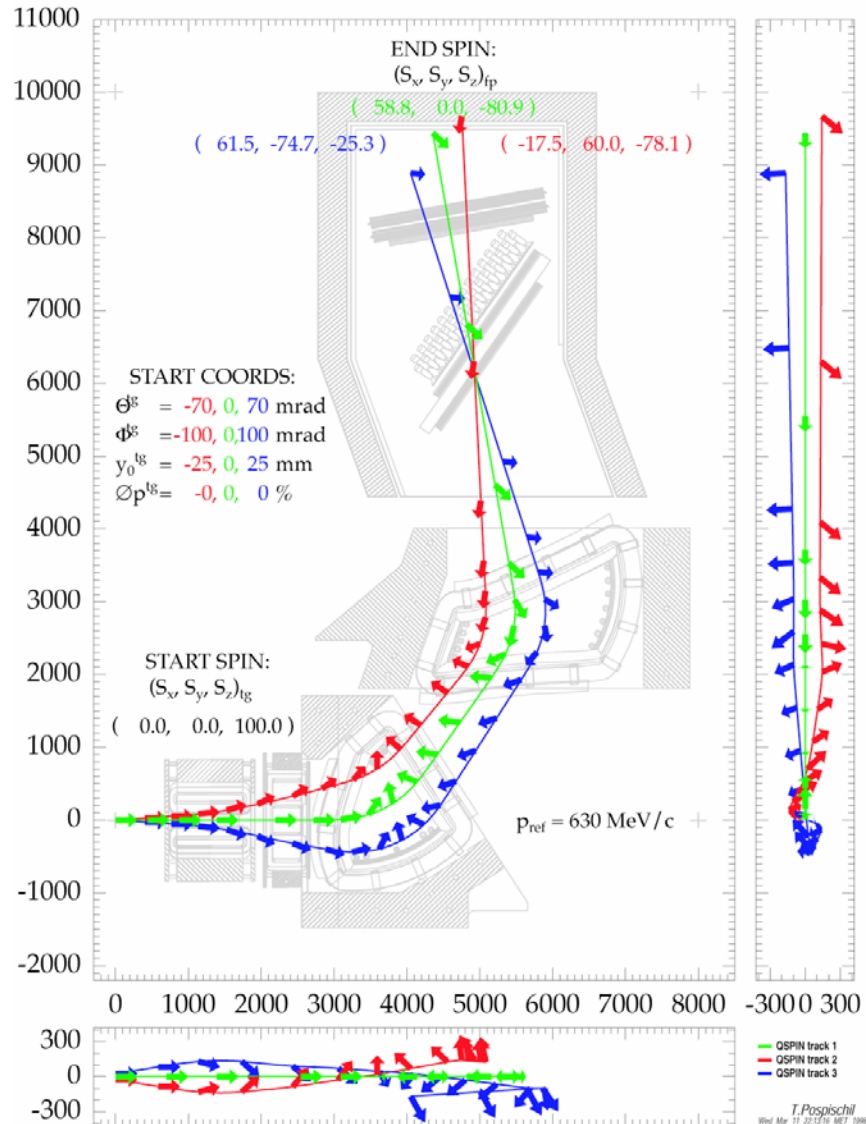
Polarimeter only sensitive to polarization components transverse to particle momentum, need magnetic field to precess particle spin

$$\chi = \gamma \theta_B (\mu_p - 1)$$

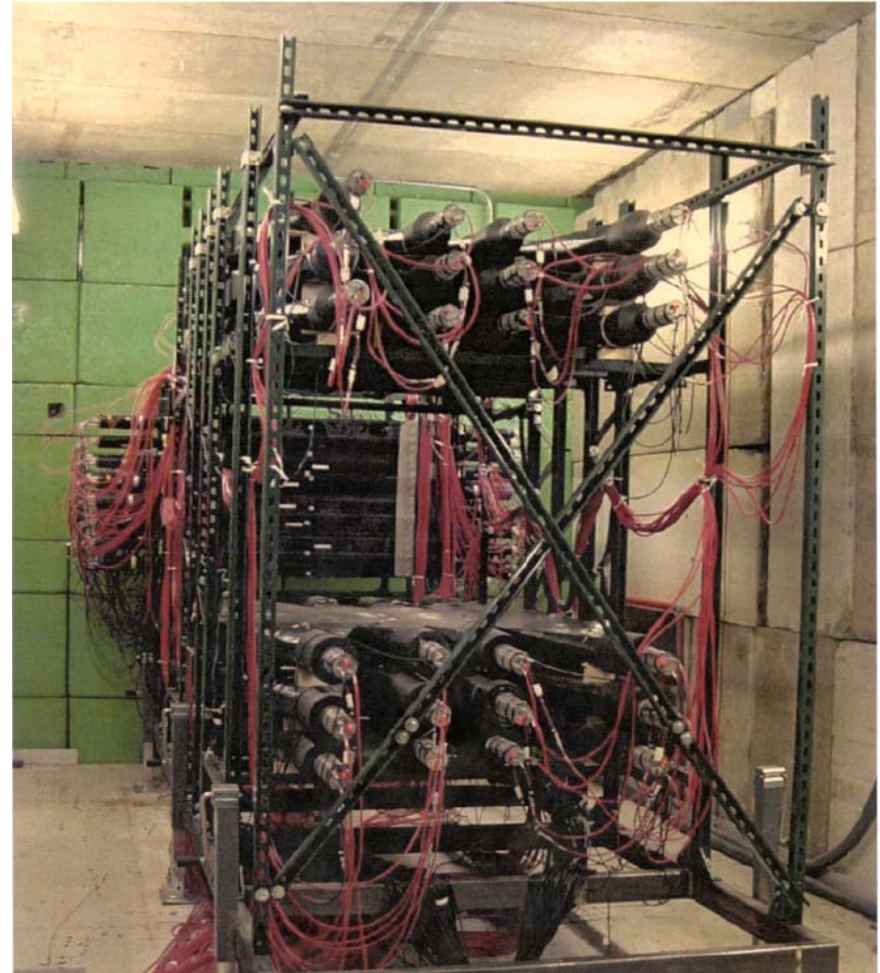
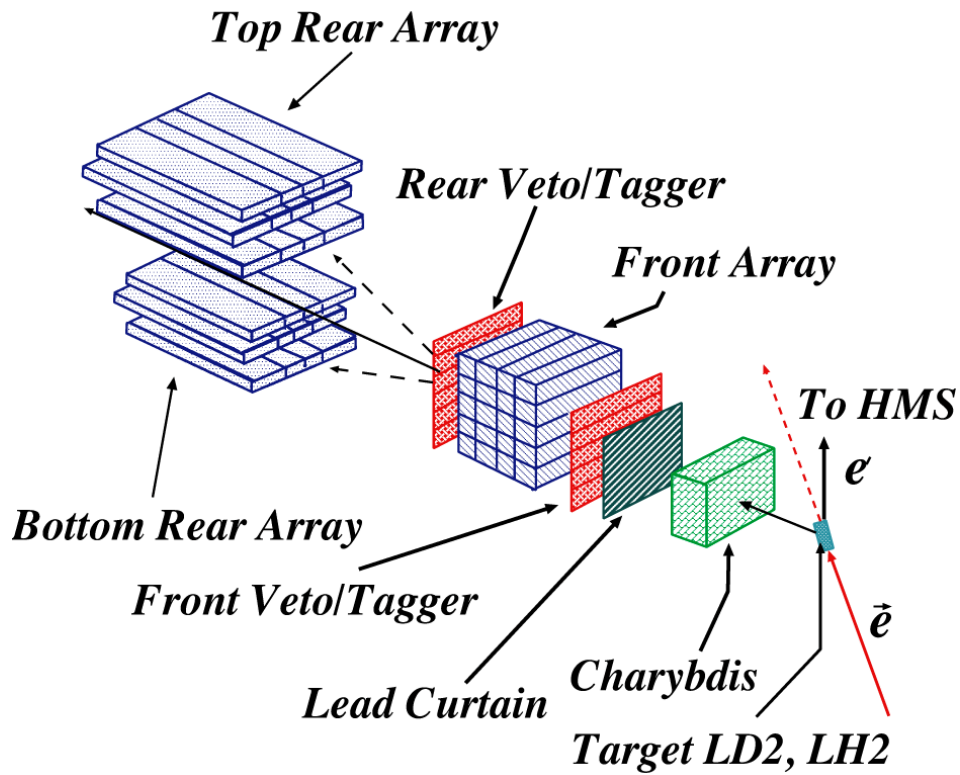
$$P_t^{FPP} = h P_t^{\text{target}}$$

$$P_l^{FPP} = \sin \chi \cdot h P_l^{\text{target}}$$

$$P_n^{FPP} = \cos \chi \cdot h P_l^{\text{target}}$$



G_E^n Experiment with Neutron Polarimeter



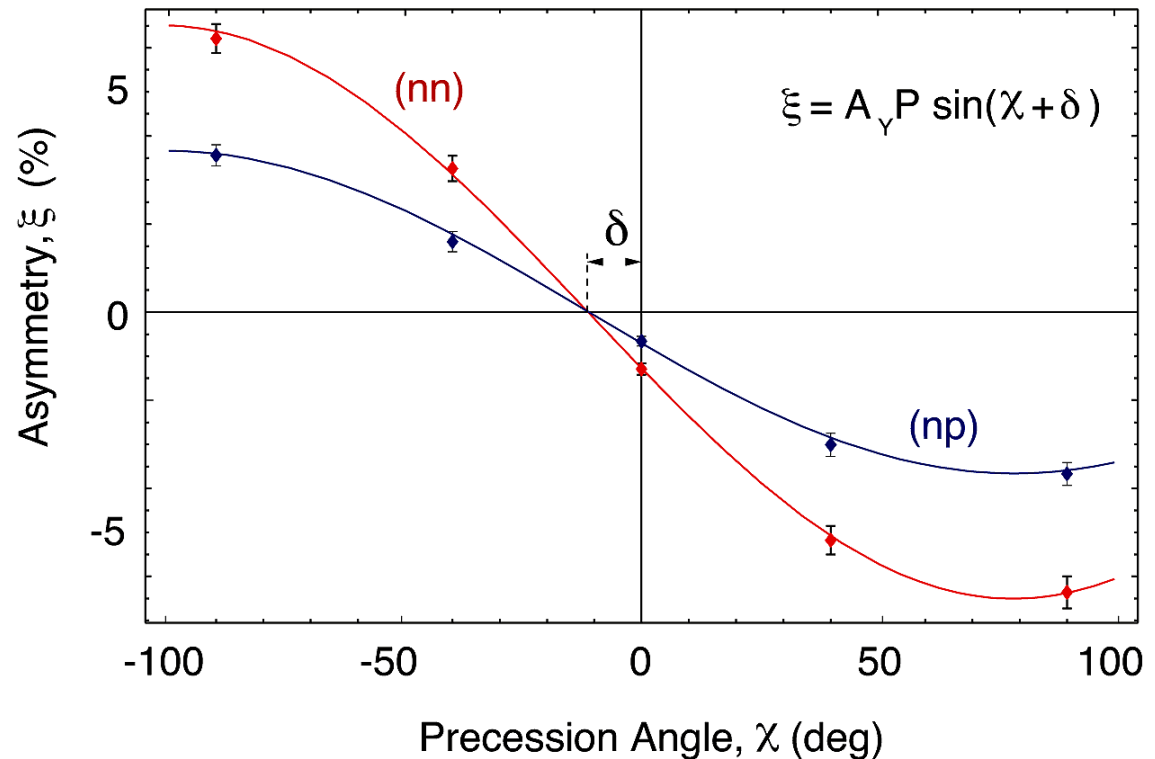
Dipole magnet (Charybdis) used to precess spin of neutron

G_E^n Experiment with Neutron Polarimeter

- Use dipole to precess neutron spin
- Up-down asymmetry ξ proportional to neutron sideways polarization
- G_E/G_M depends on phase shift δ w.r.t. precession angle χ

$$\xi \propto \sin(\chi + \delta) \Rightarrow \frac{G_E^n}{G_M^n} = -\tan\delta \sqrt{\frac{\tau(1+\varepsilon)}{2\varepsilon}}$$

Fit to Data for $Q^2 = 1.15 \text{ (GeV/c)}^2$



Instrumentation Figure of Merit (FOM)

$$\text{FOM} \equiv I_{\text{beam}} g_{\text{beam}}^{P^2} g_{\text{target}} g_{\text{target}}^{P^2} g_{\Delta\Omega_{\text{detector}}}$$

$$\text{FOM} \equiv I_{\text{beam}} g_{\text{beam}}^{P^2} g_{\text{target}} g_{\Delta\Omega_{\text{detector}}} g_{\epsilon_{\text{polarimeter}}} g_{A_{\text{polarimeter}}}^2$$

I_{beam}	beam intensity
P_{beam}	beam polarization
t_{target}	target thickness
P_{target}	target polarization
$\Delta\Omega_{\text{detector}}$	detector acceptance
$\epsilon_{\text{polarimeter}}$	polarimeter efficiency
$A_{\text{polarimeter}}$	polarimeter analyzing power

Reaction used (e,e'N)

Extended target requires capability to reconstruct target vertex
implies magnetic detector for one final state particle

Largest FOM at large Q^2 -values

for (e,e'p) FPP polarimeter with LH2 target

for (e,e'n) polarized ^3He target with neutron detector



Which instrumentation to choose?

- Polarized beam now available at high polarization ($\sim 85\%$) at current ($100 \mu\text{A}$)
- At large Q^2 recoil polarimeters preferred (for neutron also polarized ^3He target)
 - maximum Q^2 -value determined by fast drop in cross section (increasing beam energy allows more forward angle \rightarrow larger $Q^2 \rightarrow$ JLab at 12 GeV)
- At intermediate Q^2 values necessary to compare different instrumentation techniques without too much loss in measuring time, also large corrections necessary for polarized ^3He
- At low Q^2 values (up to $\sim 1 \text{ GeV}^2$) very accurate measurements feasible with storage ring + internal target + large acceptance detector (VEPP-2 at BINP in Novosibirsk, ITH at AmPS in Amsterdam, BLAST at MIT-Bates)



Review of Data

- Neutron
 - ▶ Charge Form Factor
 - ▶ Magnetic Form Factor
- Proton
 - ▶ Charge Form Factor
 - ▶ Two-Photon Exchange Contributions
- Time-like form factors



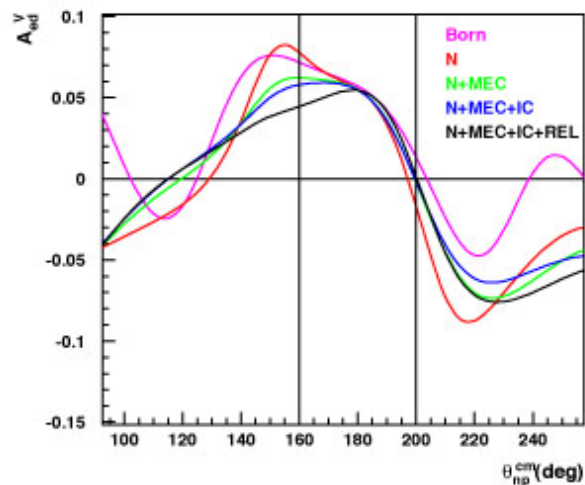
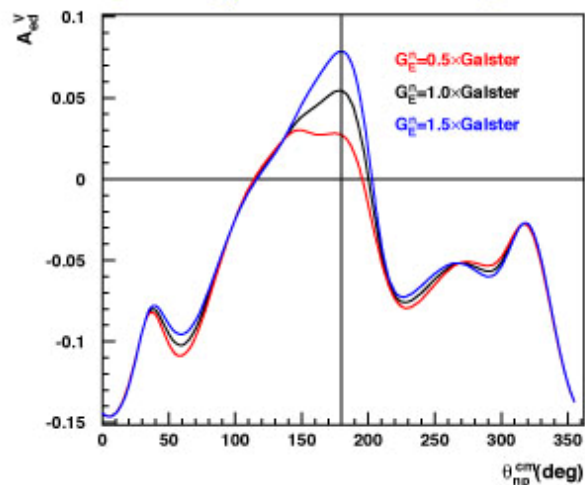
Double Polarization Experiments to Measure G_E^n

- Study the $(e,e'n)$ reaction from a polarized ND_3 target
limitations: low current (~ 80 nA) on target
deuteron polarization (~ 25 %)
- Study the $(e,e'n)$ reaction from a LD_2 target and measure the neutron polarization with a polarimeter
limitations: Figure of Merit of polarimeter
- Study the $(e,e'n)$ reaction from a polarized ^3He target
limitations: current on target ($12 \mu\text{A}$)
target polarization (40 %)
nuclear medium corrections

$$\frac{G_E^n}{G_M^n} = \frac{A_{\perp}}{A_{\parallel}} \sqrt{\tau + \tau(1 + \tau) \tan^2\left(\frac{\theta}{2}\right)}$$

How to measure G_E^n ?

Sensitivity to G_E^n – Insensitivity to Reaction



Experimental Technique for $\vec{D}(\vec{e}, e'n)p$

How to access A_{ed}^V ?

Experiment measures counts for different orientations of h and P :

$$N^{hP} \propto \sigma(h, P)$$

Beam-target Asymmetry:

$$\begin{aligned} A_{BT} &= \frac{N^{++} - N^{-+} + N^{--} - N^{+-}}{N^{++} + N^{-+} + N^{++} + N^{++}} \\ &= \frac{hPA_{ed}^V}{1 + TA_d^T} \\ &\simeq hPA_{ed}^V \end{aligned}$$

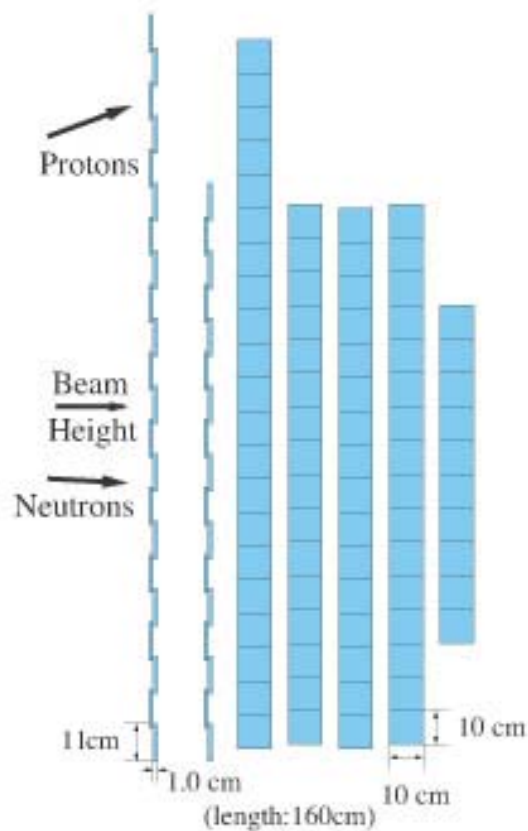
θ_{np}^{cm} : Angle between \vec{q} and relative n-p momentum in cm system; 180 deg corresponds to neutron in direction of \vec{q}



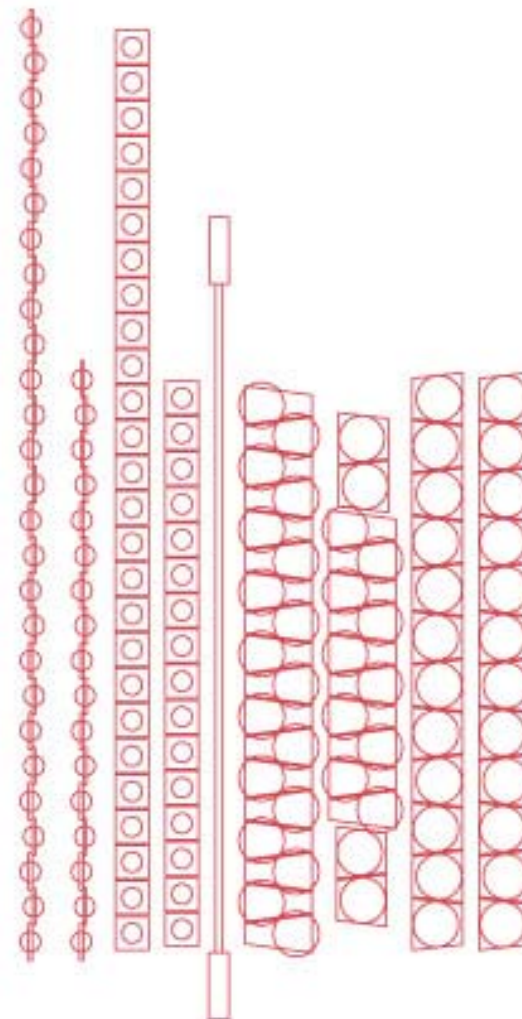
Thomas Jefferson National Accelerator Facility

Neutron Detector

Neutron detector for measurement with polarized target



1998



2001

How to measure G_E^n ?

From ε to G_E^n in Detail

The polarized beam and target electron deuteron cross section can be expressed in the form:

$$S(h, P_1^d, P_2^d) = S_0 \left[1 + hA_e + P_1^d A_d^V + P_2^d A_d^T + h(P_1^d A_{ed}^V + P_2^d A_{ed}^T) \right],$$

where $A_e, A_d^V, A_d^T, A_{ed}^V, A_{ed}^T$ are electron asymmetry, vector and tensor target asymmetries, and electron-deuteron vector and tensor asymmetries.

Comparing with the cross section expression, one can obtain expressions for the five asymmetries:

$$A_e = \frac{1}{2hS_0} [S(h, 0, 0) - S(-h, 0, 0)],$$

$$A_d^V = \frac{1}{2P_1^d S_0} [S(0, P_1^d, P_2^d) - S(0, -P_1^d, P_2^d)],$$

$$A_d^T = \frac{1}{2P_2^d S_0} [S(0, P_1^d, P_2^d) - S(0, -P_1^d, P_2^d) - 2S_0],$$

$$A_{ed}^{V,T} = \frac{1}{4hP_{1/2}^d S_0} \left\{ [S(h, P_1^d, P_2^d) - S(-h, P_1^d, P_2^d)] \mp [S(h, -P_1^d, P_2^d) - S(-h, -P_1^d, P_2^d)] \right\}.$$

Note that S_0 is in the denominator and we never measure S_0 .

$$S(+h) + S(-h) \neq S_0$$

$$\varepsilon = \frac{(L_+ - R_+) - (L_- - R_-)}{(L_+ + R_+) + (L_- + R_-)}.$$

$$L_+ = \Phi_+ n_D S(h, P_1^d, P_2^d)$$

$$L_- = \Phi_- n_D S(h, -P_1^d, P_2^d)$$

$$R_+ = \Phi_+ n_D S(-h, P_1^d, P_2^d)$$

$$R_- = \Phi_- n_D S(-h, -P_1^d, P_2^d)$$

$$\varepsilon = \frac{h \left[(1 - \beta)A_e + (1 + \alpha\beta)P_1^d A_{ed}^V + (1 - \beta\gamma)P_2^d A_{ed}^T \right]}{(1 + \beta) + (1 - \alpha\beta)P_1^d A_d^V + (1 + \beta\gamma)P_2^d A_d^T},$$

$$\alpha = -\frac{P_{1-}}{P_{1+}}$$

$$\beta = \frac{\Phi_-}{\Phi_+}$$

$$\gamma = \frac{P_2(P_{1-})}{P_2(P_{1+})}$$

$$P_2^d = 2 - \left[4 - 3(P_1^d)^2 \right]^{1/2}$$

$$A_{ed}^V = \frac{1}{h(1 + \alpha\beta)P_1^d} \left\{ \varepsilon \left[(1 + \beta) + (1 - \alpha\beta)P_1^d A_d^V + (1 + \beta\gamma)P_2^d A_d^T \right] - h \left[(1 - \beta)A_e + (1 - \beta\gamma)P_2^d A_{ed}^T \right] \right\}.$$

With full ϕ acceptance A_e, A_d^V and A_{ed}^T have zero contributions.



How to measure G_E^n ?

A_d^T remains. For $P_1^d = 20\%$, $P_2^d \simeq 3\%$

with $A_d^T \approx 10^{-2} A_d^T$ can be ignored

$$A_{ed}^V = \frac{\epsilon(1 + \beta)}{h(1 + \alpha\beta)P_1^d}$$

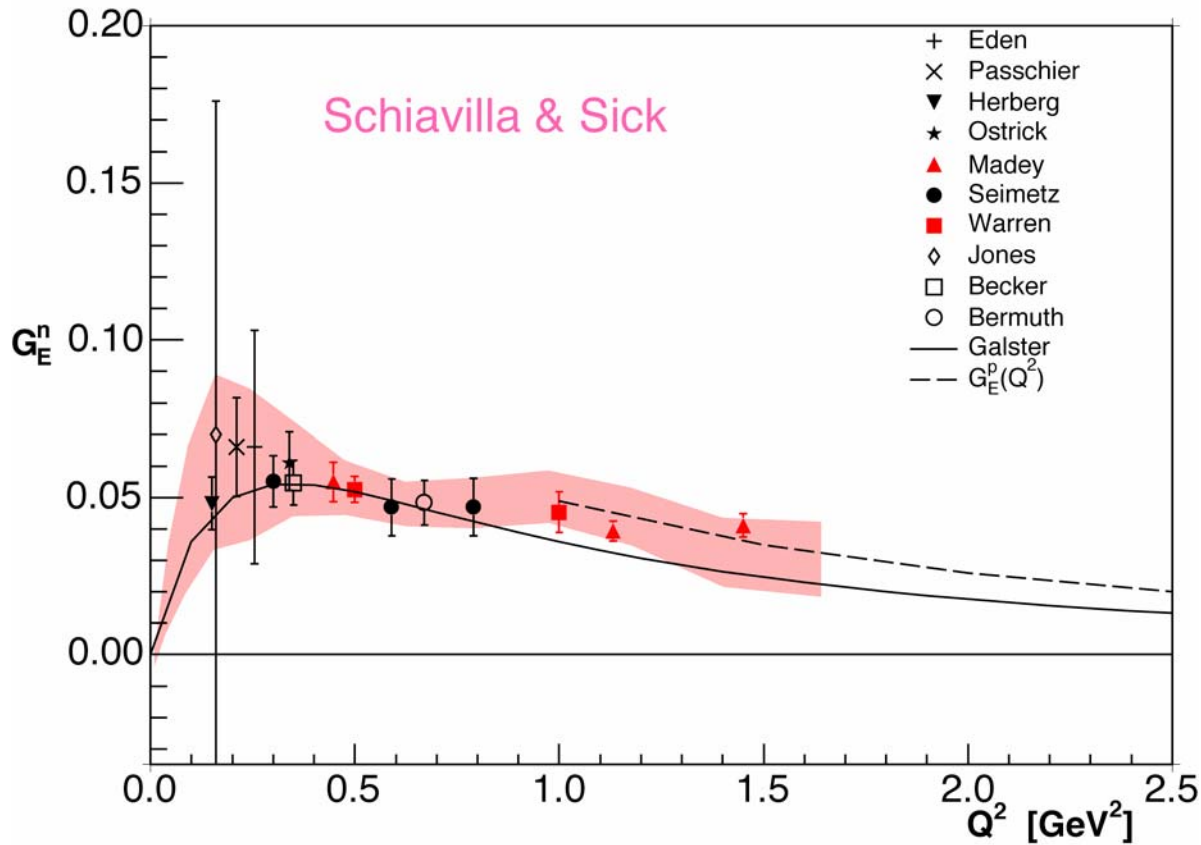
With the dilution factor

$$A_{ed}^V = \frac{\epsilon(1 + \beta)}{h(1 + \alpha\beta)P_1^d f}$$

Need cuts on
coincidence timing
neutron angle

Veto protons
Correction for
charge exchange reaction

Neutron Electric Form Factor G_E^n



Galster:
a parametrization
fitted to old (<1971)
data set of very
limited quality

For $Q^2 > 1 \text{ GeV}^2$
data hint that G_E^n has
similar Q^2 -behaviour
as G_E^p

Measuring G_M^n

Old method: quasi-elastic scattering from ^2H
large systematic errors due to subtraction of proton contribution

- Measure (en)/(ep) ratio

Luminosities cancel

Determine neutron detector efficiency

- On-line through $e+p \rightarrow e'+\pi^+(+n)$ reaction (CLAS)
- Off-line with neutron beam (Mainz)

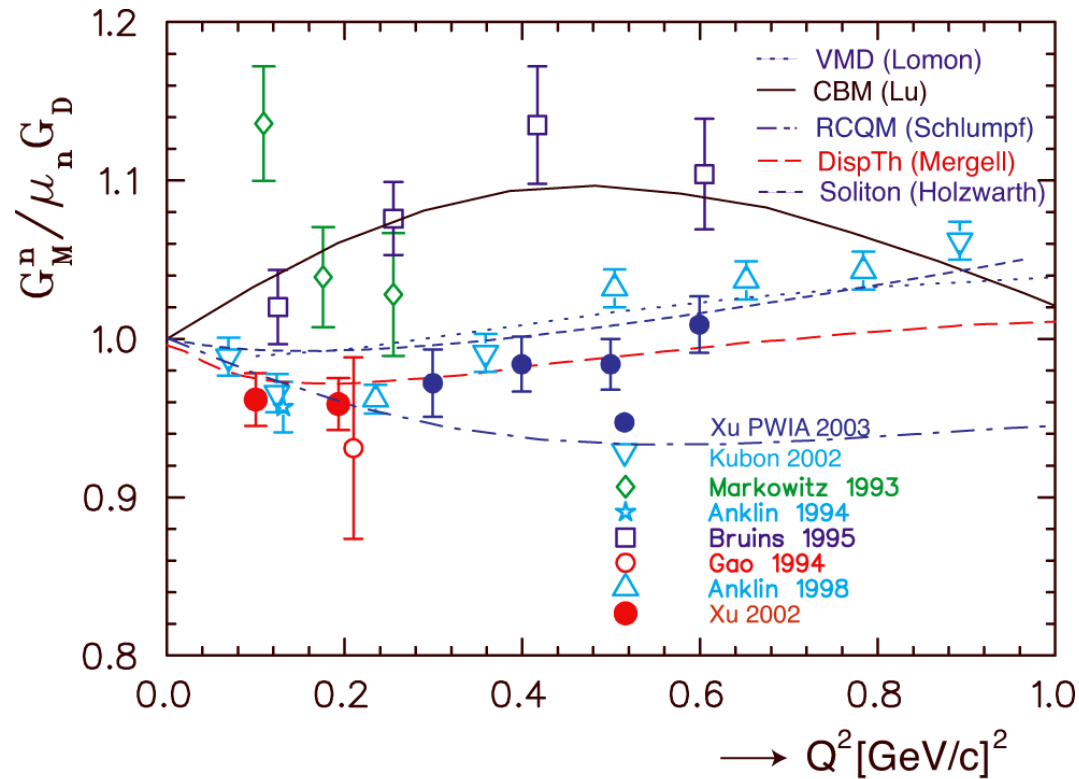
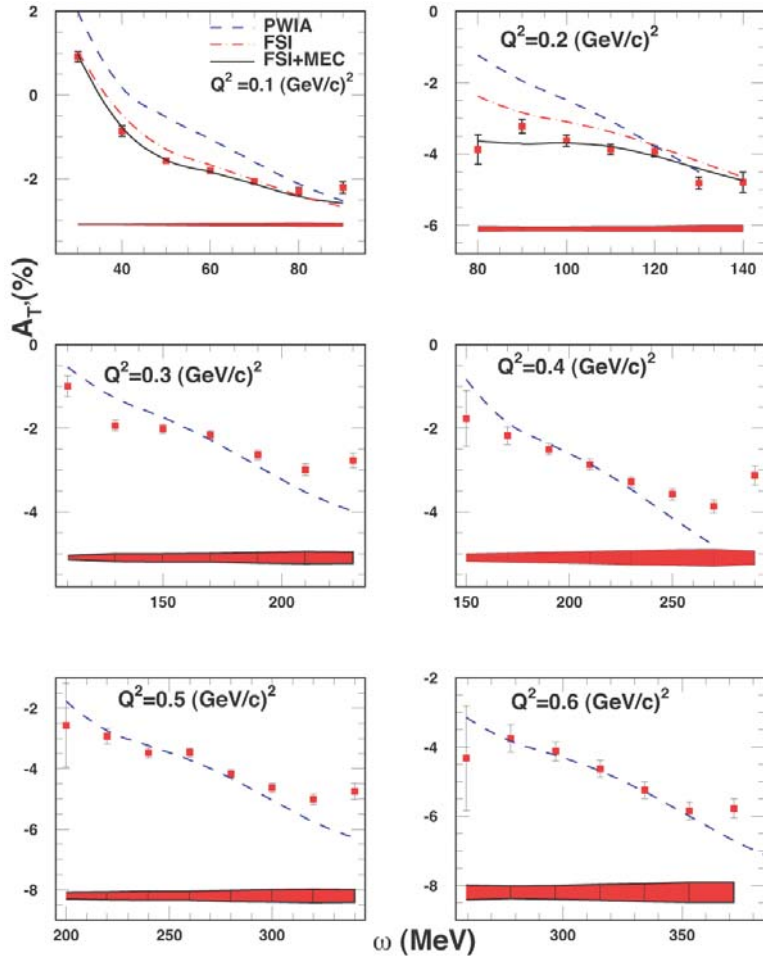
- Measure inclusive quasi-elastic scattering off polarized ^3He (Hall A)

$$R_D = \frac{\frac{d^3\sigma(eD \Rightarrow e'n(p))}{dE' d\Omega_e d\Omega_n}}{\frac{d^3\sigma(eD \Rightarrow e'p(n))}{dE' d\Omega_e d\Omega_p}}$$

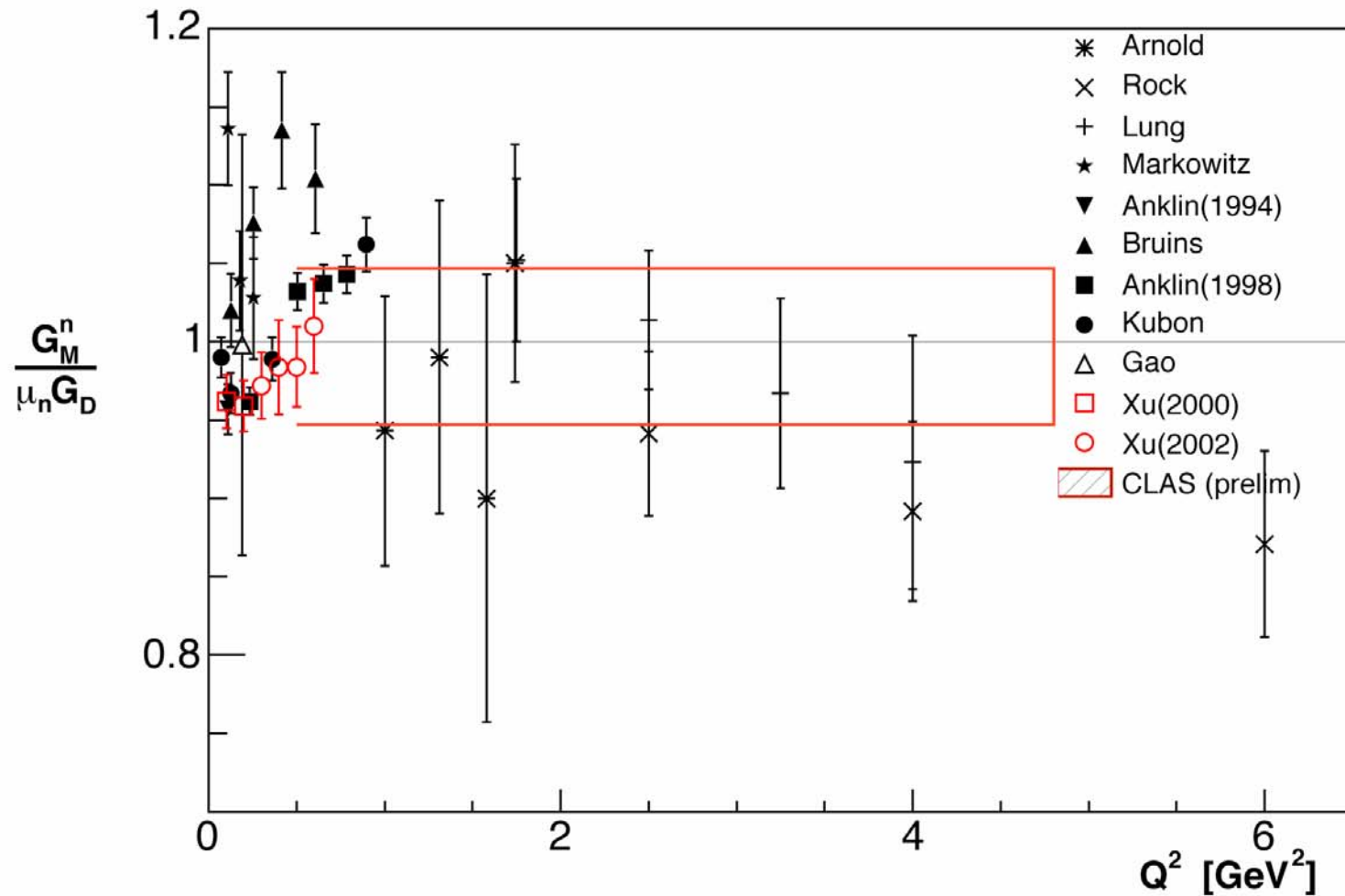
$$A = \frac{-\left(\cos\theta^* v_T R_T + 2\sin\theta^* \cos\varphi^* v_{TL} R_{TL}\right)}{v_L R_L + v_T R_T}$$

R_T directly sensitive to $(G_M^n)^2$

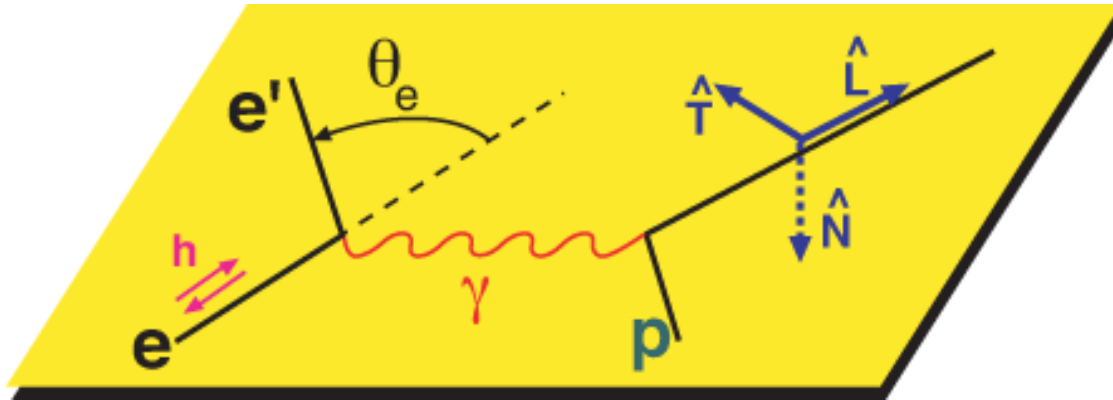
Measurement of G_M^n at low Q^2



Preliminary G_M^n Results from CLAS



Spin Transfer Reaction ${}^1\text{H}(\vec{e}, e'\vec{p})$



$$J \propto G_E^P + \sigma \times Q * G_M^P$$

Polarized electron transfers longitudinal polarization to G_E ,
but transverse polarization to G_M

$$\frac{G_E^P}{G_M^P} = -\frac{P_t}{P_l} \frac{E_e + E_{e'}}{2M} \tan\left(\frac{\theta_e}{2}\right)$$

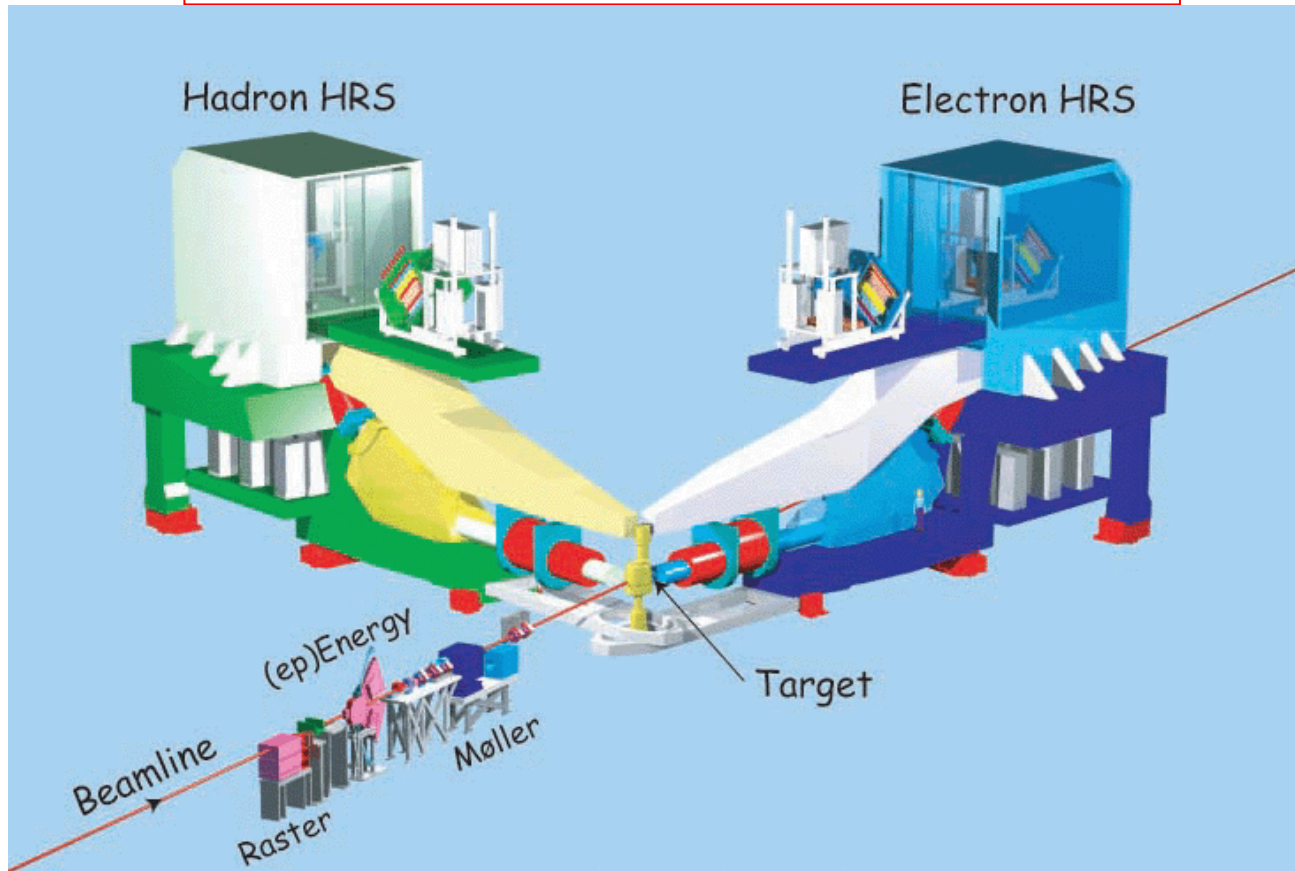
No error contributions from

- analyzing power
- beam polarimetry

Measuring G_E^p in JLab Hall A

Two High Resolution Spectrometers

p_{\max}	4 GeV/c
momentum resolution	10^{-4}
solid angle	6 msr

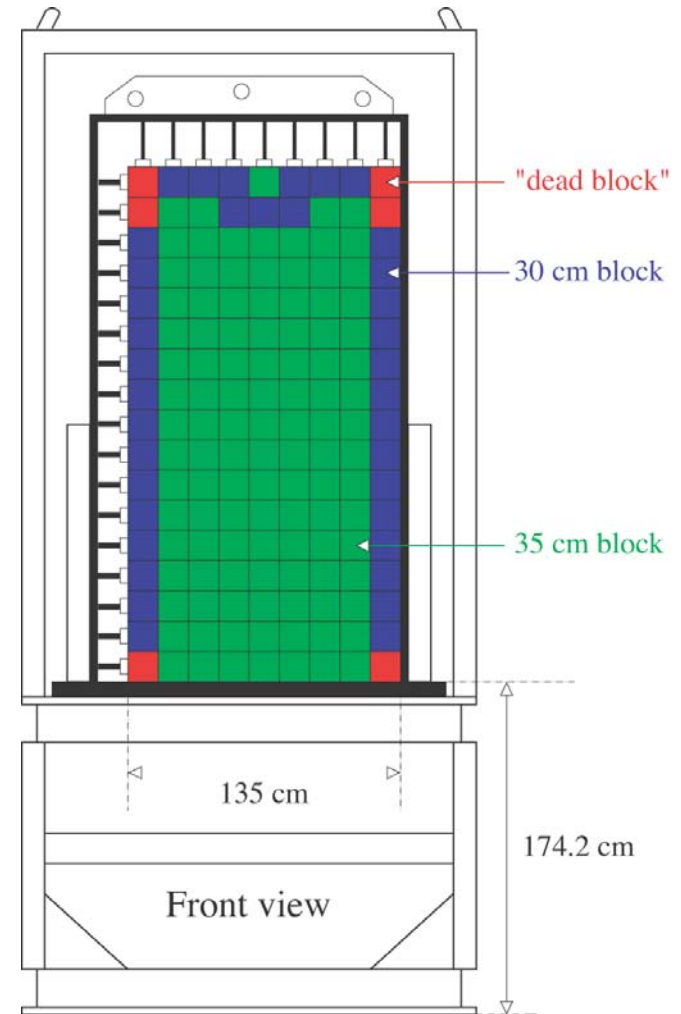


Lead Glass Calorimeter

At larger Q^2 -values protons are focused into smaller solid angle \rightarrow increase electron acceptance
At a beam energy of 4.6 GeV

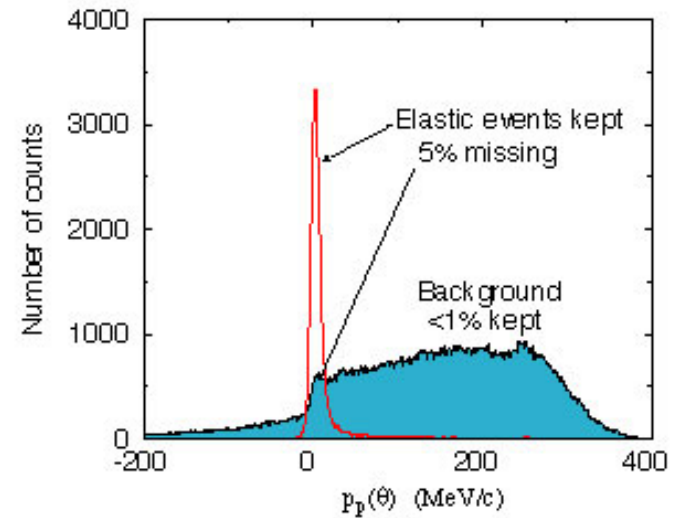
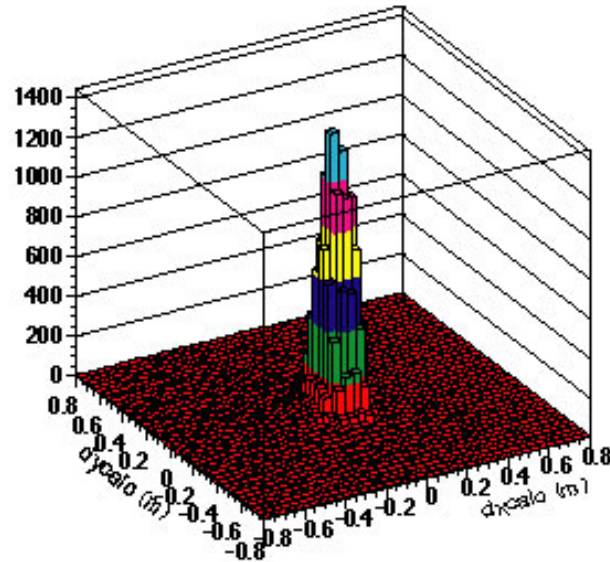
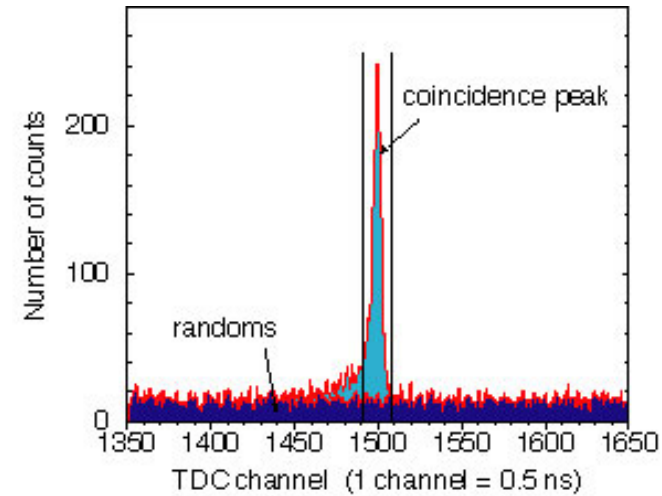
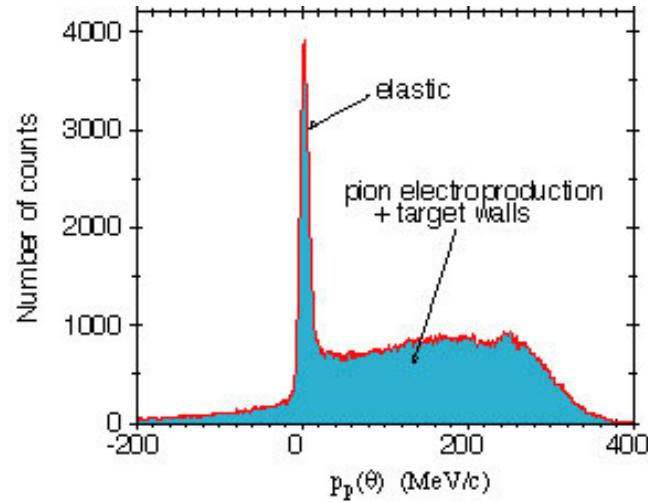
Q^2 [GeV ²]	p_p [GeV/c]	θ_p	θ_e	solid angle _e
4.0	2.92	28.6°	34.5°	11.9
4.8	3.36	23.8°	42.1°	22.0
5.6	3.81	19.4°	51.4°	42.5

- HRS solid angle is ~ 6 msr
- Assembled 1.4×2.5 m² calorimeter
17 rows, 9 columns of 15×15 cm² lead-glass blocks
- Optimized distance to target at each Q^2



Calorimeter Performance

- Clean identification of elastic events through coincidence requirement



Systematic Errors

Spin Precession

$$\chi = \gamma \theta_B (\mu_p - 1)$$

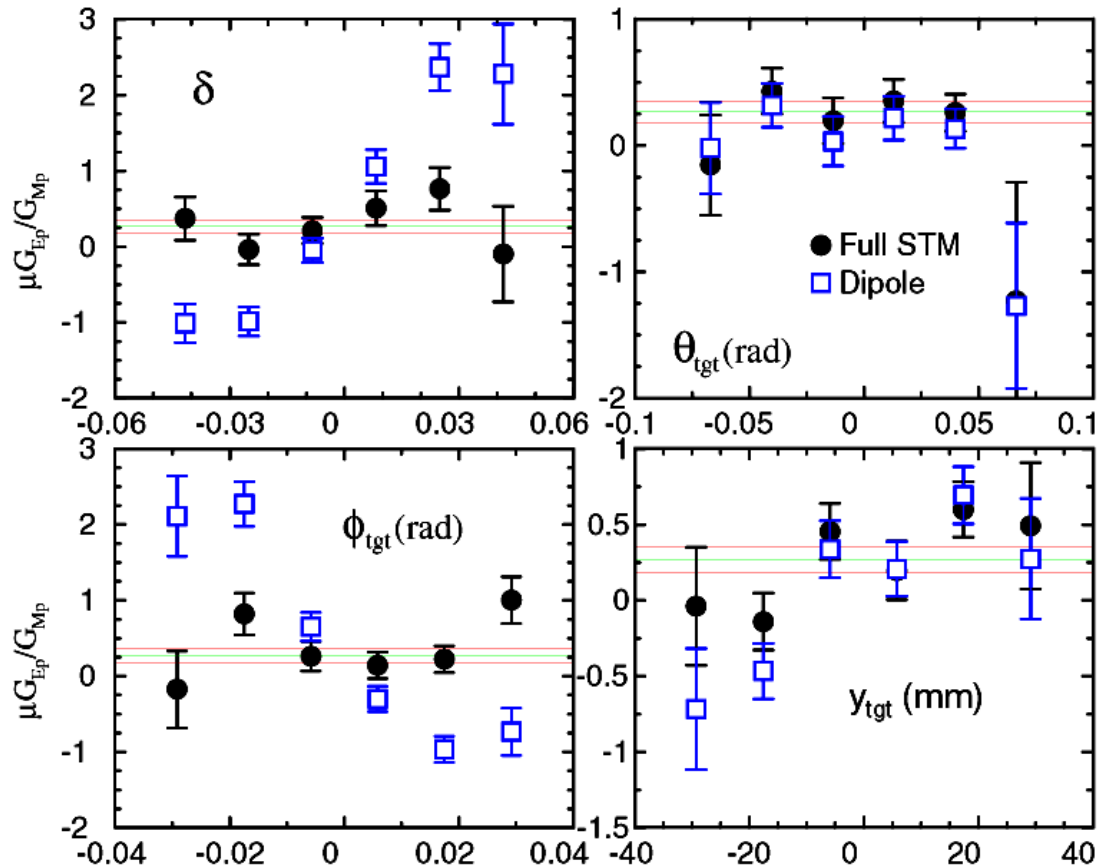
$$P_t^{FPP} = h P_t^{\text{target}}$$

$$P_l^{FPP} = \sin \chi \cdot h P_l^{\text{target}}$$

Open squares:
only dipole precession

Full circles:
event-by-event correction

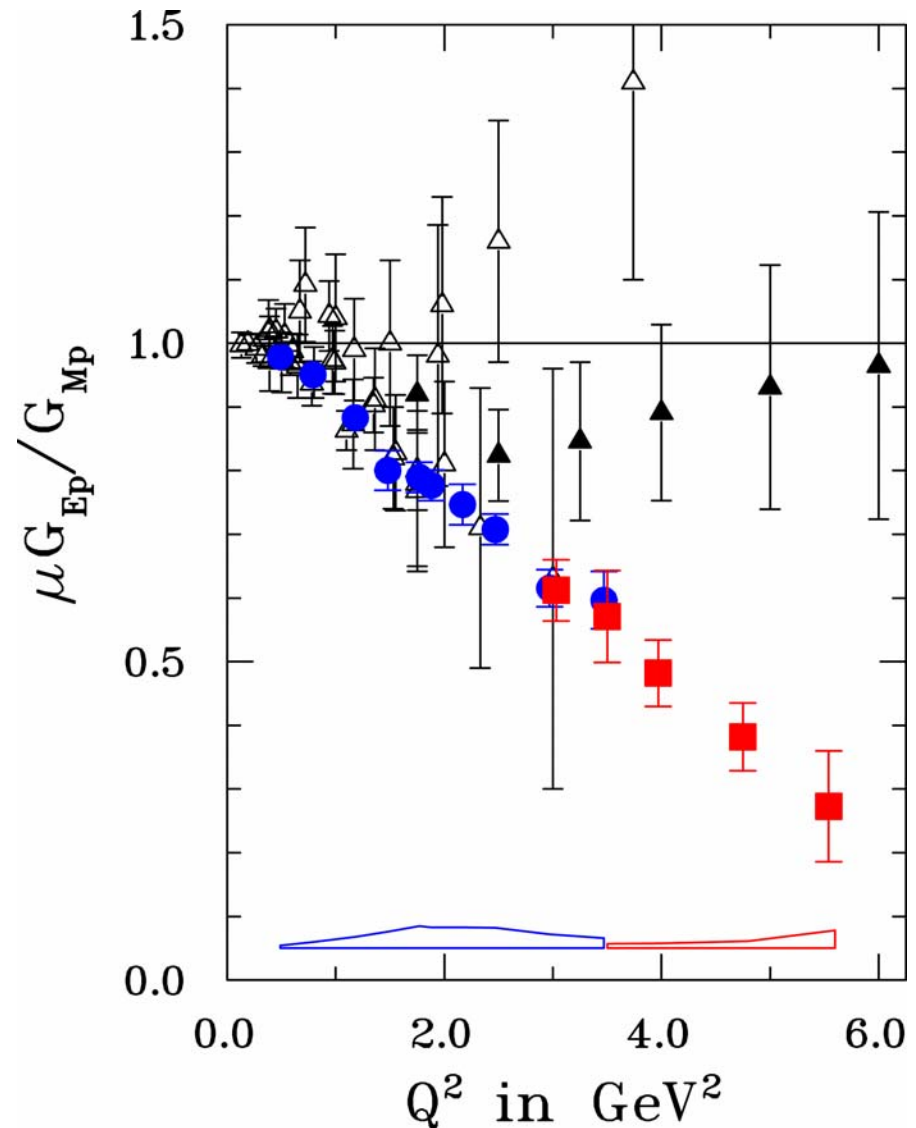
No dependence of G_E/G_M on
either δ , θ , ϕ or y_{targ}



JLab Polarization Transfer Data

- E93-027 PRL 84, 1398 (2000)
Used both HRS in Hall A with FPP
- E99-007 PRL 88, 092301 (2002)
used Pb-glass calorimeter for electron
detection to match proton HRS
acceptance
- Reanalysis of E93-027 (Pentchev)
Using corrected HRS properties

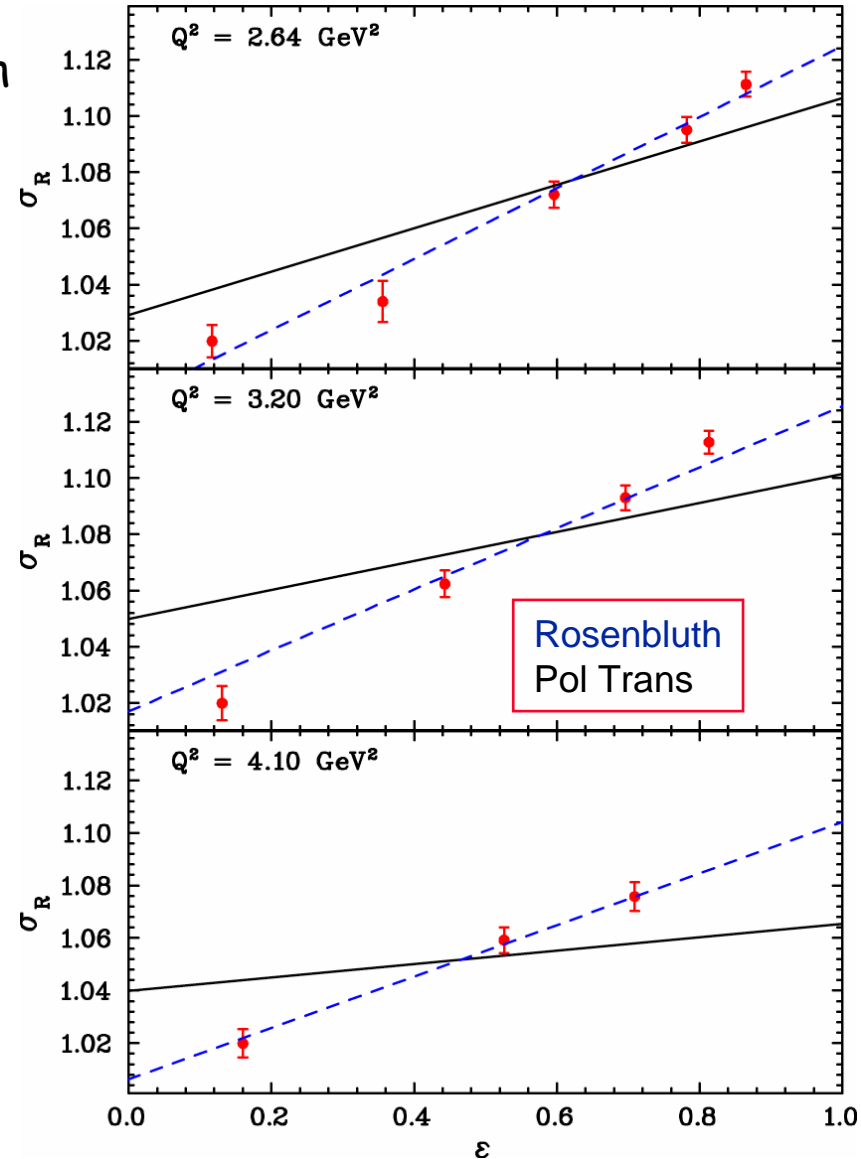
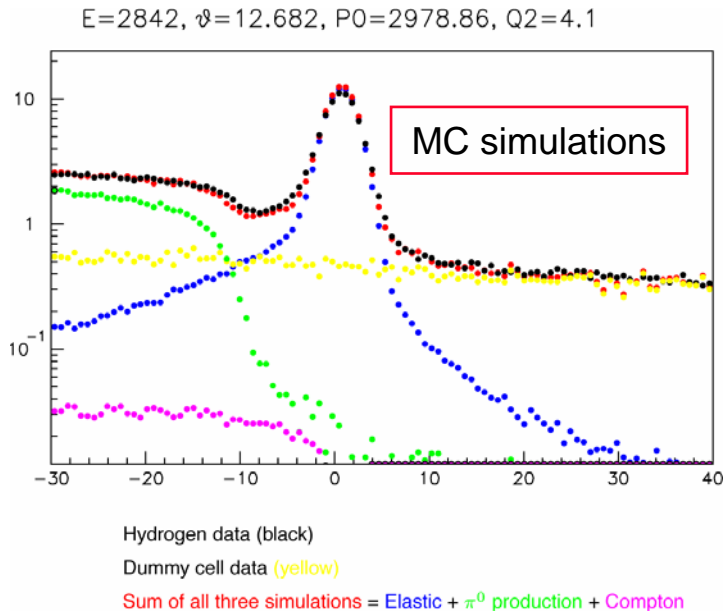
Colored data polarization transfer
Black/white Rosenbluth separation



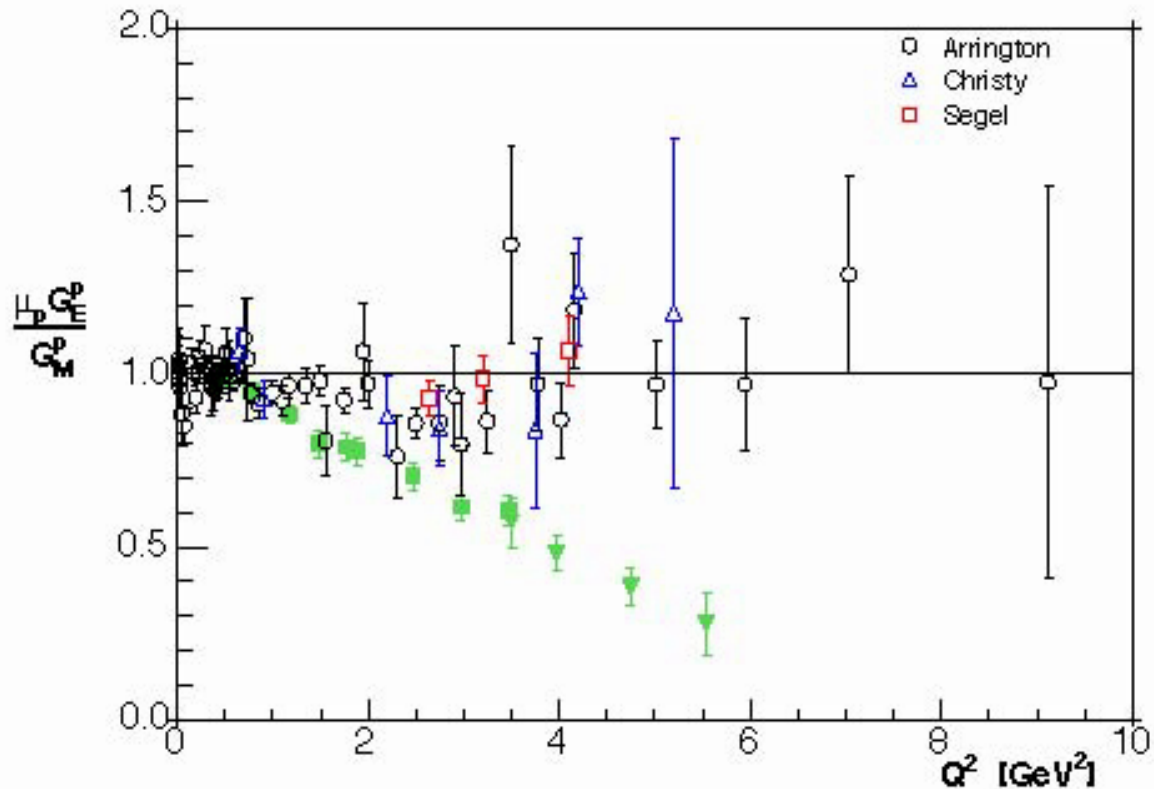
Super-Rosenbluth (E01-001)

J. Arrington and R. Segel

- Detect recoil protons in HRS-L to diminish sensitivity to:
 - Particle momentum
 - Particle angle
 - Rate
- Use HRS-R as luminosity monitor
- Very careful survey



Rosenbluth Compared to Polarization Transfer

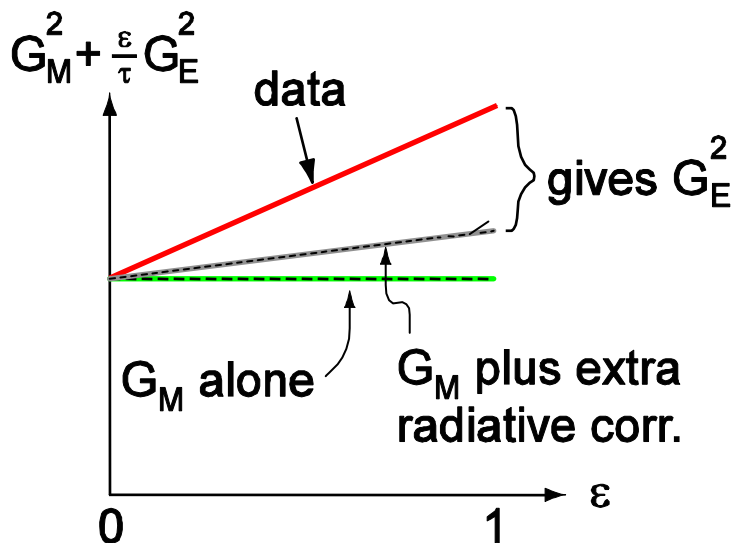


- John Arrington performed detailed reanalysis of SLAC data
- Hall C Rosenbluth data (E94-110, Christy) in agreement with SLAC data
- No reason to doubt quality of either Rosenbluth or polarization transfer data
- Investigate possible theoretical sources for discrepancy

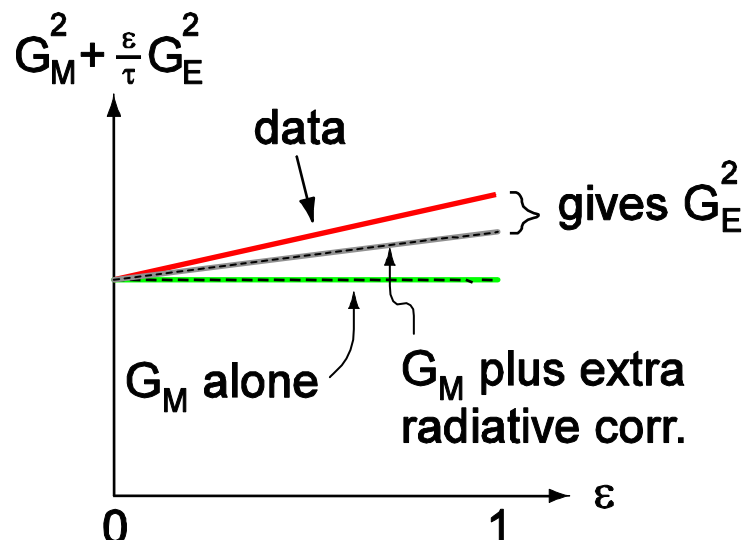
Speculation : missing radiative corrections

Speculation : there are radiative corrections to Rosenbluth experiments that are important and are not included in the analysis

missing correction : linear in ϵ , not strongly Q^2 dependent



Low τ (Low Q^2)



High τ (High Q^2)

$Q^2 = 6 \text{ GeV}^2$

G_E term is proportionally smaller at large Q^2

$$\frac{G_E^2}{\tau G_M^2} = \frac{4 M^2}{Q^2 \mu_p^2} = 7.5\%$$

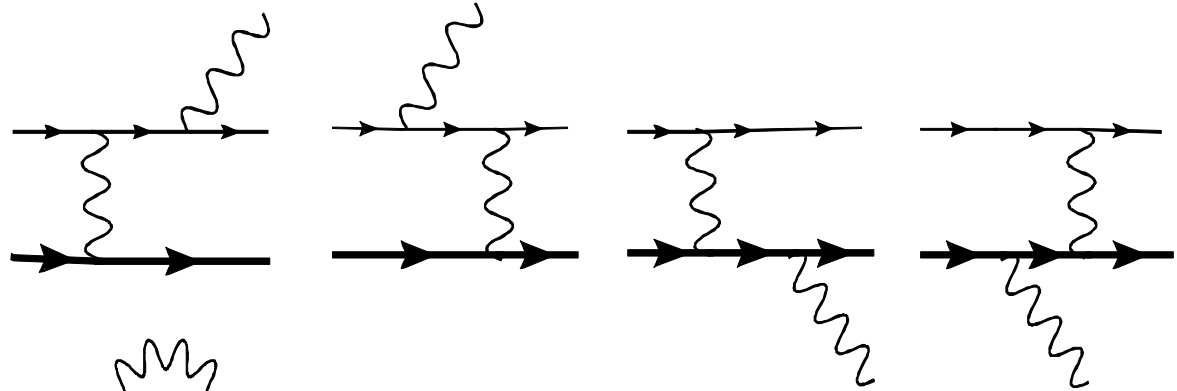
effect more visible at large Q^2

if both FF scale in same way

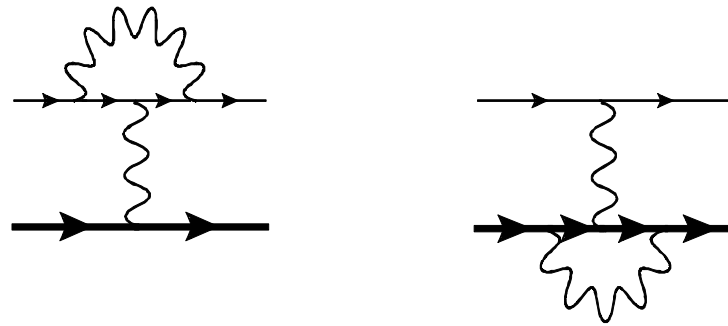


Radiative correction diagrams

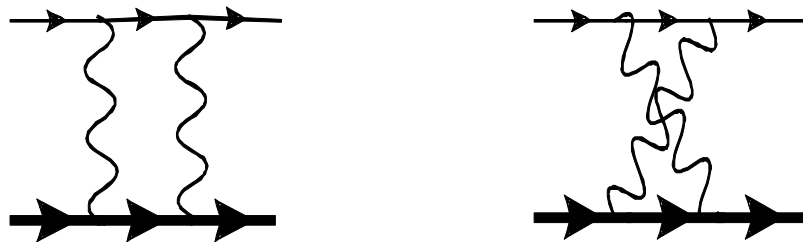
bremsstrahlung



vertex corrections



two-photon exchange
box diagrams



Comments on radiative corrections

- Radiative corrections at **electron side**,



well understood and taken care of

- **Soft bremsstrahlung**

involves long-wavelength photons

compositeness of nucleon only enters through



on-shell form factors

- **Box diagrams** involve photons of all wavelengths

long-wavelength (soft photon) part is included in radiative correction



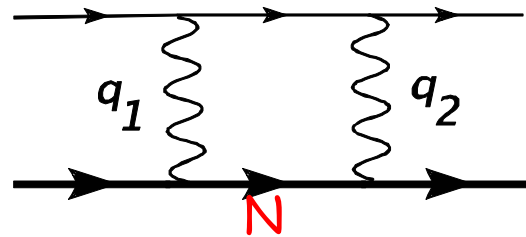
(IR divergence is cancelled with electron-proton bremsstrahlung interference)

short-wavelength contributions :

neglected in "old" days



Status of radiative corrections



- Tsai (1961), Mo & Tsai (1968)

box diagram calculated using **only nucleon intermediate state** and using $q_1 \sim 0$ or $q_2 \sim 0$ in both numerator and denominator (calculate 3-point function) \rightarrow **gives correct IR divergent terms**

- Maximon & Tjon (2000)

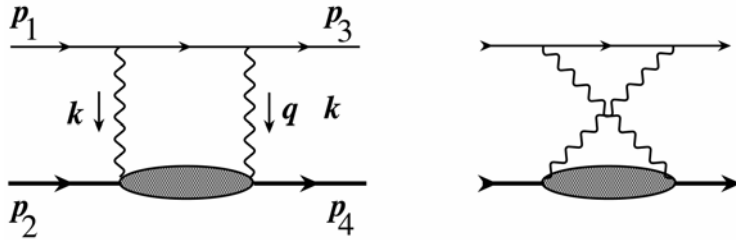
same as above, but make the above approximation only in numerator (calculate 4-point function)

+ use **on-shell nucleon form factors** in loop integral

- Blunden, Melnitchouk, Tjon (2003)

further improvement by keeping the full numerator

Two-photon Contributions

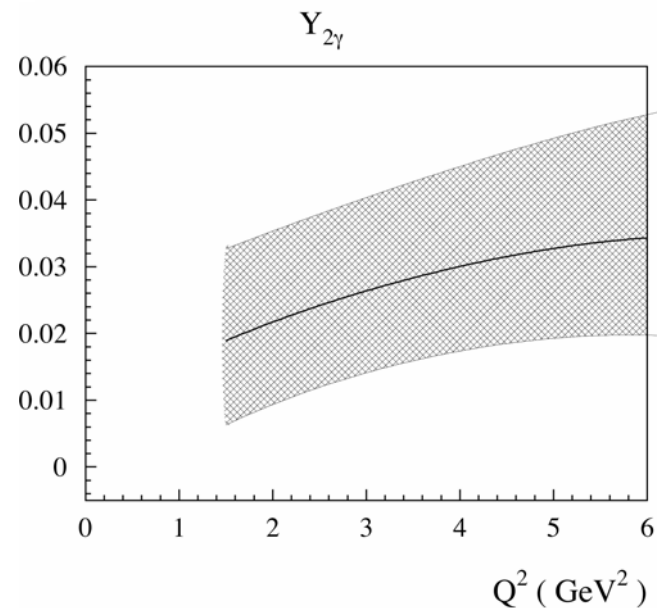
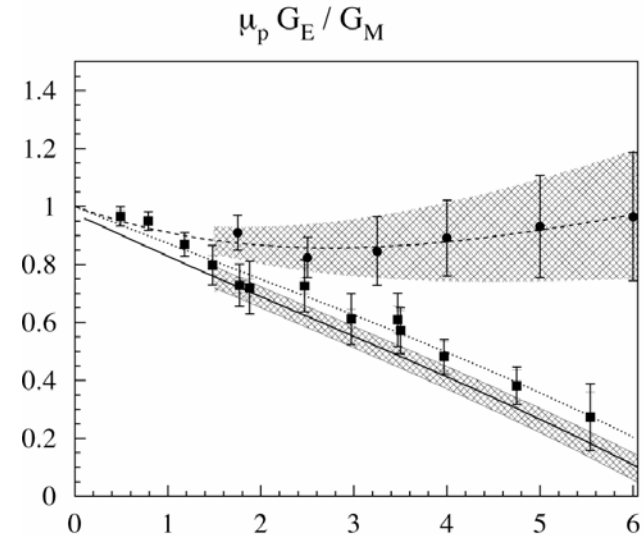


Guichon and Vanderhaeghen (PRL 91 (2003) 142303) estimated the size of two-photon corrections (TPE) necessary to reconcile the Rosenbluth and polarization transfer data

$$\frac{d\sigma}{d\Omega} \propto \frac{|\tilde{G}_M|^2}{\tau} \left\{ \tau + \varepsilon \frac{|\tilde{G}_E|^2}{|\tilde{G}_M|^2} + 2\varepsilon \left(\tau + \frac{|\tilde{G}_E|}{|\tilde{G}_M|} \right) Y_{2\gamma}(v, Q^2) \right\}$$

$$\frac{P_t}{P_l} \approx -\sqrt{\frac{2\varepsilon}{\tau(1+\varepsilon)}} \left\{ \frac{|\tilde{G}_E|}{|\tilde{G}_M|} + \left(1 - \frac{2\varepsilon}{1+\varepsilon} \frac{|\tilde{G}_E|}{|\tilde{G}_M|} \right) Y_{2\gamma}(v, Q^2) \right\}$$

Need ~3% value for $Y_{2\gamma}$ (6% correction to ε -slope), independent of Q^2 , which yields minor correction to polarization transfer

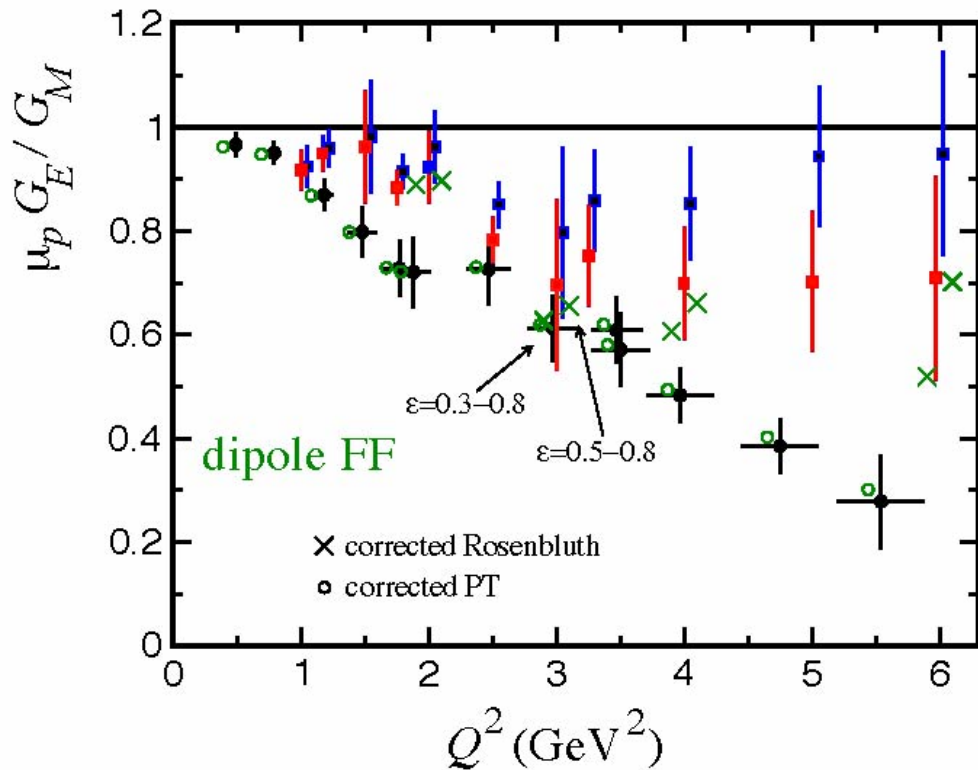


Two-Photon Contributions (cont.)

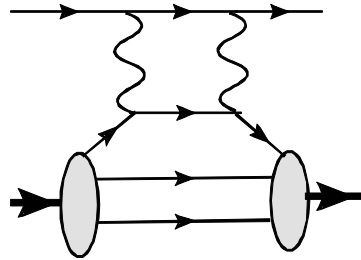
Blunden, Melnitchouk and Tjon (nucl-th/0306076) investigated the box (and cross) diagram in the radiative correction, but only the **elastic** contribution. The γp form factor was assumed to follow a **monopole** dependence.

Need estimate of inelastic (resonance) contributions!

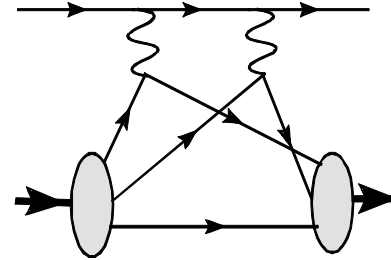
Recent calculations use a more realistic **dipole** form factor, decreases the discrepancy even more



Partonic calculation of two-photon exchange contribution



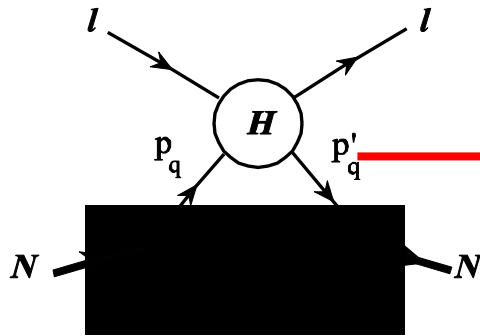
"handbag"



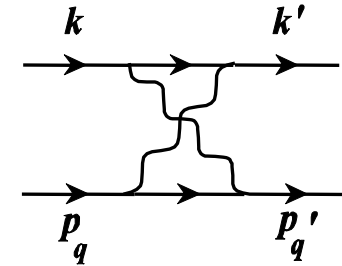
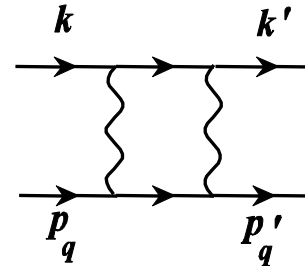
"cat's ears"

- main contribution at large Q^2 :
handbag diagrams (one active quark)
- to reproduce the IR divergent contribution at nucleon correctly (i.e. to satisfy the Low Energy Theorem)
need cat's ears diagrams (two active quarks)

Calculation of hard scattering amplitude



hard
scattering
amplitude



$$H_{h,\lambda} = \frac{(ee_q)^2}{Q^2} \bar{u}(k', h) \gamma_\mu u(k, h) \cdot \bar{u}(p'_q, \lambda) \left(\tilde{f}_1 \gamma^\mu + \tilde{f}_3 \gamma \cdot K P_q^\mu \right) u(p_q, \lambda)$$

electron helicity

quark helicity

$$K \equiv (k + k')/2$$

$$P_q \equiv (p_q + p'_q)/2$$

Calculation for $e_\mu \rightarrow e_\mu$ can be found in literature

(e.g. [van Nieuwenhuizen \(1971\)](#)), which was verified explicitly

IR divergences of boxes must disappear or cancel in the end,
regularize through photon mass λ

Separation soft-hard parts in electron-quark box

Follow the decomposition of **Grammer and Yennie (1973)** :

soft part calculated as 3-point function

reproduces Low Energy Theorem

kinematics partonic subprocess : $\hat{s} \equiv (k + p_q)^2$, $\hat{u} \equiv (k - p'_q)^2$, $\hat{s} + \hat{u} = Q^2$

$$\mathcal{R}(\tilde{f}_1^{soft}) = \frac{e^2}{4\pi^2} \left\{ \ln \left(\frac{\lambda^2}{\sqrt{-\hat{s}\hat{u}}} \right) \ln \left| \frac{\hat{s}}{\hat{u}} \right| + \frac{\pi^2}{2} \right\}$$

$$\mathcal{R}(\tilde{f}_1^{hard}) = \frac{e^2}{4\pi^2} \left\{ \frac{1}{2} \ln \left| \frac{\hat{s}}{\hat{u}} \right| + \frac{Q^2}{4} \left[\frac{1}{\hat{u}} \ln^2 \left| \frac{\hat{s}}{Q^2} \right| - \frac{1}{\hat{s}} \ln^2 \left| \frac{\hat{u}}{Q^2} \right| - \frac{1}{\hat{s}} \pi^2 \right] \right\}$$

$$\mathcal{R}(\tilde{f}_3) = \frac{e^2}{4\pi^2} \frac{1}{\hat{s}\hat{u}} \left\{ \hat{s} \ln \left| \frac{\hat{s}}{Q^2} \right| + \hat{u} \ln \left| \frac{\hat{u}}{Q^2} \right| + \frac{\hat{s} - \hat{u}}{2} \left[\frac{\hat{s}}{\hat{u}} \ln^2 \left| \frac{\hat{s}}{Q^2} \right| - \frac{\hat{u}}{\hat{s}} \ln^2 \left| \frac{\hat{u}}{Q^2} \right| - \frac{\hat{u}}{\hat{s}} \pi^2 \right] \right\}$$

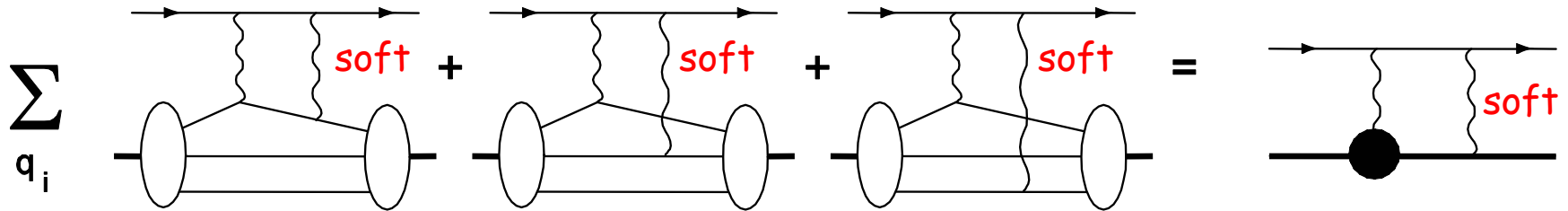
Calculation of soft part at nucleon level

LET : sum of soft contributions from the partonic calculation has to match the soft contributions at nucleonic level

To satisfy the LET, one has to include the

soft-photon contributions from the cats' ears diagrams

Pictorially :

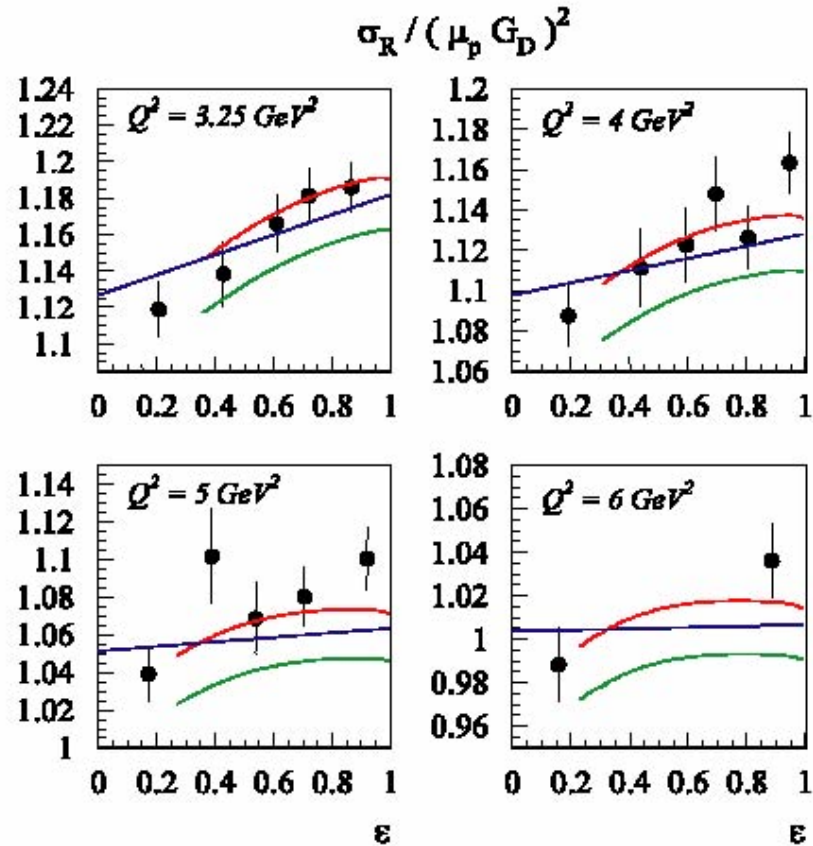
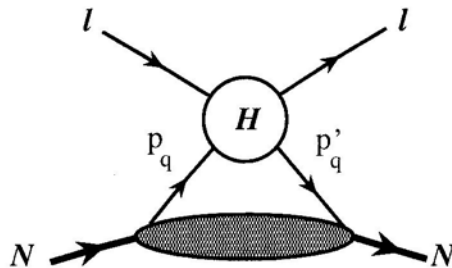


Two-Photon Contributions (cont.)

Chen et al., hep/ph-0403058

Model schematics:

- Hard eq-interaction
- GPDs describe quark emission/absorption
- Soft/hard separation
- Assume factorization



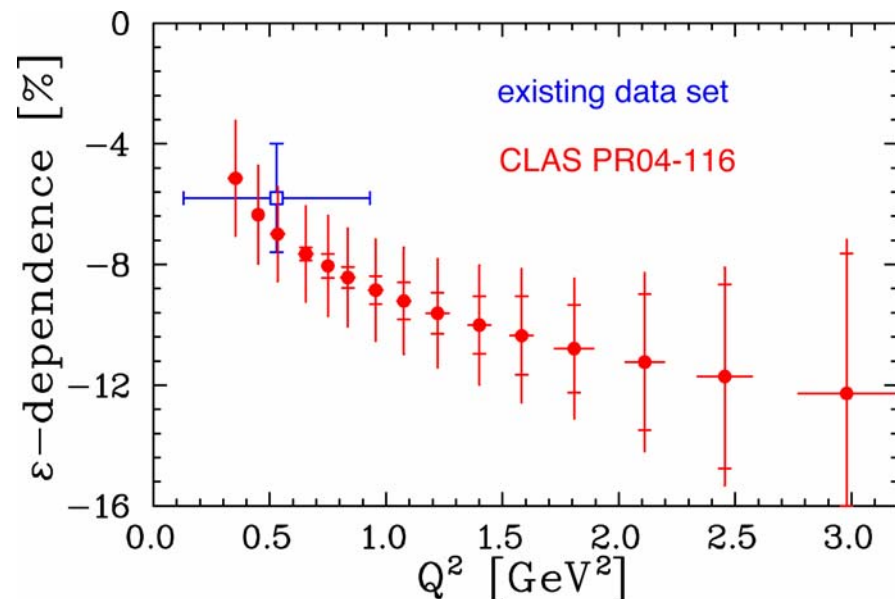
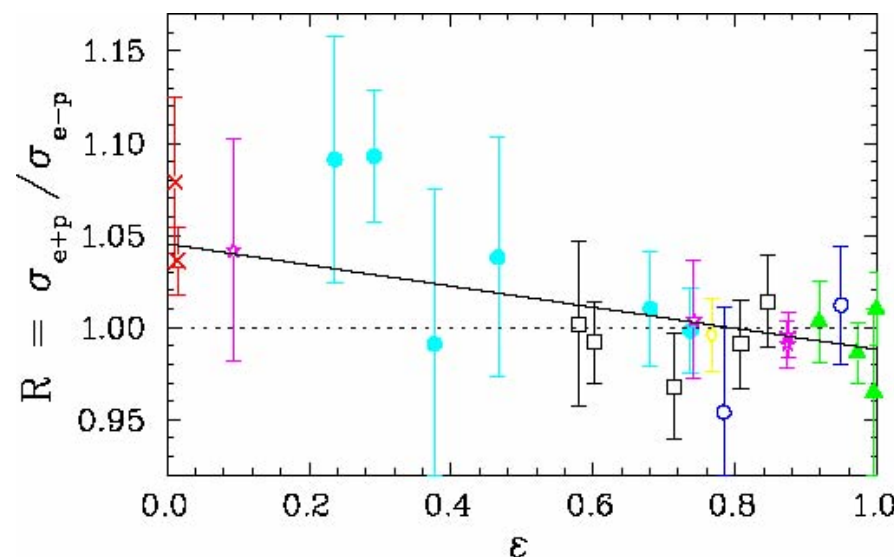
Polarization transfer
 $1\gamma+2\gamma(\text{hard})$
 $1\gamma+2\gamma(\text{hard+soft})$

Experimental Verification of TPE contributions

Experimental verification

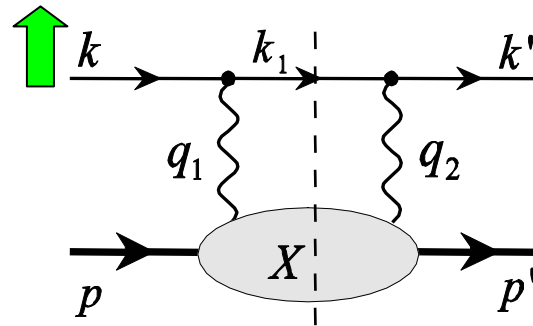
- non-linearity in ε -dependence (test of model calculations)
- transverse single-spin asymmetry (imaginary part of two-photon amplitude)
- ratio of e^+p and e^-p cross section (direct measurement of two-photon contributions)

CLAS experiment E04-116 aims at a measurement of the ε -dependence for Q^2 -values up to 2.0 GeV^2



SSA in elastic eN scattering

spin of **beam** OR **target**
NORMAL to scattering
 plane



$$s = (k + p)^2$$

on-shell intermediate state ($M_X = W$)

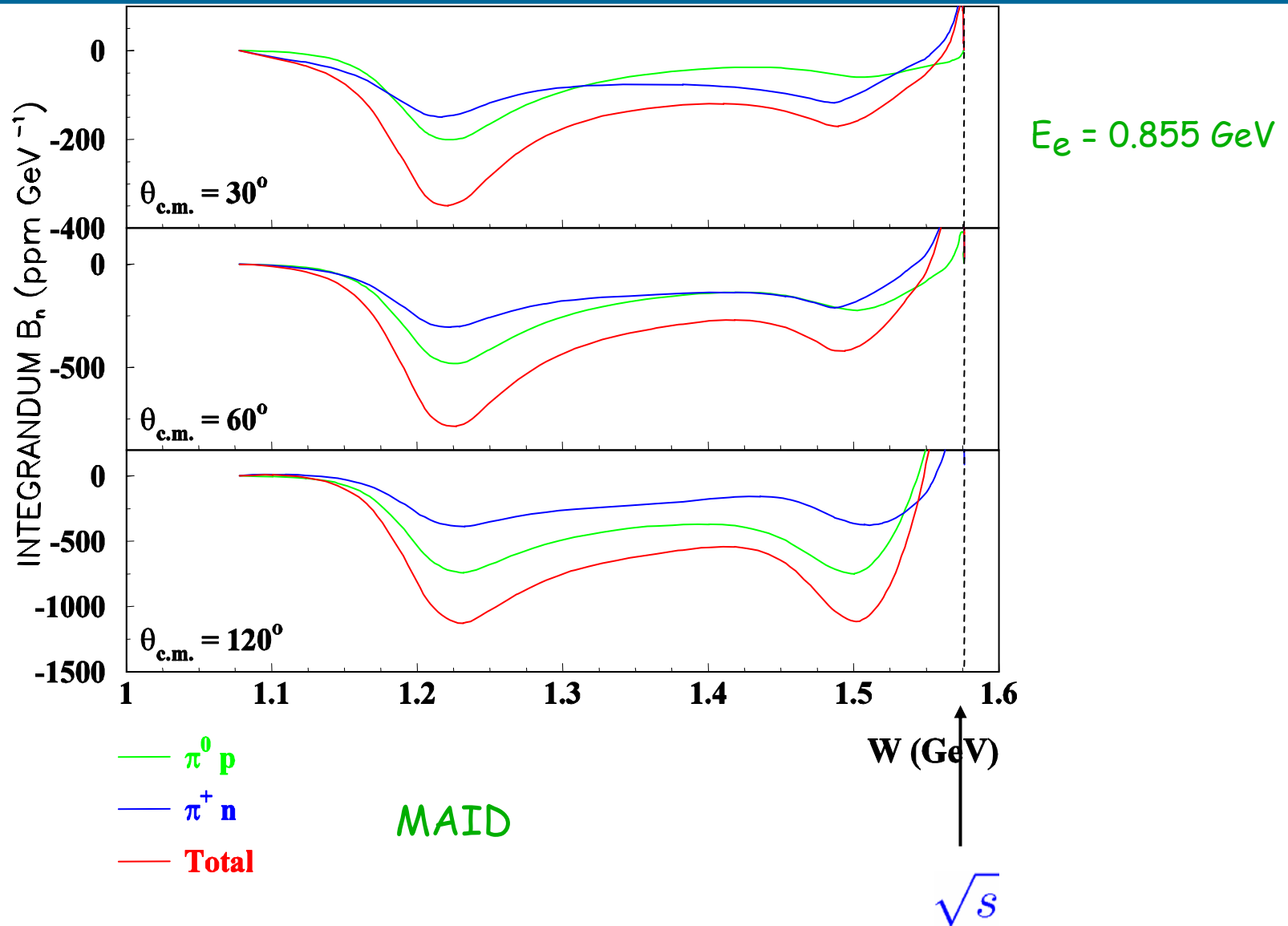
$$A_n = -\frac{1}{(2\pi)^3} \frac{e^2 (1 - \varepsilon)}{8 Q^2} \int_{M^2}^s dW^2 \frac{|\vec{k}_1|^2}{4\sqrt{s}} \int d\Omega_{k_1} \frac{1}{Q_1^2 Q_2^2} \mathcal{I}(L_{\alpha\mu\nu} H^{\alpha\mu\nu})$$

lepton $L_{\alpha\mu\nu} = \bar{u}(k', h') \gamma_\mu (\gamma \cdot k_1 + m_e) \gamma_\nu u(k, h) \cdot [\bar{u}(k', h') \gamma_\alpha u(k, h)]^*$

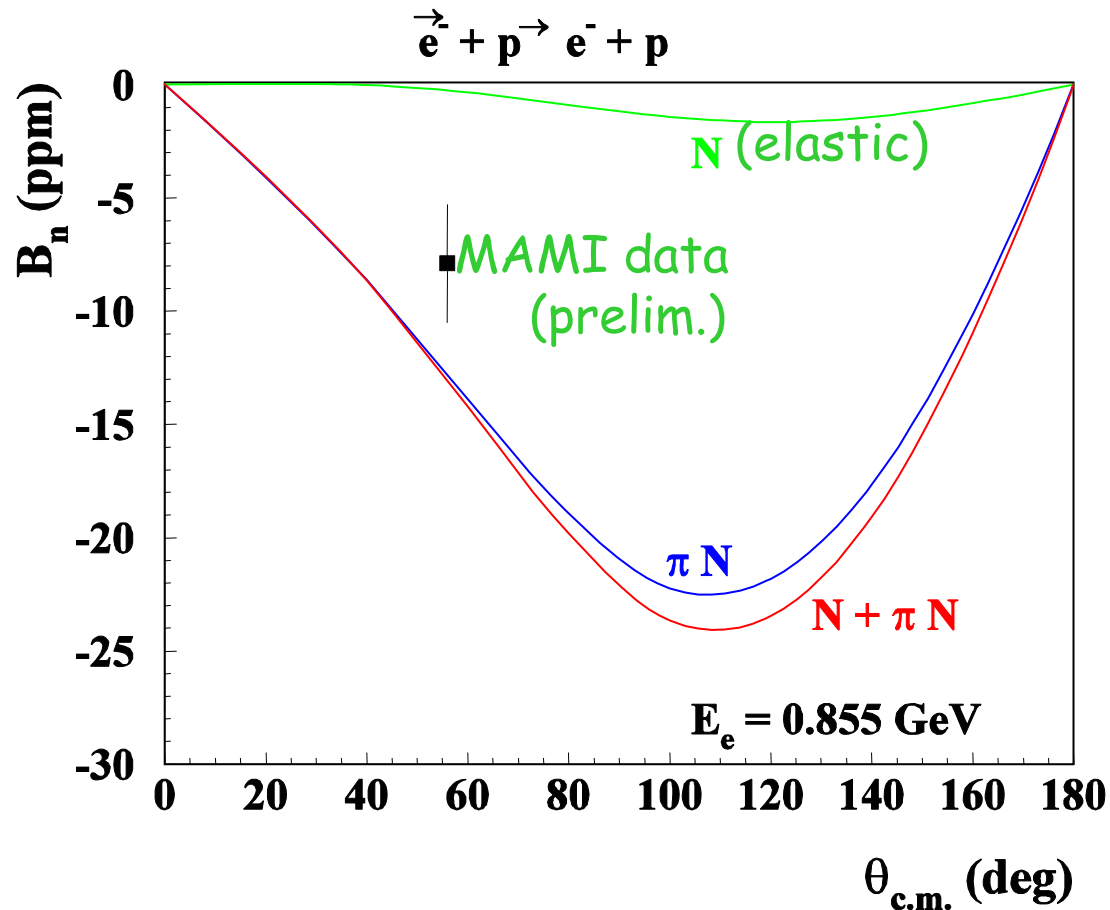
hadron $H^{\alpha\mu\nu} = W^{\mu\nu} \cdot \left[\bar{u}(p', \lambda'_N) \left(G_M \gamma^\alpha - F_2 \frac{P^\alpha}{M} \right) u(p, \lambda_N) \right]^*$

$$W^{\mu\nu} = \sum (2\pi)^4 \delta^4(p + q_1 - p_X) \langle p' \lambda'_N | J^\mu(0) | X \rangle \langle X | J^\nu(0) | p \lambda_N \rangle$$

Integrand : **beam** normal spin asymmetry



Beam normal spin asymmetry



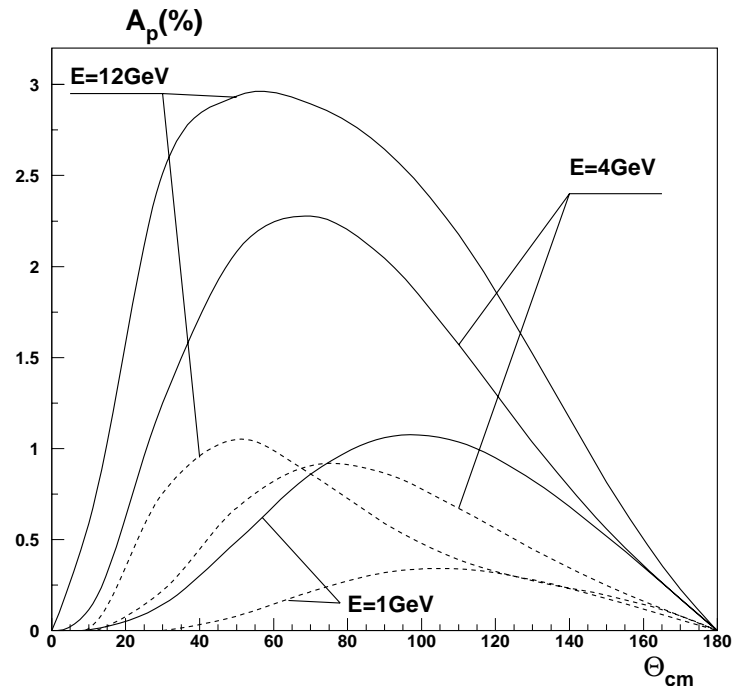
Single-spin (beam or target) asymmetries

Normal beam asymmetry

- Requires electron helicity flip
- $\sim 10^{-5}$ effect, measurable in parity-violation experimental setup
- Inelastic intermediate excitations lead to the enhanced normal beam asymmetry by large double logarithms $\sim \log^2(Q^2/m_e^2)$ due to emission of hard collinear quasi-real photons
- When beam energy exceeds a few GeV, at fixed Q^2 the asymmetry reaches a constant limit controlled by the total photoproduction cross section $\sigma_{\gamma p}$

A. Afanasev, N. Merenkov, accepted in PRL

Normal target asymmetry=polarization



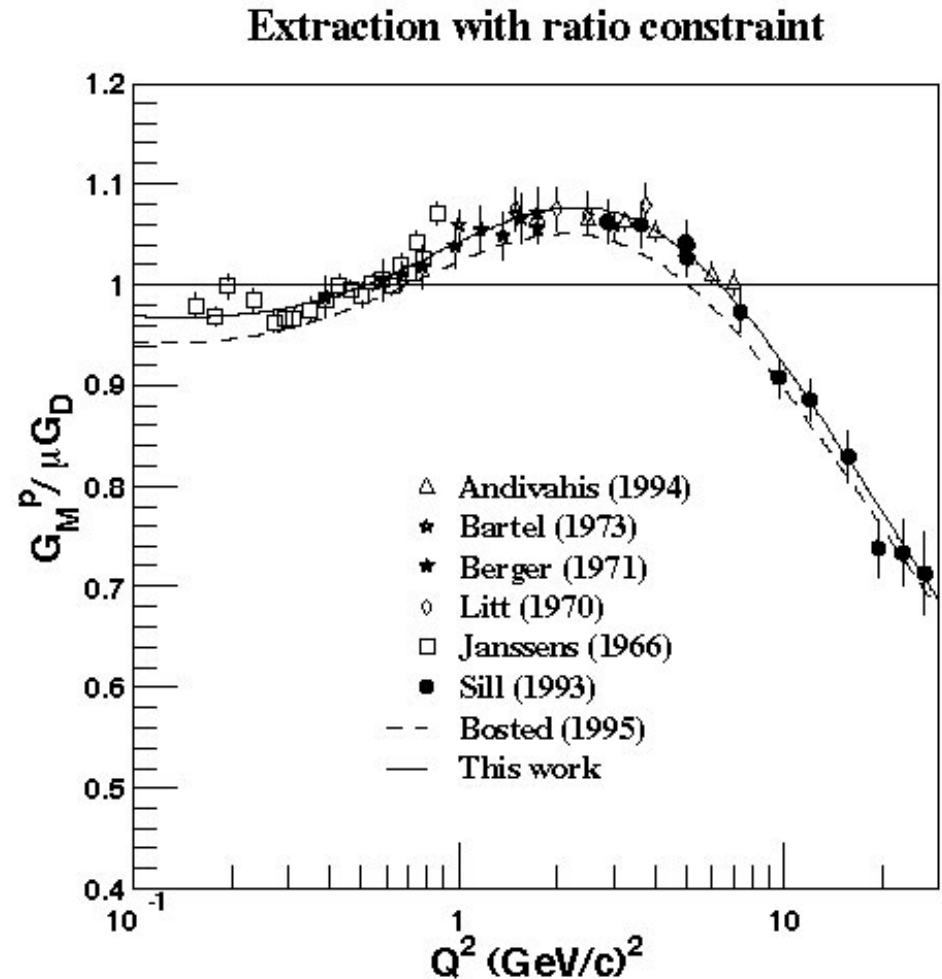
Dotted: Unexcited intermediate proton,

Solid: Total, using a model for non-forward Compton amplitude

A.Afanasev et al., hep-ph/0208260

Reanalysis of SLAC data on G_M^p

E. Brash *et al.*, PRC 65, 051001 (2002), have reanalyzed the SLAC data with JLab G_E^p/G_M^p results as constraint, using a similar fit function as Bosted. The reanalysis results in 1.5-3% increase of the G_M^p data.



Summary of Experimental Data

- Very active experimental program at Bates, Mainz, JLab on nucleon form factors thanks to development of polarized beam ($> 100 \mu\text{A}$, $> 75\%$), polarized targets and polarimeters with large analyzing powers
- G_E^p Precise data set up to $Q^2 = 5.6 \text{ GeV}^2$
charge FF differs from magnetization FF
discrepancy between Rosenbluth and polarization transfer not an experimental problem, probably due to TPE in radiative corrections
- G_E^n 3 successful experiments, precise data up to $Q^2 = 1.5 \text{ GeV}^2$
- G_M^n $Q^2 < 1 \text{ GeV}^2$ data from ${}^3\text{He}(e, e')$
 $Q^2 < 5 \text{ GeV}^2$ data from ${}^2\text{H}(e, e'n)/{}^2\text{H}(e, e'p)$ in CLAS
- Strong support from theory community on two-photon exchange contributions



Theory

- ▲ Low Q^2
- ▲ Vector Meson Dominance
- ▲ Chiral Soliton
- ▲ Lattice QCD
- ▲ Relativistic Constituent Quarks
- ▲ High Q^2
- ▲ Quark Orbital Angular Momentum
- ▲ The shape of the proton

Charge and Magnetization Radii

$$\langle r^2 \rangle \equiv 4\pi \int \rho(r) r^4 dr = -\frac{6}{G(0)} \frac{dG(Q^2)}{dQ^2} \Big|_{Q^2=0}$$

Experimental values

$$\langle r_{E,p}^2 \rangle^{1/2} = 0.895 \pm 0.018 \text{ fm}$$

$$\langle r_{M,p}^2 \rangle^{1/2} = 0.855 \pm 0.035 \text{ fm}$$

$$\langle r_{E,n}^2 \rangle = -0.0119 \pm 0.003 \text{ fm}^2$$

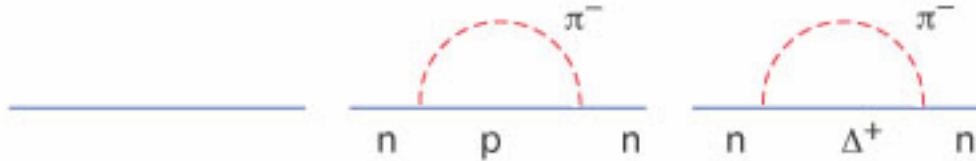
$$\langle r_{M,n}^2 \rangle^{1/2} = 0.87 \pm 0.01 \text{ fm}$$

- Ingo Sick has proven that it is essential to include Coulomb distortion effects, even in the low Q^2 -region
- The three non-zero radii are identical within experimental accuracy
- The proton charge radius is in excellent agreement with three-loop QED calculation of hydrogen Lamb shift
- Neutron charge radius was determined by measuring the transmission of slow neutrons through atomic electrons of a heavy atom (Bi,Pb)

Why is neutron charge radius negative?

Hadron Picture

$p\pi^-$ component in neutron wavefunction
 π^- cloud on outside



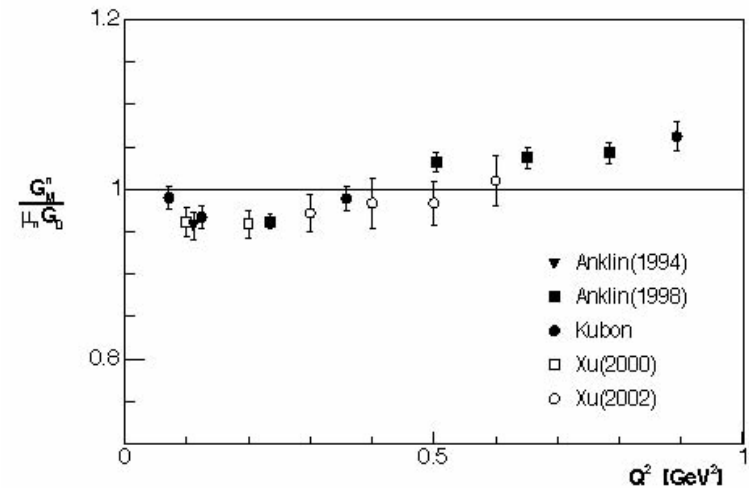
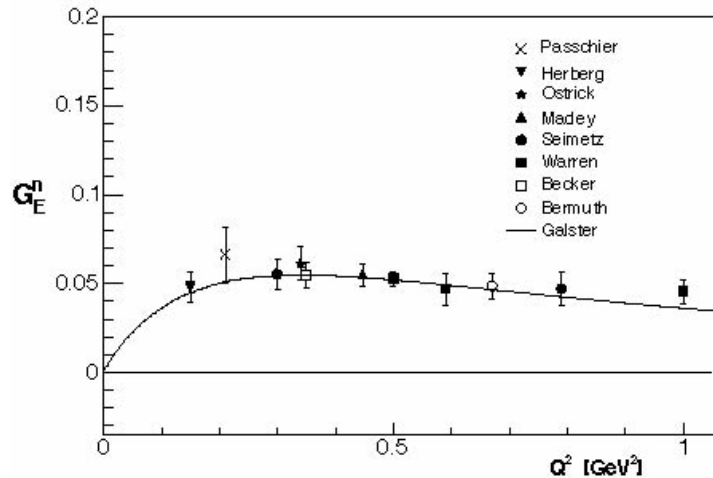
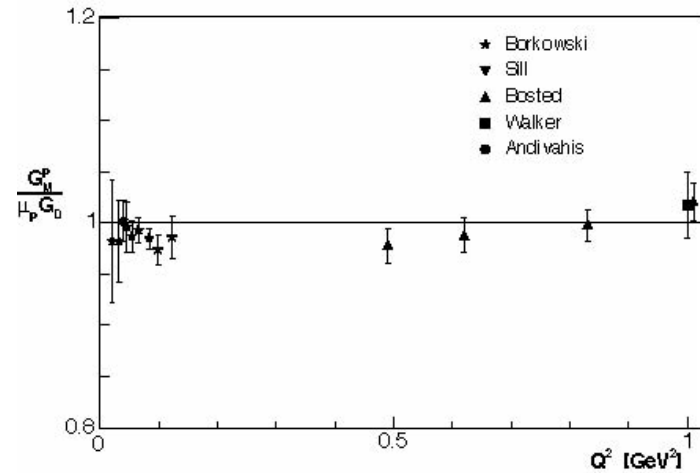
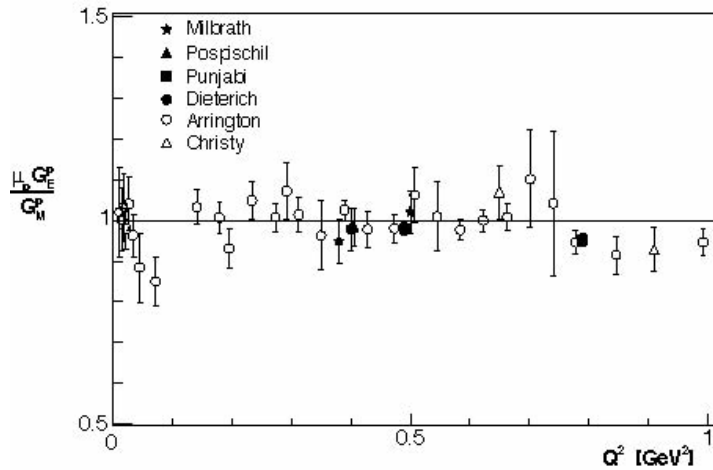
CQM

neutron = udd and spin-spin forces create a charge segregation

$$\left. \frac{dG_E^n(Q^2)}{dQ^2} \right|_{Q^2=0} = \left. \frac{dF_1^n(Q^2)}{dQ^2} \right|_{Q^2=0} - \frac{F_2^n(0)}{4M^2}$$

Foldy term = -0.0126 fm^2 canceled by relativistic corrections (Isgur)
implying neutron charge distribution is determined by G_E^n

Low- Q^2 Behaviour

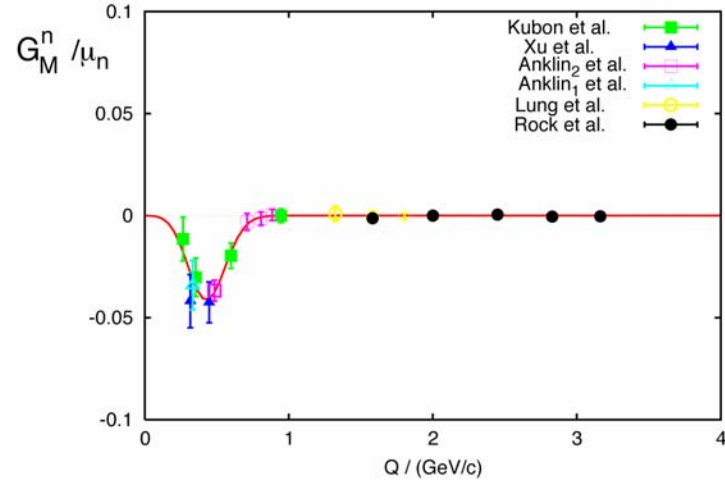
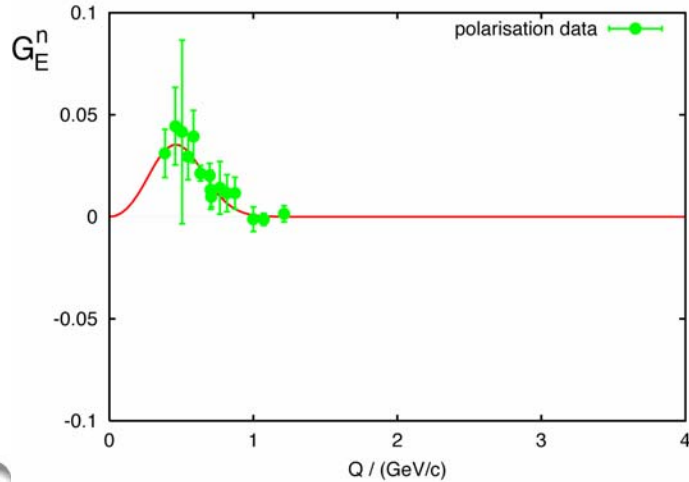
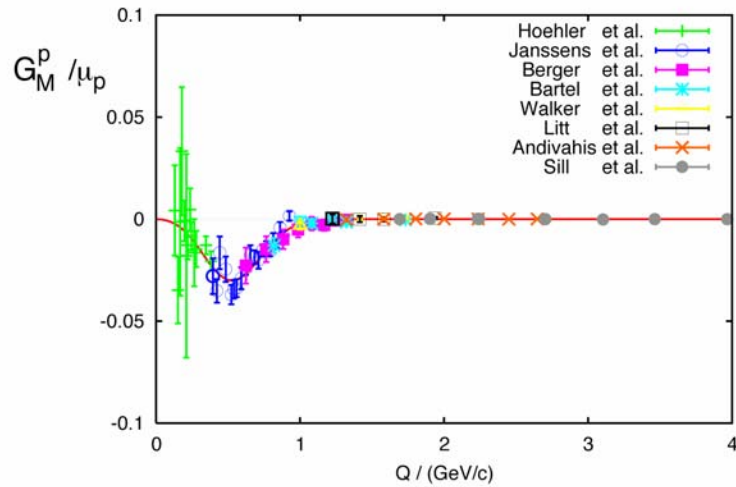
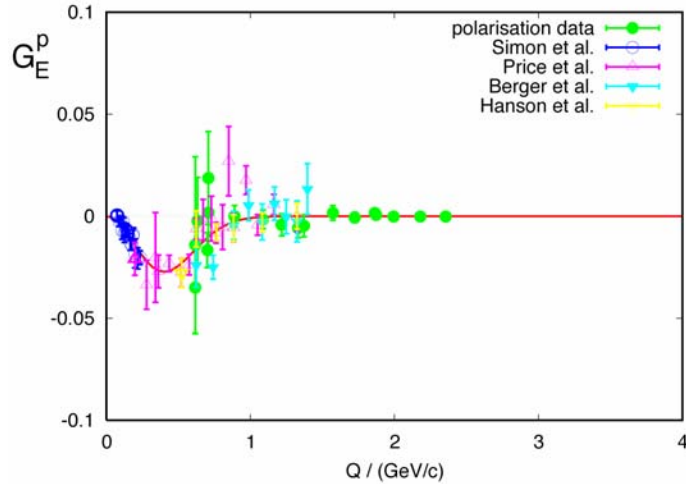


All EMFF allow shallow minimum (max for G_E^n) at $Q \sim 0.5$ GeV

Analysis by Friedrich & Walcher

Formfactors - “smooth contribution”

“smooth contribution” = 2 dipoles, “bump” = “Gaussian”

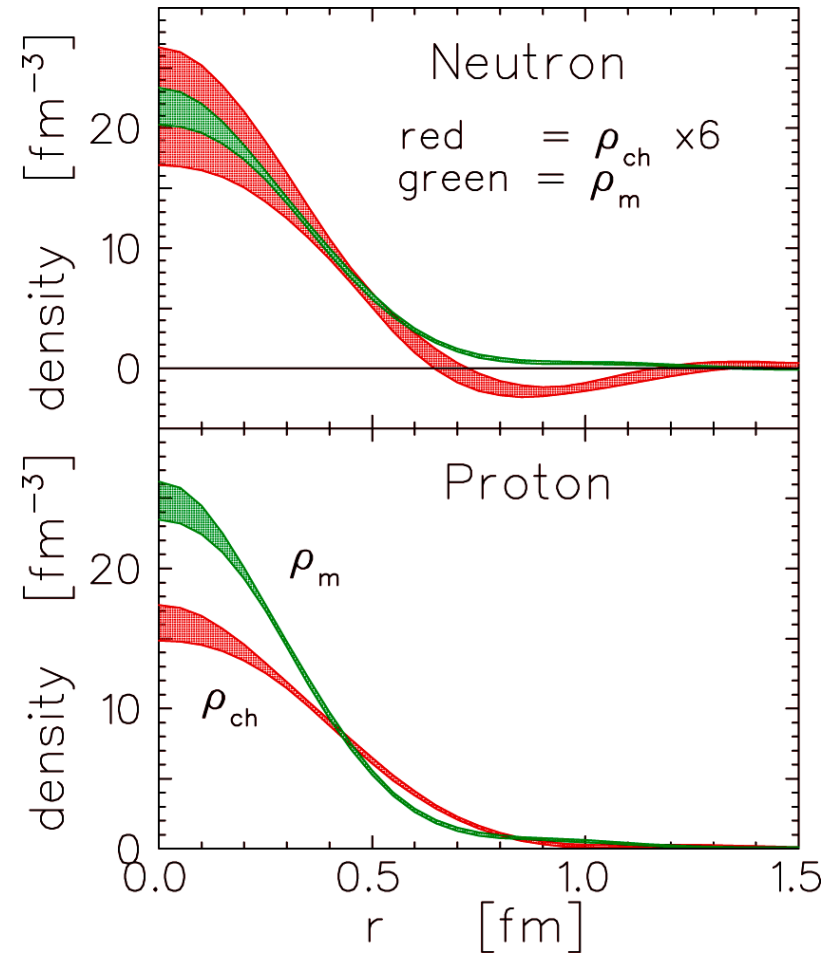


Pion Cloud

- Kelly has performed simultaneous fit to all four EMFF in coordinate space using a Laguerre-Gaussian expansion and first-order approximation for Lorentz contraction of local Breit frame

$$\tilde{G}_{E,M}(k) = G_{E,M}(Q^2)(1 + \tau)^2 \quad \text{with} \quad k^2 = \frac{Q^2}{1 + \tau} \quad \text{and} \quad \tau = \left(\frac{Q}{2M}\right)^2$$

- He observes a structure in the proton and neutron densities at ~ 0.9 fm which he assigns to a (single-loop) pion cloud



- Using dispersion relations Hammer et al. have extracted the pion cloud assigned to the $NN2\pi$ component which they find to peak at ~ 0.4 fm

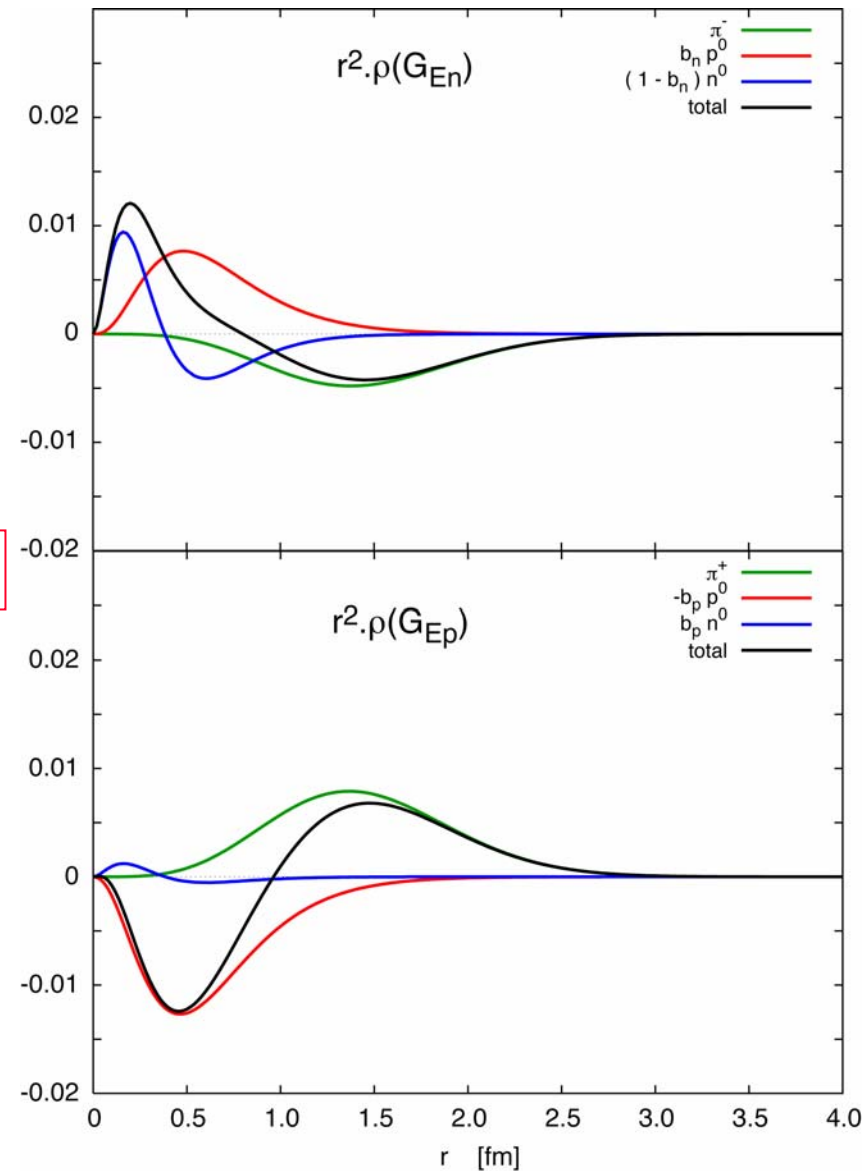
Analysis by Friedrich & Walcher (cont.)

- A Gaussian peaking at $Q \sim 0.4-0.5 \text{ GeV}$ transforms into a structure in coordinate space peaking at $\sim 1.2-1.5 \text{ fm}$
- Friedrich & Walcher analyzed the world data set describing the nucleons as the sum of a bare nucleon plus a polarisation part:

$$G_{n,p} = G_{n,p}^0 + G_{n,p}^{pol} \quad \text{with} \quad G_{n,p}^{pol} = b_{n,p} [G_{p,n}^0 - G_{n,p}^0 + G^{\pi}]$$

- The bare nucleon FF were described as the sum of constituent-quark FF with a dipole behaviour
- The pion FF was assumed to have a HO-type wave function
- Isospin invariance was also imposed:

$$G^{up} \approx G^{dn} \quad G^{dp} \approx G^{un} \quad G^{\pi^+} \approx G^{\pi^-}$$



Theory

$$F_{1,2}^{is,iv} = \sum g_X \frac{m_X^2}{m_X^2 + Q^2} F_{1,2}(Q^2)$$

▲ Vector Meson Dominance

Photon couples to nucleon exchanging vector meson (ρ, ω, ϕ)

Adjust high- Q^2 behaviour to pQCD scaling

Include 2π -continuum in finite width of ρ

- Lomon 3 isoscalar, isovector poles, intrinsic core FF
- Iachello 2 isoscalar, 1 isovector pole, intrinsic core FF
- Hammer 4 isoscalar, 3 isovector poles, no additional FF

▲ Relativistic chiral soliton model

- Holzwarth one VM in Lagrangian, boost to Breit frame
- Goeke NJL Lagrangian, few parameters

▲ Lattice QCD (Schierholz, QCDSF)

quenched approximation, box size of 1.6 fm, $m_\pi = 650$ MeV

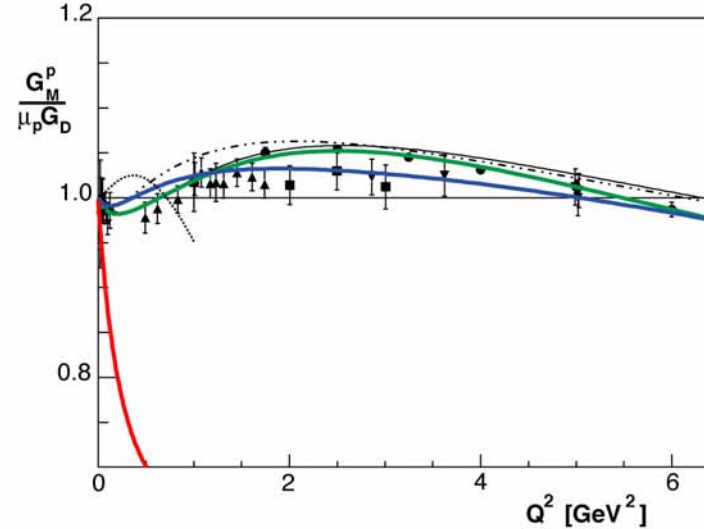
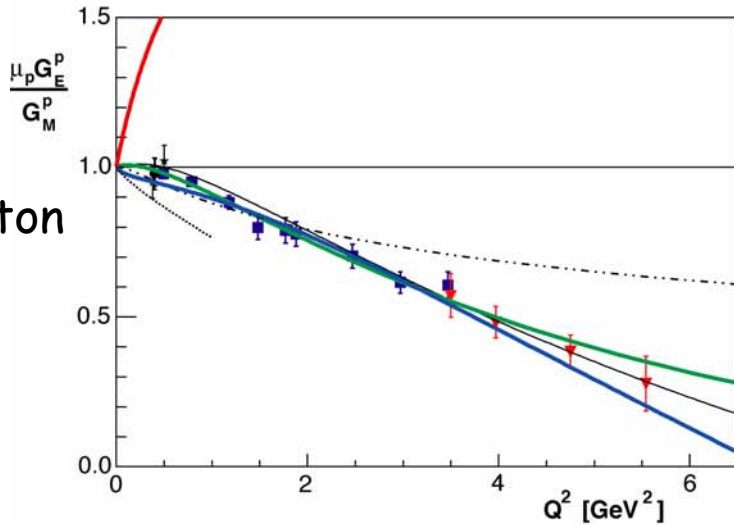
chiral extrapolation to $m_\pi = 140$ MeV (Adelaide)

Vector-Meson Dominance

charge

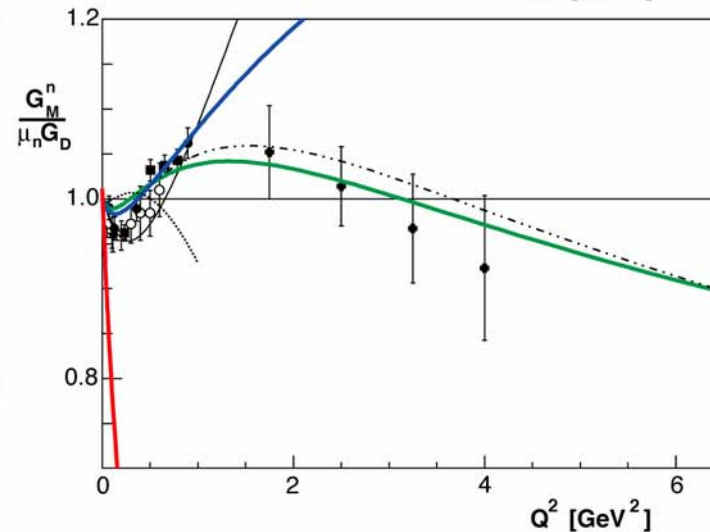
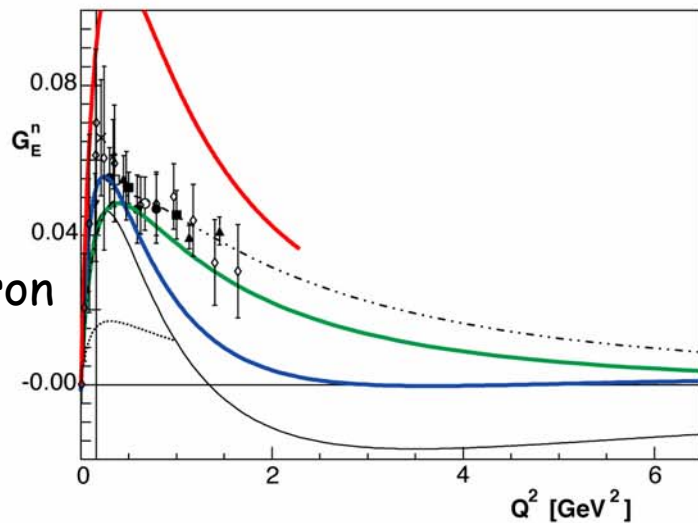
magnetization

proton



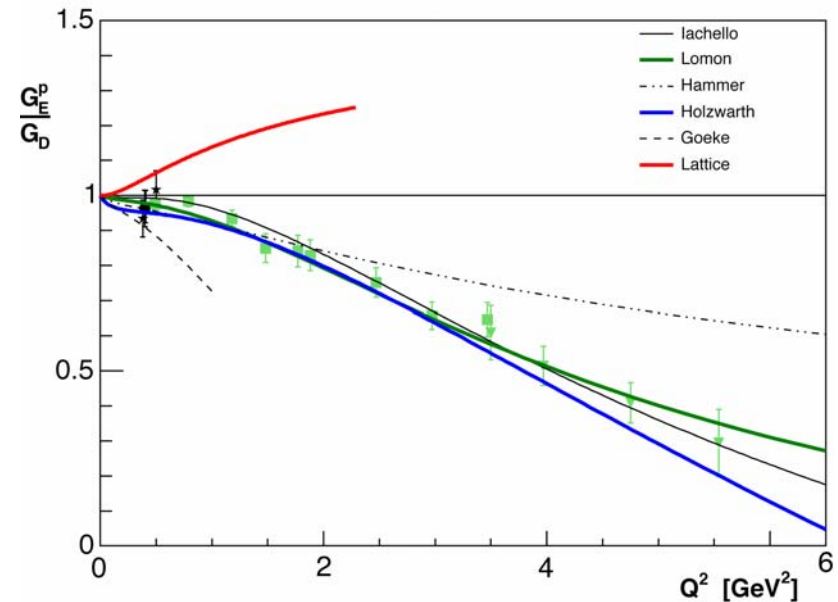
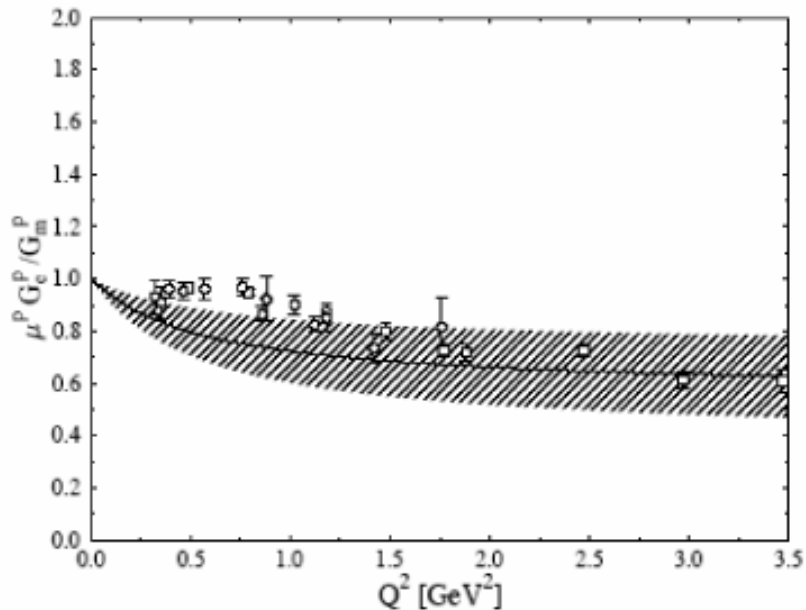
- Lachello
- Lomon
- · - · Hammer
- Holzwarth
- Goeke
- Lattice

neutron



Chiral Extrapolation of Lattice QCD

- Problem is how to extrapolate LQCD results to the physical pion mass
- QCDSF group uses a linear extrapolation in m_π for the dipole mass fitted to the FF
- Adelaide group uses the same for the isoscalar radii, but an $a/m_\pi + b \ln(m_\pi)$ behaviour for the isovector radii
- Additionally, one should question whether a chiral extrapolation is valid at $m_\pi=650$ MeV



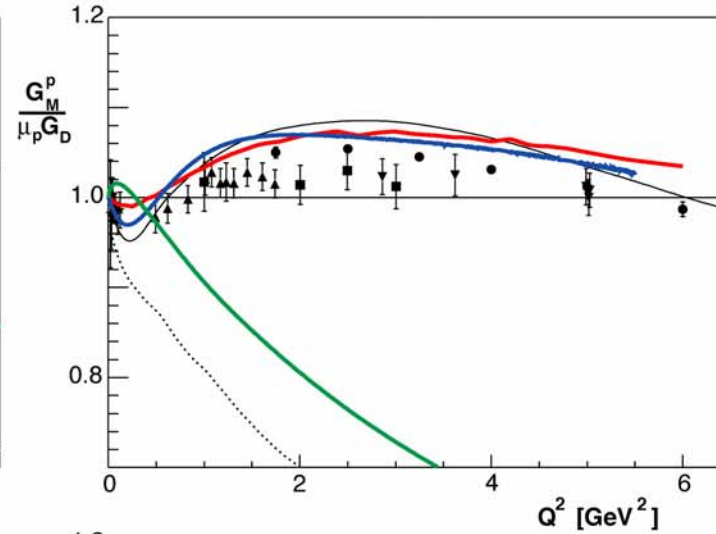
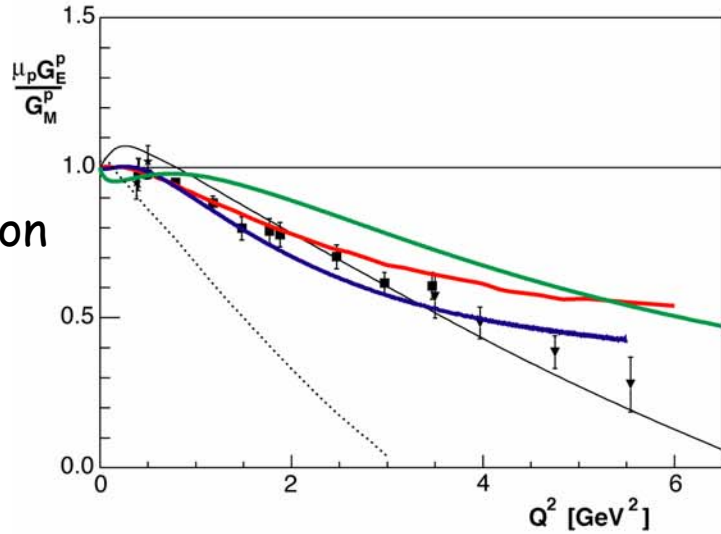
Theory

- Relativistic Constituent Quark Models
Variety of q - q potentials (harmonic oscillator, hypercentral, linear)
Non-relativistic treatment of quark dynamics, relativistic EM currents
- Miller: extension of cloudy bag model, light-front kinematics
wave function and pion cloud adjusted to static parameters
- Cardarelli & Simula
Isgur-Capstick one-gluon-exchange potential, light-front kinematics, constituent quark FF in agreement with DIS data
- Wagenbrunn & Plessas
point-form spectator approximation
linear confinement potential, Goldstone-boson exchange
- Giannini et al.
gluon-gluon interaction in hypercentral model
boost to Breit frame
- Metsch et al.
solve Bethe-Salpeter equation, linear confinement potential

Relativistic Constituent Quark

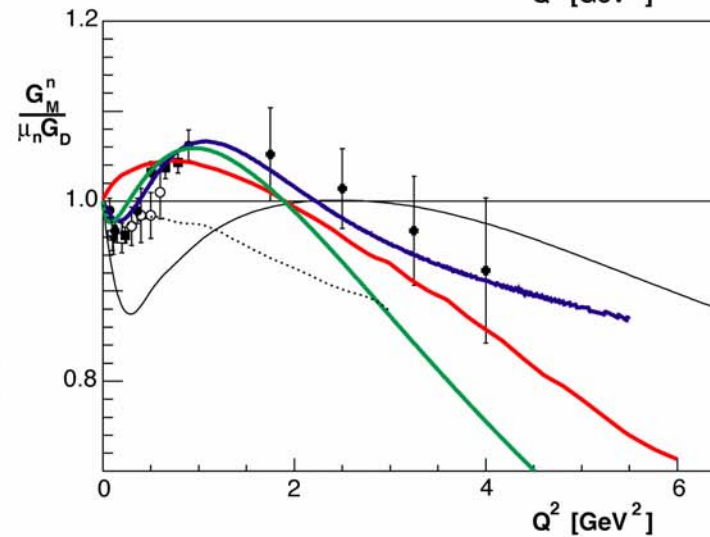
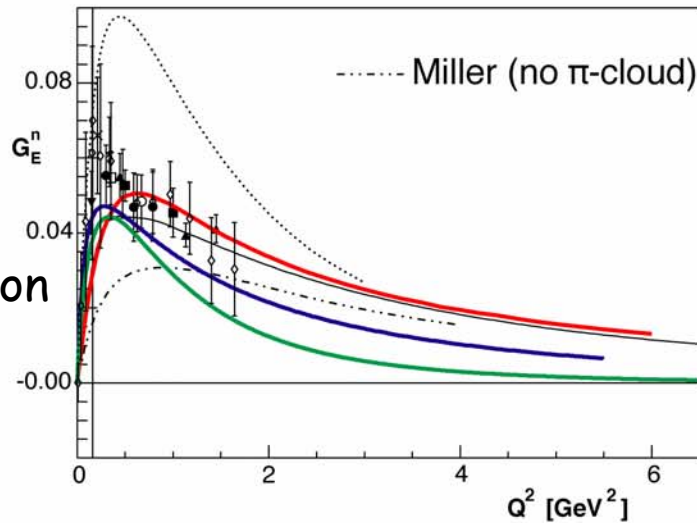
charge

magnetization



- Miller
- Simula
- Giannini
- Plessas
- Metsch

proton



neutron



Thomas Jefferson National Accelerator Facility

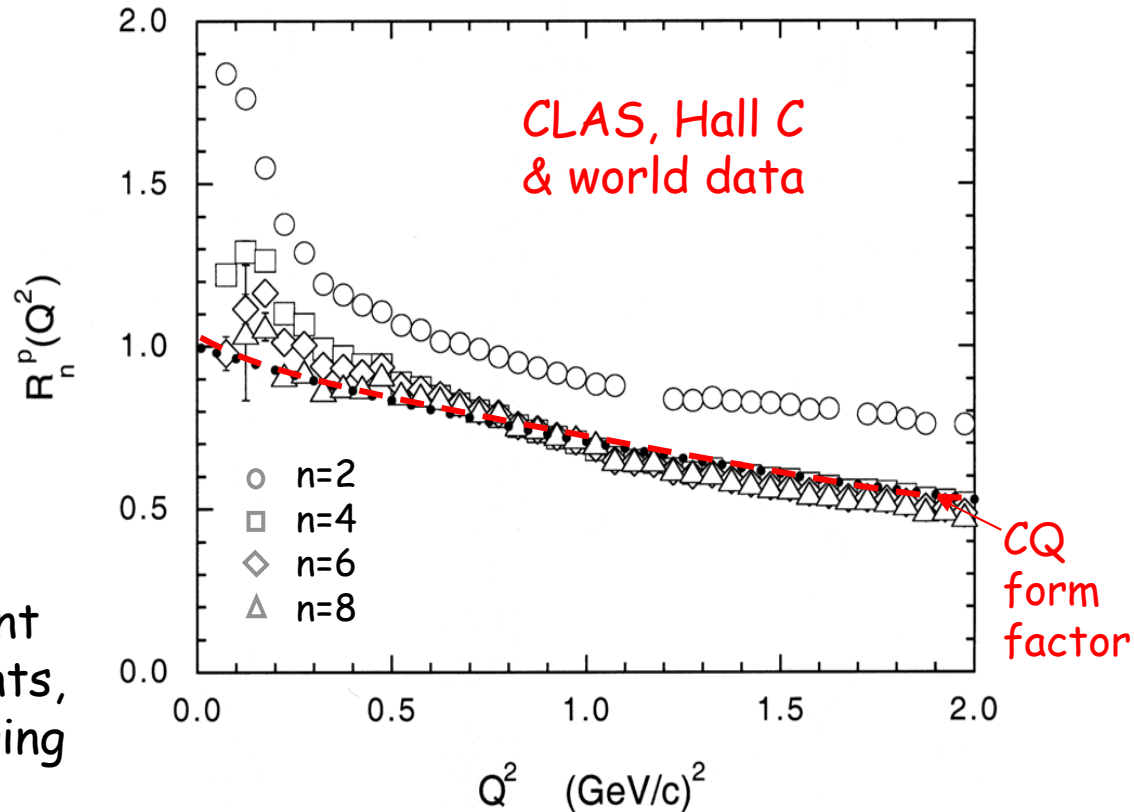
Constituent Quarks as Extended Objects?

$$R_n^p(Q^2) = M_n^p(Q^2)/M_n^p(Q^2)$$

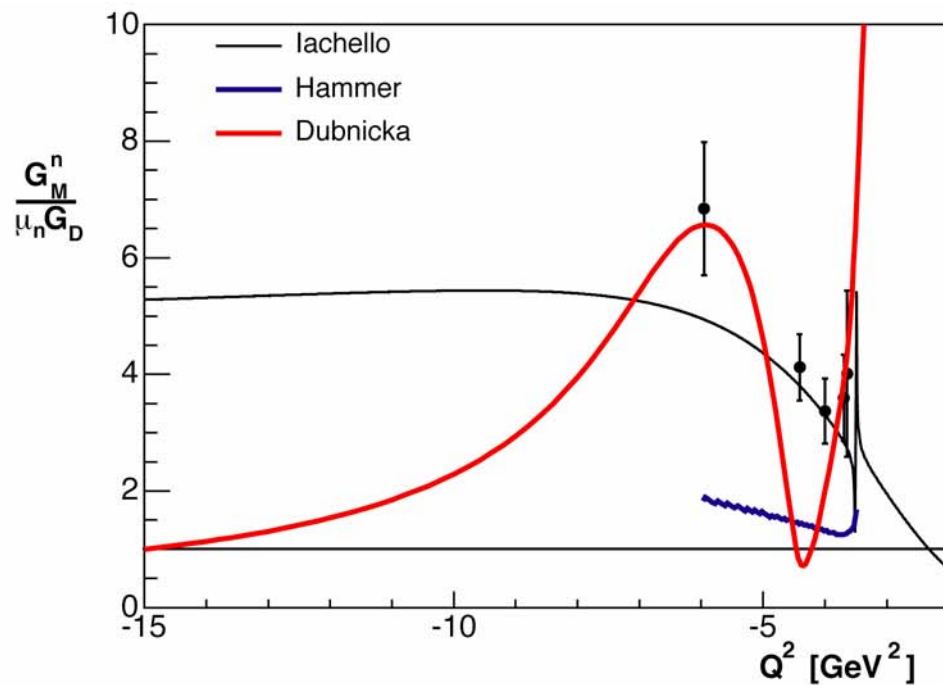
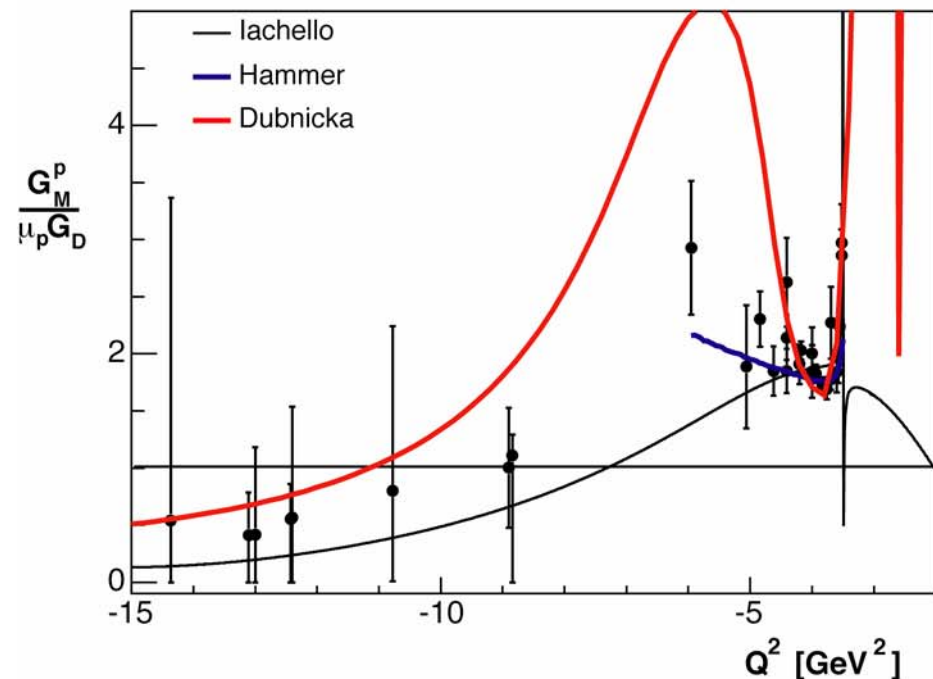
M_n^p - Theoretical moments of the model with point-like CQs

R. Petronzio, S. Simula, G. Ricco,
PRD 67, 09404 (2003)

The scaling behavior in the Q^2 -dependence observed for different orders n in the Nachtmann moments, is interpreted as "elastic" scattering off CQs with radius $\sim 0.2-0.3$ fm



Time-Like Region



- Data quality insufficient to separate charge and magnetization contributions
- No scaling observed with dipole form factor
- Iachello only model in reasonable agreement with data

Role of Quark Orbital Angular Momentum (OAM)

▲ Vital!

Image there is no OAM:

- $F_2 \otimes 0$,
- $\mathcal{E} \otimes 0$ (would have been discovered in 1933)

▲ Models consistent with the QCD picture:

- **Meson cloud model**

In which the anomalous magnetic moment is generated by orbital motion of pions around a bare nucleon

- **MIT bag model**

\mathcal{E} is proportional to the lower component of the quark wave function which is a p-wave

- ▲ It should not have been so surprising that the quark OAM might play a significant role in the nucleon spin

High- Q^2 behaviour

Basic pQCD (Bjorken) scaling predicts

$$F_1 \propto 1/Q^4; F_2 \propto 1/Q^6$$

$$\boxtimes F_2/F_1 \propto 1/Q^2 \text{ (Brodsky \& Farrar)}$$

Data clearly do not follow this trend

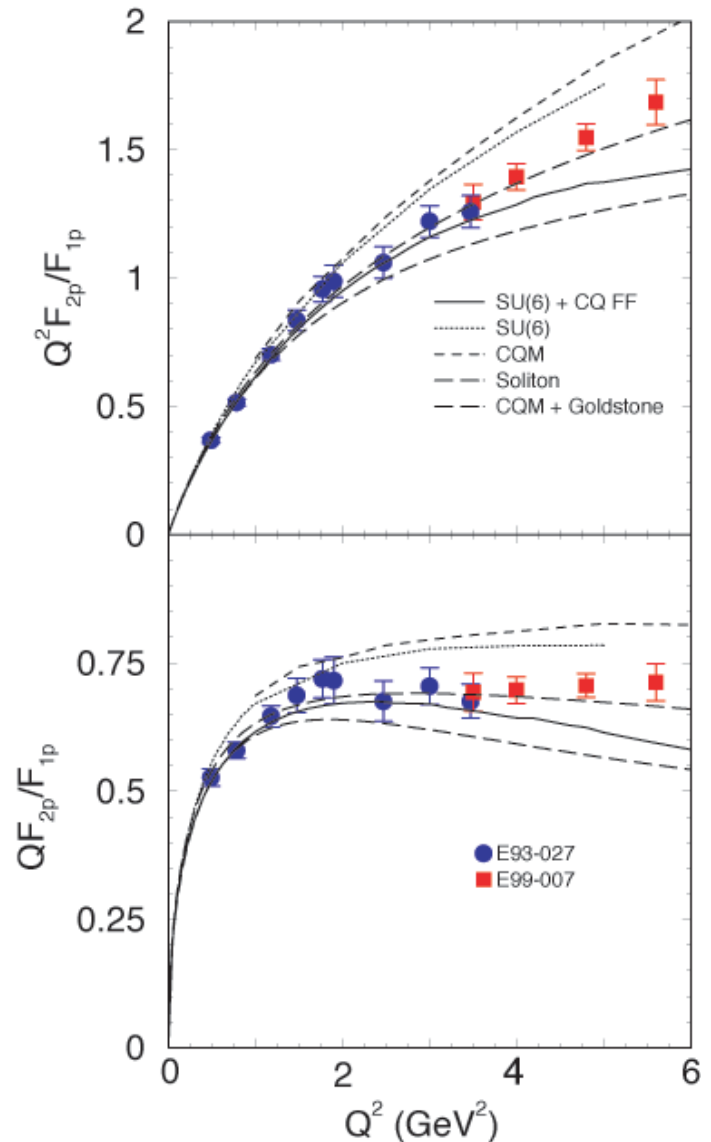
Schlumpf (1994), Miller (1996) and Ralston (2002) agree that by

- freeing the $p_T=0$ pQCD condition
- applying a (Melosh) transformation to a relativistic (light-front) system
- an orbital angular momentum component is introduced in the proton wf (giving up helicity conservation) and one obtains

$$\boxtimes F_2/F_1 \propto 1/Q$$

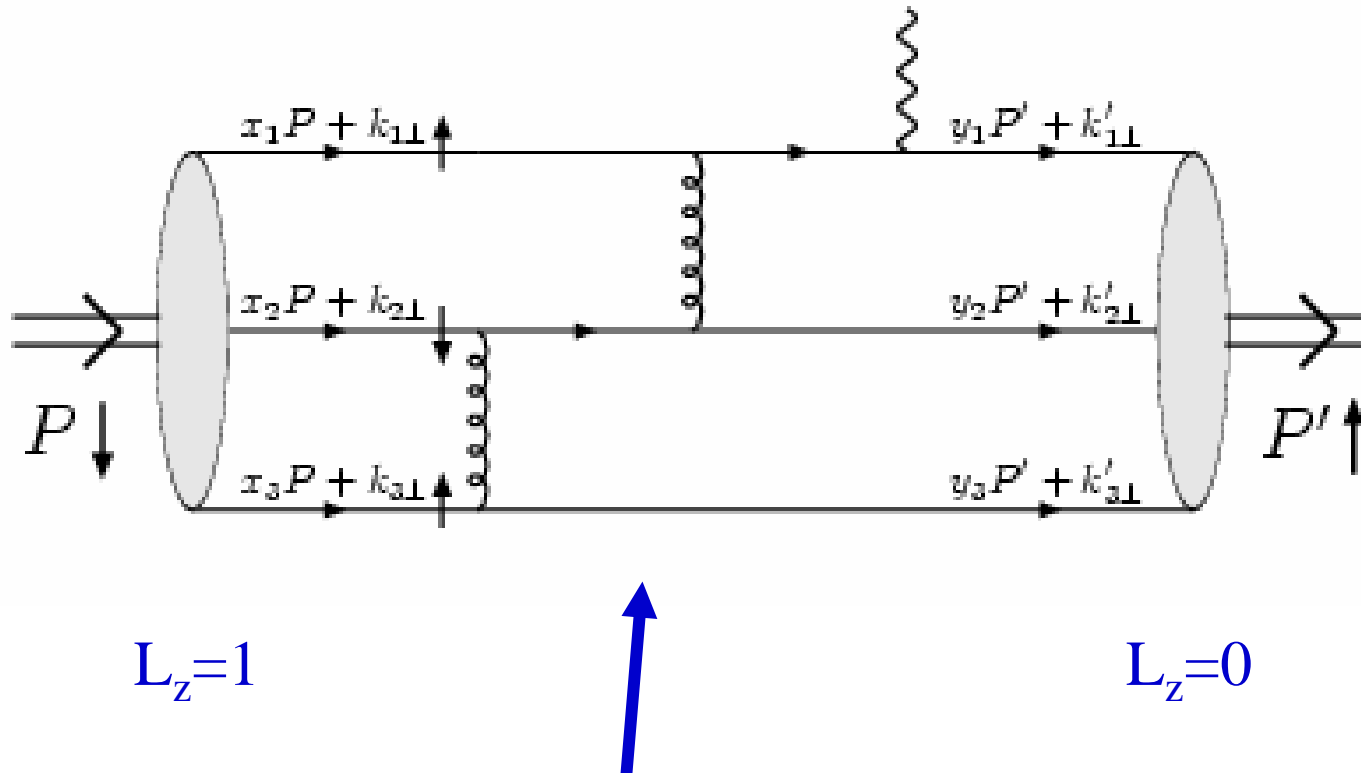
- or equivalently a linear drop off of G_E/G_M with Q^2

Brodsky argues that in pQCD limit non-zero OAM contributes to both F_1 and F_2



A pQCD Calculation of $F_2(Q)$

Belitsky, Ji & Yuan, PRL 91, 092003 (2003)



The hard part must create one unit of OAM. This can happen as easily for small- x quarks as for large- x ones.

Physics of Logs:

it has to do with the hard scattering

- ▲ The pQCD hard scattering must change the direction of three valence quarks.
- ▲ For F_2 , it also must create one unit of OAM
- ▲ The small x quarks contribute little to the linear momentum, but can contribute to the OAM just as easily as the large x quarks
 - Therefore, one needs to count the number of small x quarks,
↓ dx/x
- ▲ However, for $x < \Lambda/Q$, the quark is *de-localized* and its contribution is strongly suppressed because of the color (Sudakov suppression)

$$\int dx/x \sim \log Q$$

Result

They predict that F_2 goes like $\mathcal{O}_s^2(\ln^2 Q^2)/Q^6$ and so

$$\frac{F_2(Q^2)}{F_1(Q^2)} \sim \frac{1}{Q^2} \log^2(Q^2 / \Lambda^2)$$

The power behavior confirms the Brodsky et al. scaling prediction but it is accurate to logarithms!

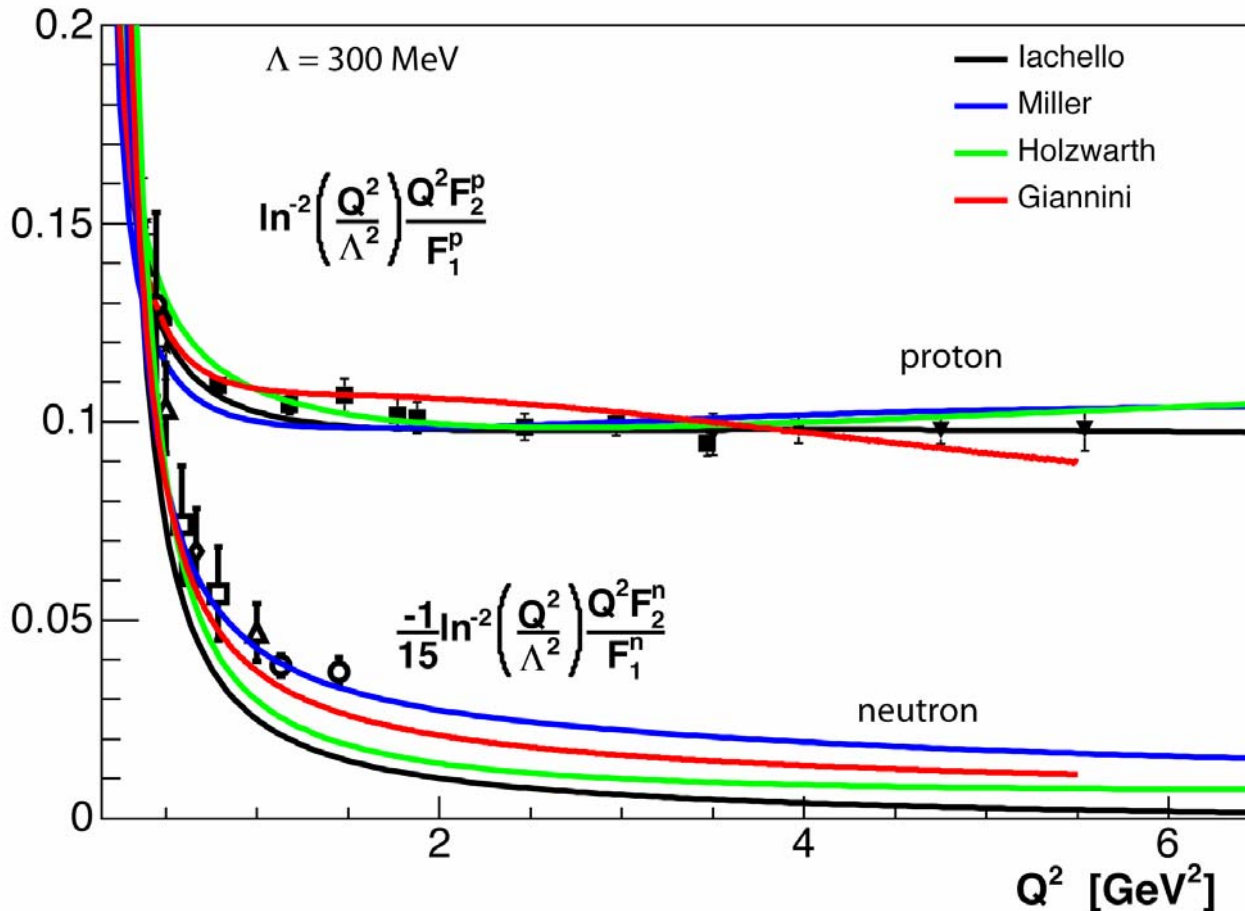
Brodsky, Hiller & Hwang

$$\frac{F_2(Q^2)}{F_1(Q^2)} = \frac{\mu_A}{1 + (Q^2/c) \ln^b(1 + Q^2/a)}$$

$$(b = \approx 0.6)$$

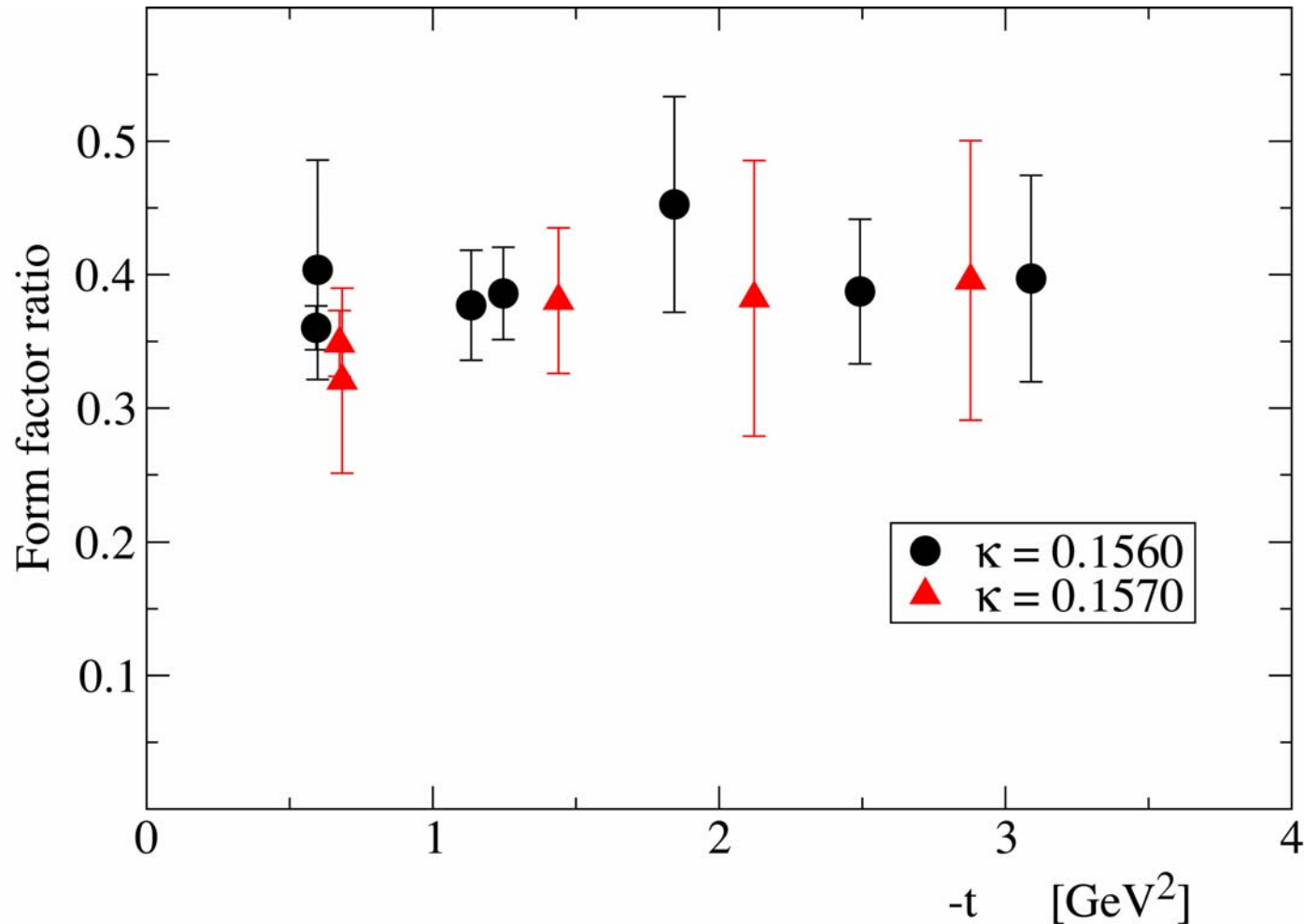
High- Q^2 Behaviour

Belitsky et al. have included logarithmic corrections in pQCD limit



They warn that the observed scaling could very well be precocious

LQCD calculation of Belitsky's ratio



LHPC collaboration

Unquenched

$m_\pi = 750, 960$ MeV

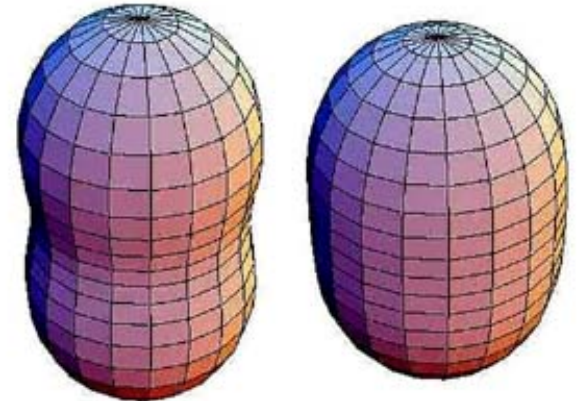
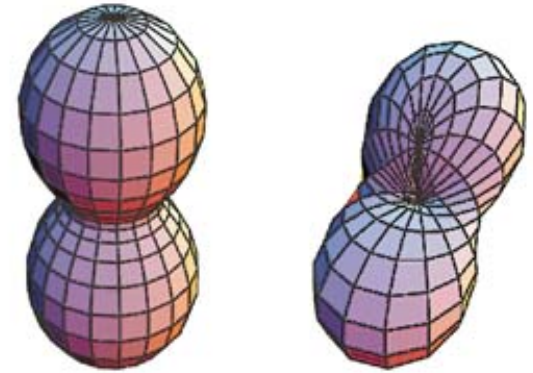


Thomas Jefferson National Accelerator Facility

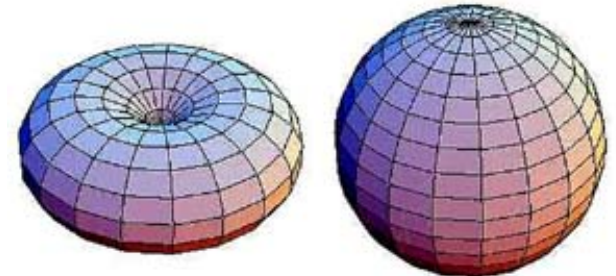
Shapes of the proton

- Jerry Miller has developed a procedure to calculate 3D images of the proton as a function of the momentum of the quark probed by the virtual photon, for different orientations of the spin of that quark relative to that of the proton

quark spin parallel
to nucleon spin



quark spin antiparallel
to nucleon spin



Viewing the proton through x-momentum filters

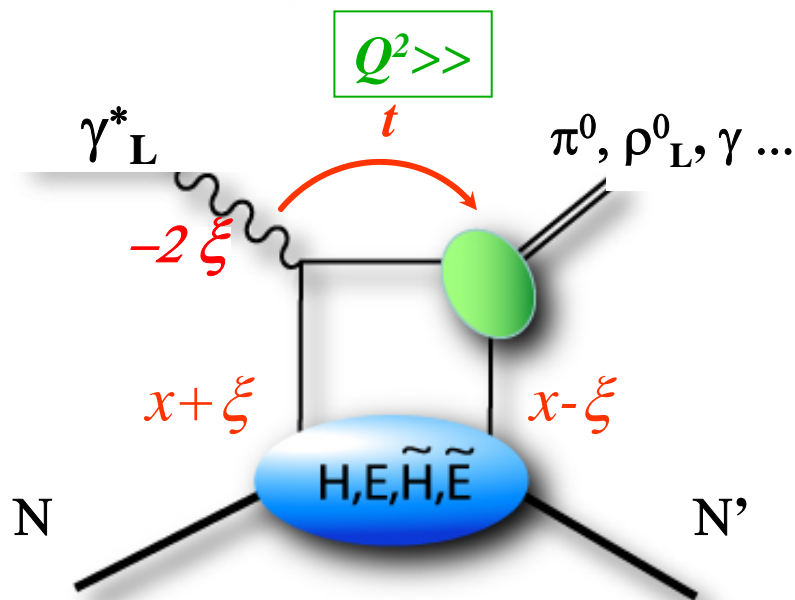
- Ji has developed a method to utilize the quantum-mechanical phase-space distributions developed by Wigner in 1932 to visualize the proton for any choice of the Bjorken-x variable
- The distribution is related to the Generalized Parton Distributions (GPDs) introduced not too long ago

$$f_{\Gamma}(\mathbf{r}, x) = \frac{1}{2M} \int \frac{d^3\mathbf{q}}{(2\pi)^3} e^{-i\mathbf{q}\cdot\mathbf{r}} F_{\Gamma}(x, \xi, t)$$

$$\frac{1}{2M} F_{\gamma^+}(x, \xi, t) = [H(x, \xi, t) - \tau E(x, \xi, t)] + i(\mathbf{s} \times \mathbf{q})_z \frac{1}{2M} [H(x, \xi, t) + E(x, \xi, t)]$$

Generalized Parton Distributions (GPDs)

-Mueller (1994) -
- Ji & Radyushkin (1996) -



→ 4 GPDs defined for each quark flavour:

H^q

\tilde{H}^q

conserve nucleon helicity

E^q

\tilde{E}^q

flip nucleon helicity

↓
unpolarized

↓
polarized

→ 3 variables: x, ξ, t

$x+\xi$ Longitudinal momentum fraction of the quark

-2ξ Exchanged longitudinal momentum fraction

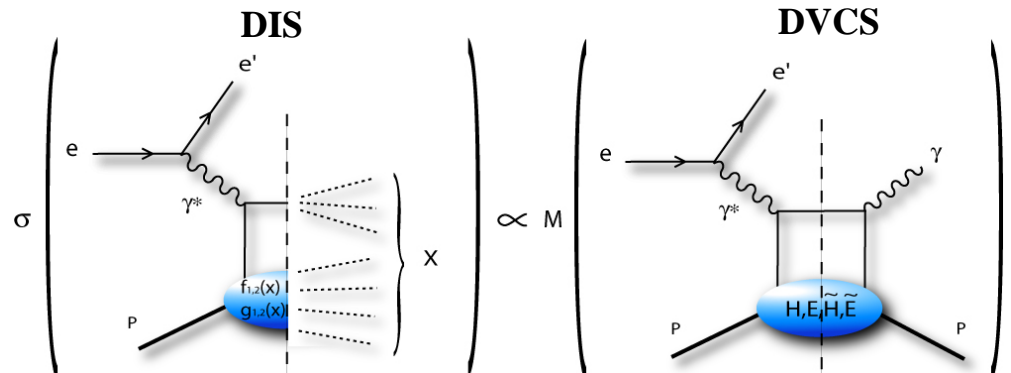
t Squared momentum transfer

$$\xi = \frac{1}{2} \frac{x_B}{1 - \frac{x_B}{2}}$$

→ GPDs = probability amplitude for N to emit a parton ($x+\xi$) and for N' to absorb it ($x-\xi$)

Limiting cases and sum rules

Forward limit ($t \rightarrow 0, \xi \rightarrow 0$)



$$H^q(x, \xi=0, t=0) = \mathbf{q}(x) \quad \tilde{H}^q(x, \xi=0, t=0) = \Delta \mathbf{q}(x)$$

Sum rules

$$\int_{-1}^{+1} dx H^q(x, \xi, t) = \mathbf{F}_1^q(t)$$

$$\int_{-1}^{+1} dx \tilde{H}^q(x, \xi, t) = \mathbf{g}_A^q(t)$$

$$\int_{-1}^{+1} dx E^q(x, \xi, t) = \mathbf{F}_2^q(t)$$

$$\int_{-1}^{+1} dx \tilde{E}^q(x, \xi, t) = \mathbf{h}_A^q(t)$$

Ji sum rules

$$\int_{-1}^{+1} (H(x, \xi, t=0) + E(x, \xi, t=0)) x dx = \mathbf{J}_{\text{quark}} = 1/2 \Delta \Sigma + \Delta L_z$$

~30%(DIS)

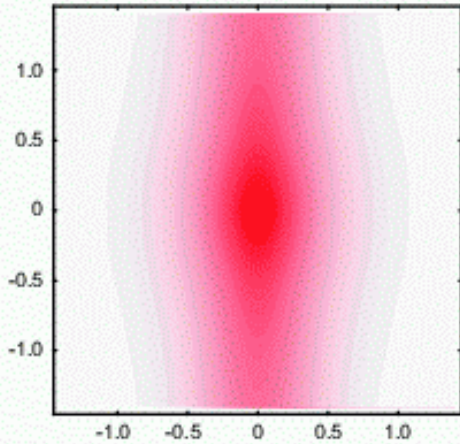


Thomas Jefferson National Accelerator Facility

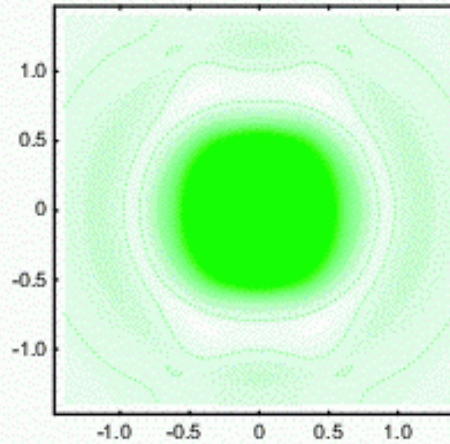
Proton Images at Fixed x

Up-quark densities

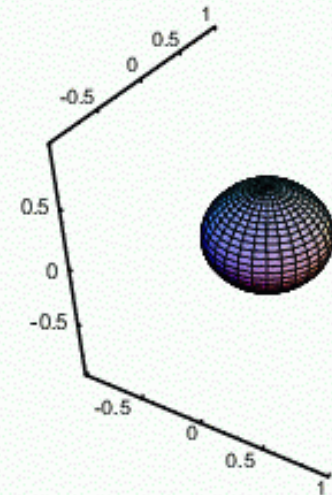
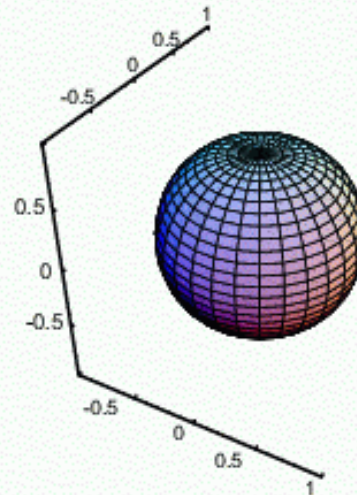
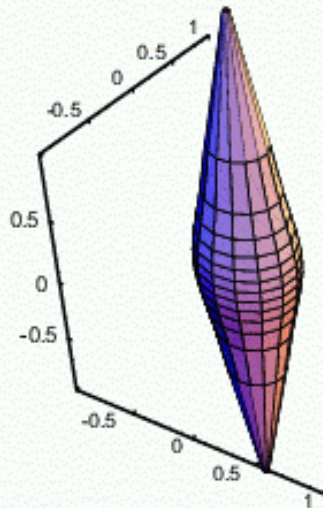
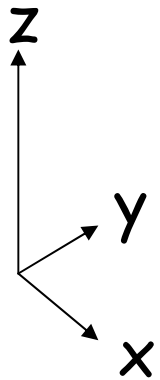
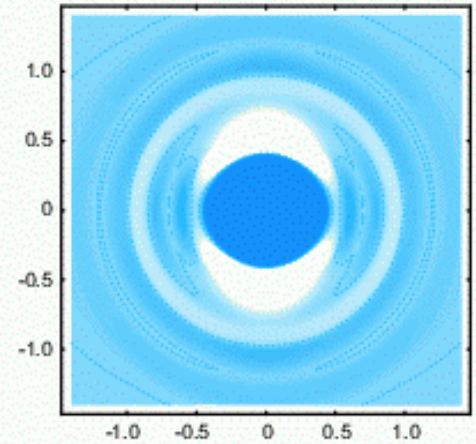
$x = 0.01$



$x = 0.4$



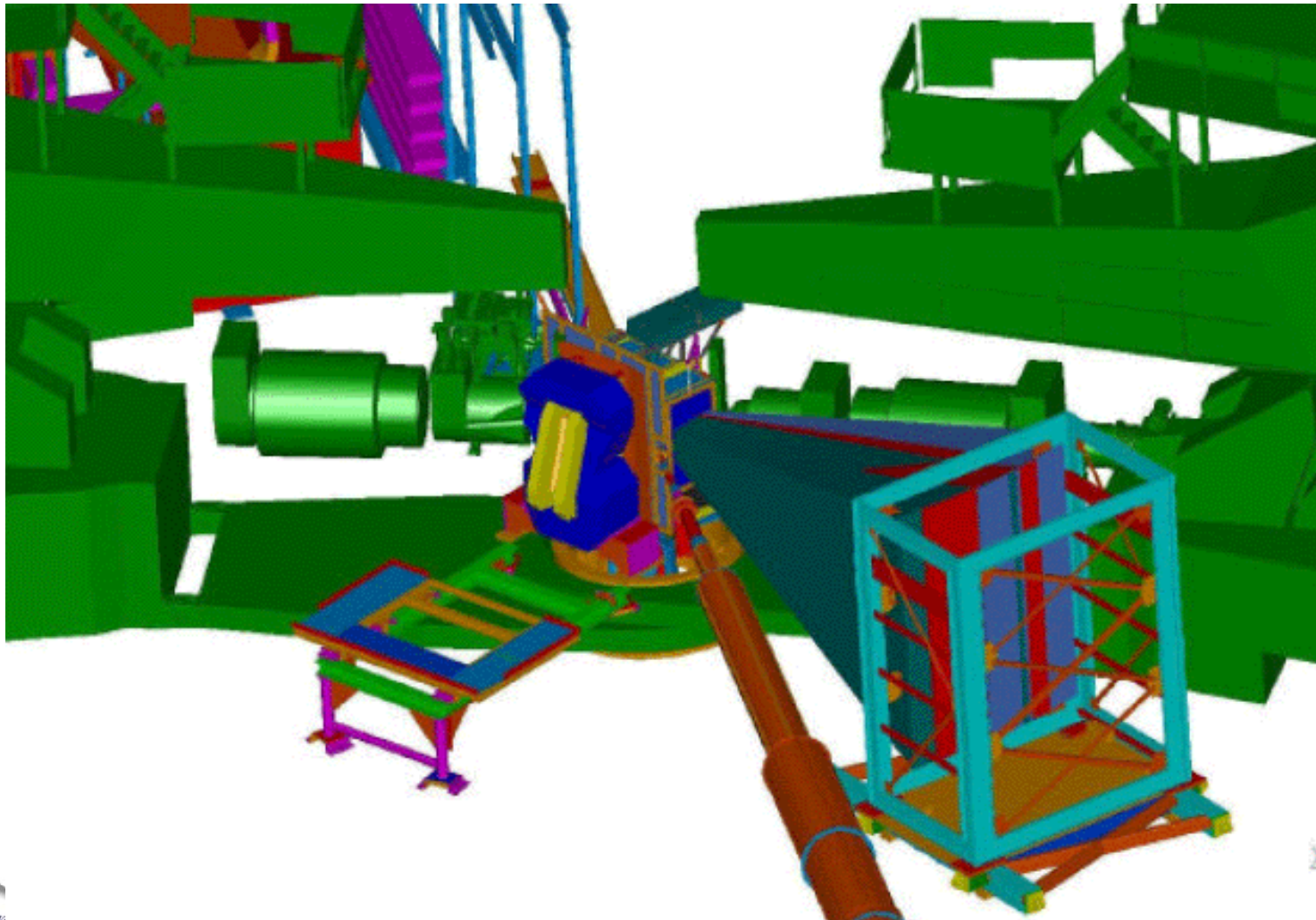
$x = 0.7$



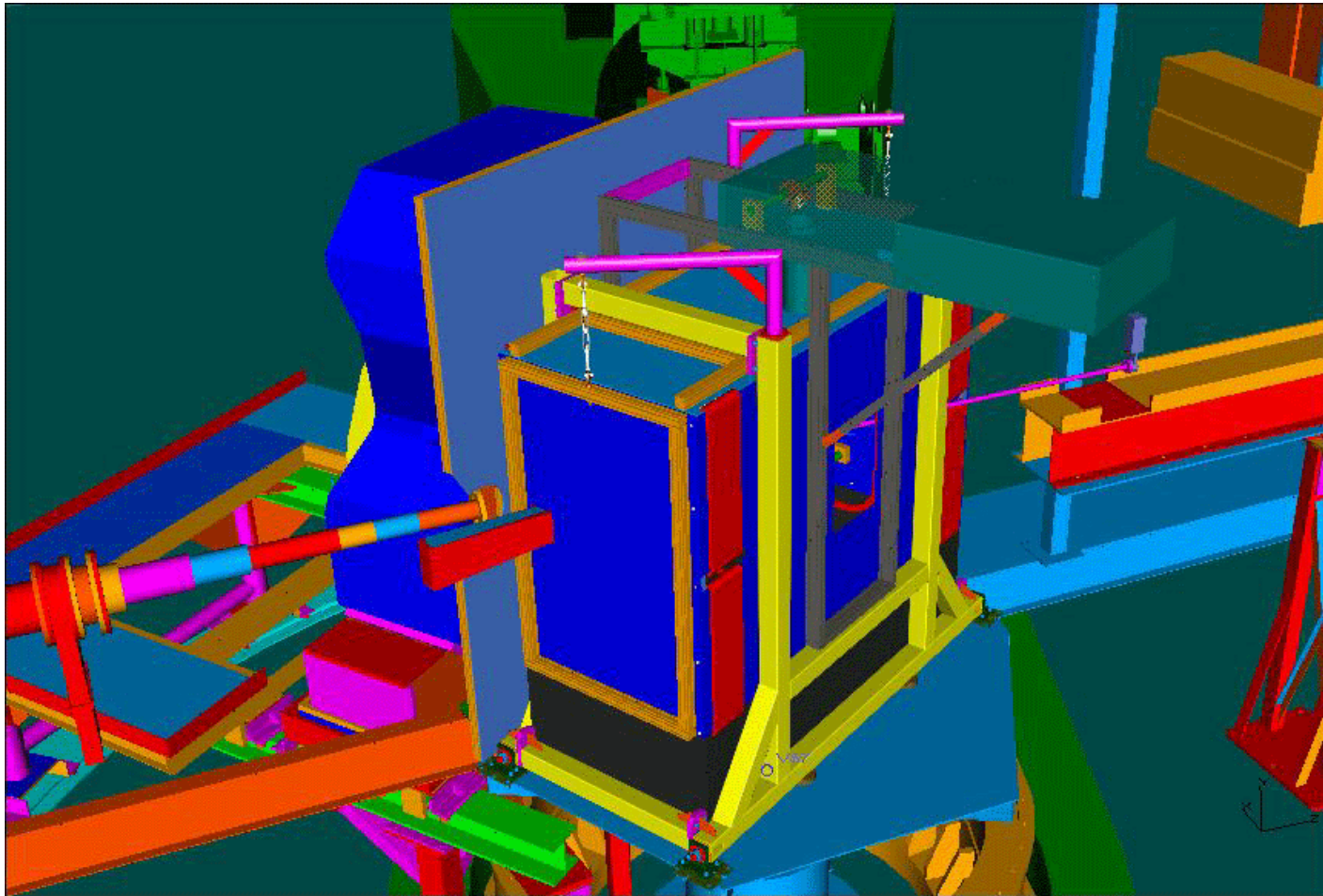
Future measurement of G_E^n at high Q^2

100 msr electron detector

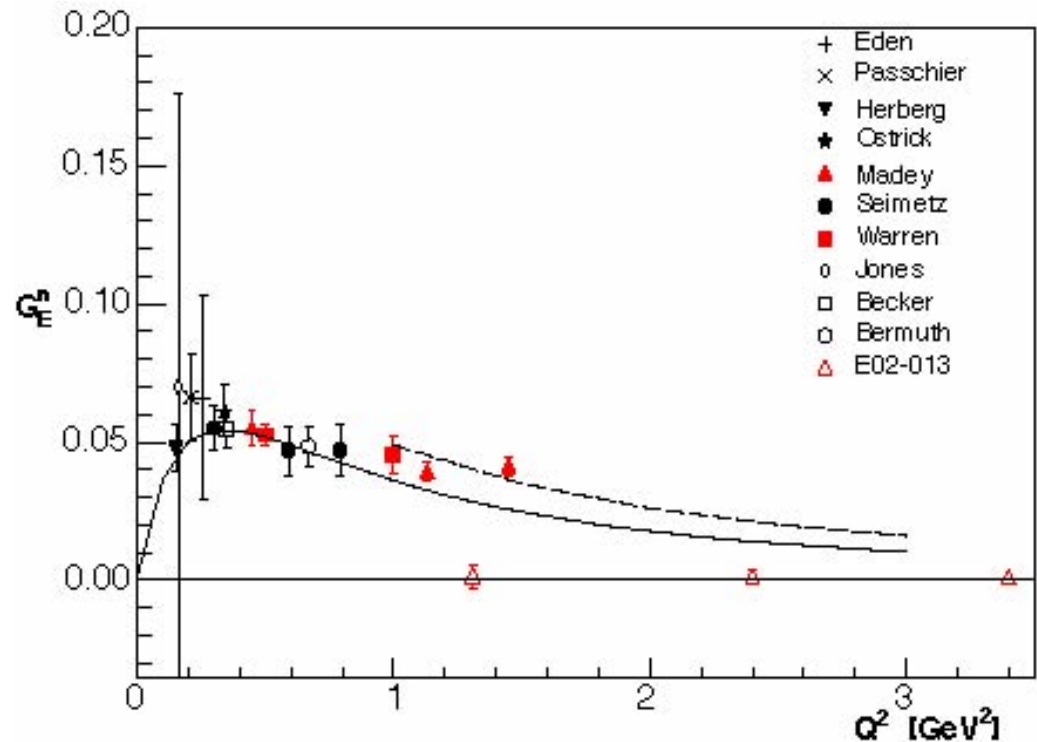
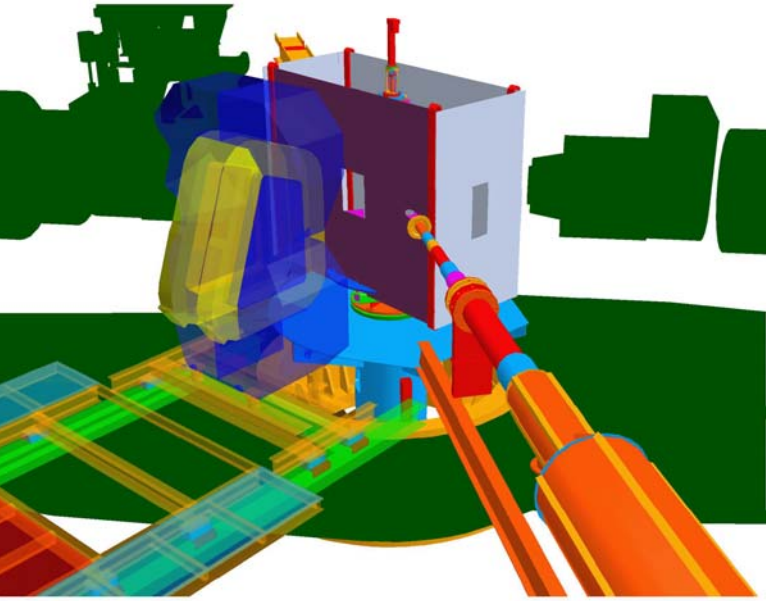
Large acceptance neutron detector



Target to measure G_E^n at high Q^2

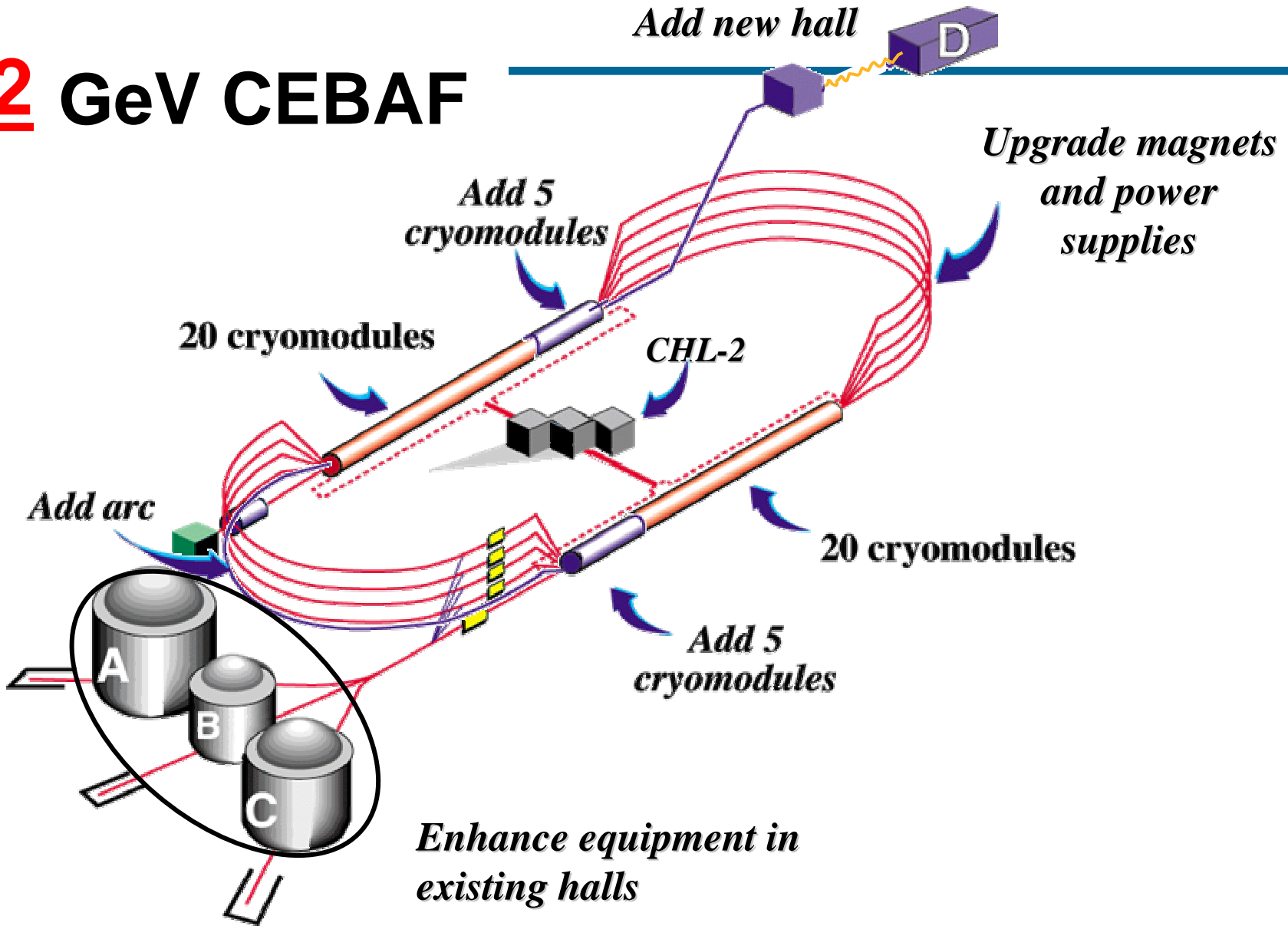


Future Extensions for G_E^n



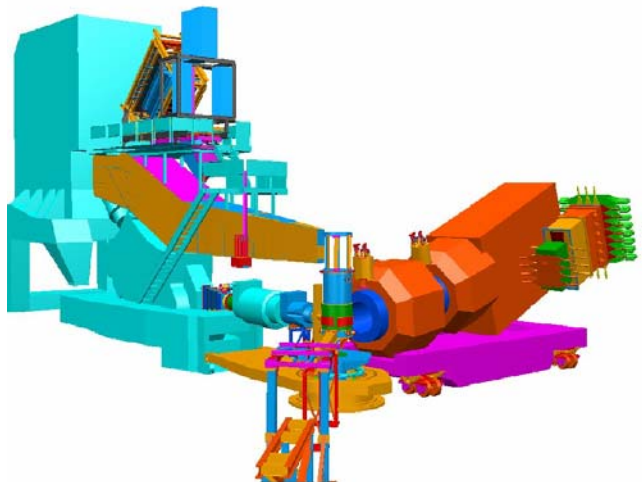
- E02-013 (Hall A) - polarized beam, polarized ^3He target, 100 msr electron detector and neutron detector allow extension to 3.4 GeV^2
- At 11 GeV further improvements of polarized ^3He target extension to $>5 \text{ GeV}^2$

12 GeV CEBAF



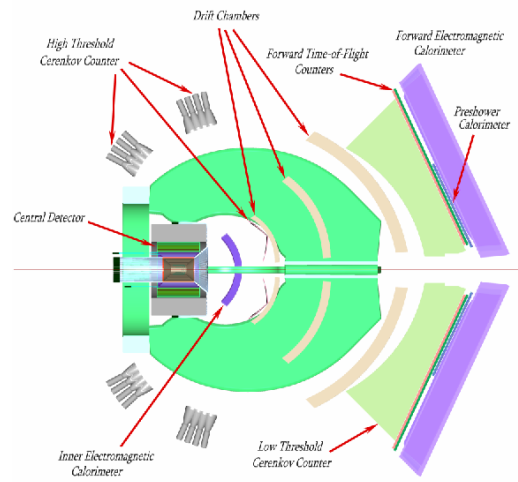
Upgraded Equipment in Halls A, B, C and a New Hall D

A



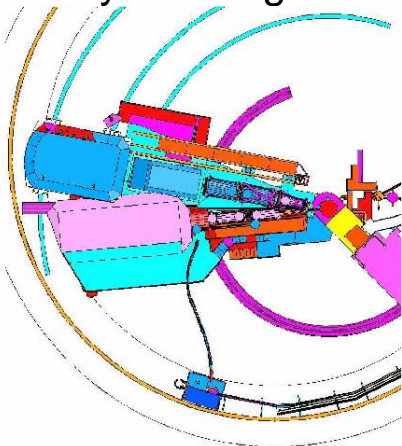
Medium Acceptance Detector (MAD) at high luminosity and large acceptance

B



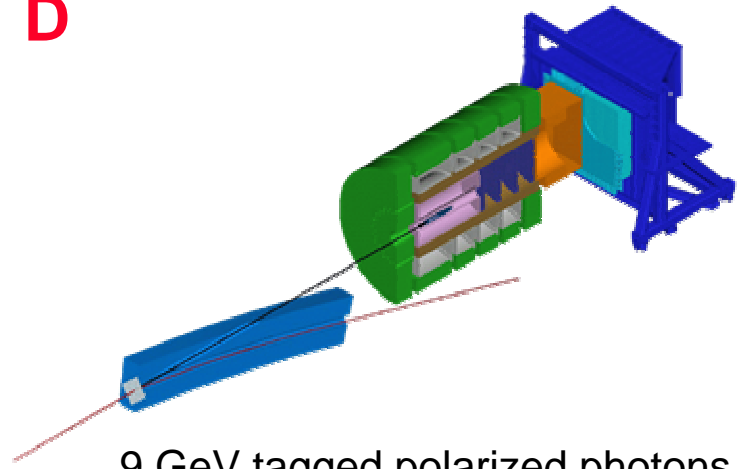
CLAS upgraded to higher (10^{35}) luminosity and coverage

C



Super High Momentum Spectrometer (SHMS) at high luminosity and forward angles

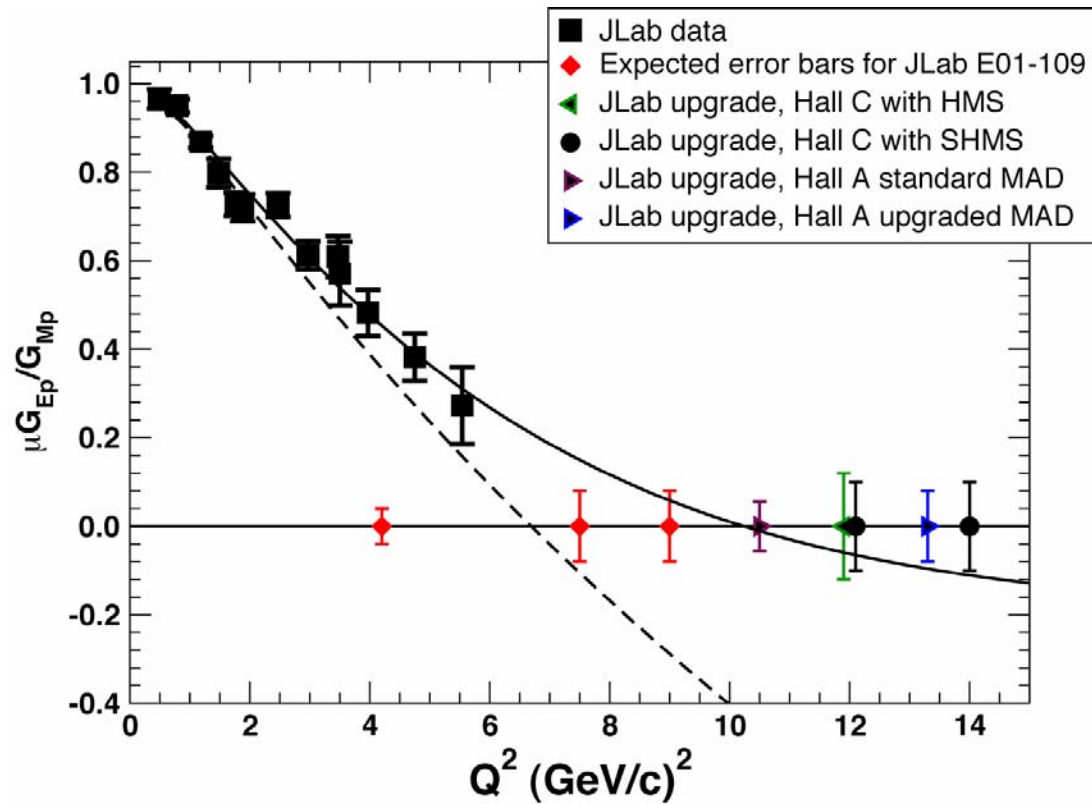
D



9 GeV tagged polarized photons and a 4π hermetic detector



Future extensions for G_E^p



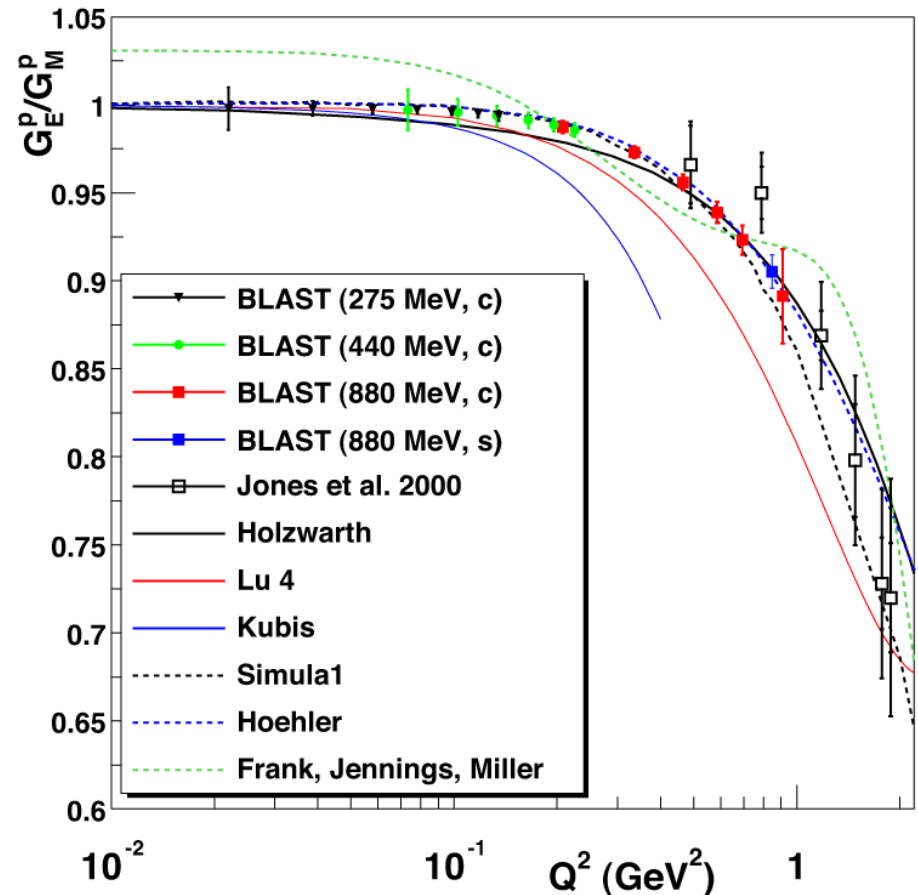
- Perdrisat *et al.* **E01-109**
Use Hall C HMS (with new FPP) and larger Pb-glass calorimeter
- MAD in Hall A or SHMS in Hall C at 11 GeV

High-accuracy measurement at BLAST

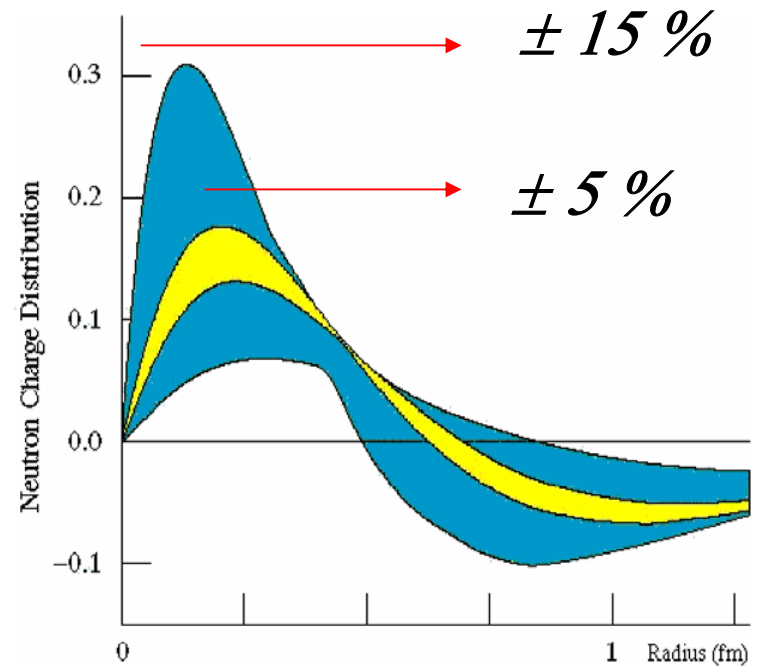
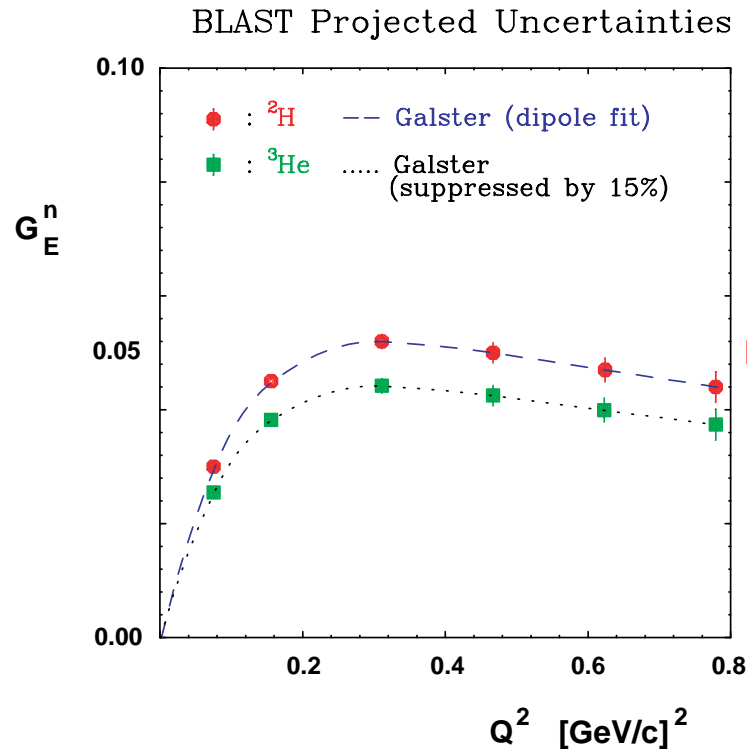
$$R = \frac{A_{\text{left}}}{A_{\text{right}}} = \frac{2\tau v_T \cos\theta_{\text{left}}^* (G_M^P)^2 + 2\sqrt{2\tau(1+\tau)} v_{LT} \sin\theta_{\text{left}}^* \cos\theta_{\text{left}}^* G_M^P G_E^P}{2\tau v_T \cos\theta_{\text{right}}^* (G_M^P)^2 + 2\sqrt{2\tau(1+\tau)} v_{LT} \sin\theta_{\text{right}}^* \cos\theta_{\text{right}}^* G_M^P G_E^P}$$

- BLAST with its two identical detector sectors allows a simultaneous measurement of the above super-ratio R in which beam and target polarization cancel
- Expected accuracy in G_E^P/G_M^P **0.3-1.2 %**

H. Gao, J.R. Calarco, H. Kolster



G_E^n measurements from BLAST



Key features of BLAST measurement:

- Effective neutron targets in common apparatus
- Technique minimizes systematic uncertainties
- Many channels simultaneously over broad range of kinematics

Summary

- In the last decade the field of nucleon electromagnetic form factors has opened up again, thanks to the development of powerful new polarization instrumentation
- Many surprising new data have been produced, the most exciting the difference between the Q^2 -dependence of the proton charge and magnetic form factors
- The apparent discrepancy between polarization transfer and Rosenbluth separation has very probably been resolved by the inclusion of TPE effects
- The large body of accurate data now available has provided a sensitive tests for a variety of nucleon properties at scales ranging from 1 fm to smaller than 0.1 fm
- Future experiments will extend data to higher Q^2
 - Does G_E^p change sign?
 - Does G_E^n show scaling similar to G_E^p ?
- Will also provide highly accurate data at low Q^2

